

FINAL REPORT

ALPHA FOUNDATION FOR THE IMPROVEMENT OF MINE SAFETY AND HEALTH

Grant Number: AFC518-67

Project Title: Demonstration of a UAV-based Digital Photogrammetry System for Geological Mapping and Geotechnical Characterization of Fractured Rock Masses at Hazardous Underground Sites

Reporting Period: July 1, 2017 through December 31, 2018

Organization Name: Montana Technological University, Butte, Montana

Principal Investigator: Professor Mary M. MacLaughlin
Department of Geological Engineering
Montana Tech of The University of Montana
1300 West Park St., MG 213B
Butte, MT 59701 USA
Phone: 406-496-4655
Fax: 406-496-4260
Email: mmaclaughlin@mtech.edu

ACKNOWLEDGEMENT/DISCLAIMER:

This study was sponsored by the Alpha Foundation for the Improvement of Mine Safety and Health, Inc. (ALPHA FOUNDATION). The views, opinions, and recommendations expressed herein are solely those of the authors and do not imply any endorsement by the ALPHA FOUNDATION, its Directors and staff.

EXECUTIVE SUMMARY

The overall goal of this research was to contribute to development of a new geosensing tool that allows engineers and geologists to identify and quantify geological features and loose ground that may adversely affect the safety and production of an underground mine in areas that are inaccessible to mine personnel. Due to their ability to access unsupported areas and locations with uneven ground while simultaneously collecting imagery for creating photogrammetric point clouds, unmanned aerial vehicles (UAVs) offer an opportunity for mine personnel to view and better understand the geologic structures in areas that are otherwise inaccessible. A georeferenced, photogrammetry-based point cloud of these unsupported openings allows geological structures to be identified and measured. ***Having a more detailed and thorough understanding of these areas allows for geotechnical analyses and risk assessments to be completed more accurately, thoroughly, efficiently, and safely.*** UAVs also have the potential to significantly improve the ability to create high quality 3D models and maps of accessible areas, as well, allowing expeditious collection of imagery data which can then be manipulated in the safety of the office. UAVs have the potential to allow high quality geologic mapping and basic geotechnical characterization of large, unsupported underground openings ***if the challenges associated with flight control, lighting, and image georeferencing can be overcome.***

The original focus of the research described in this report was to assess and quantify 1) the ability of UAV-based systems developed using modestly priced off-the-shelf components to a) survive flights within an unsupported underground opening, b) capture high-quality georeferenced imagery that is sufficiently lit and georeferenced, c) collect forward looking infrared (FLIR) thermal imagery that can be georeferenced, and 2) the ability of available software packages to generate photogrammetric models from the imagery and FLIR data which allow accurate definition of the geometry of the underground opening and the geological features that control its stability. The study was focused on underground hardrock mining so permissibility was not a concern. Issues encountered during the project created challenges but also opportunities to expand the research to investigate the performance of more sophisticated (and expensive) UAV-based systems involving LiDAR and SLAM, and multispectral imagery. The basic off-the-shelf system assembled to fly on the DJI M100 platform is evaluated to have a NASA Technology Readiness Level (TRL) of 5 (full scale prototype in intended environment). The TRLs of the more expensive, sophisticated systems range from 5 to 9 (full commercial application). The Hovermap system by Emesent, Ranger by Inkonova, and Elios by Flyability are reasonably rugged and able to navigate beyond line-of-sight. A significant contribution associated with this project is development of a set of trials that are used to evaluate the performance of the systems in a variety of situations.

3D models were successfully produced from visual (RGB), thermal, and multispectral imagery collected with the UAV systems, using four different commercially available photogrammetry software packages. Although the models created by the different packages vary somewhat in quality, the quality can be increased by adjusting parameters within the software to create higher resolution models (which are associated with larger files that are more difficult to manipulate). Construction of models using thermal and multispectral imagery requires special attention.

Continued development of a low-cost, reasonably robust system is worthwhile to pursue due to the inherent risk associated with the underground mining environment (and likelihood that the equipment will be lost), and the continual improvement in available technology. The ultimate goal is to provide a safe working environment and minimize personnel underground.

TABLE OF CONTENTS

1.0 Concept Formulation and Mission Statement	4
2.0 Project Component 1: Basic UAV Systems and Imagery Acquisition	7
2.1 PC-1 Proof-of-Concept (Prototype) Technology Components	7
2.2 PC-1 Proof-of-Concept (Prototype) Evaluation	10
3.0 Project Component 1B: Systems for Enhanced Navigation	18
3.1 PC-1B Proof-of-Concept (Prototype) Technology Components	18
3.2 PC-1B Proof-of-Concept (Prototype) Evaluation	21
3.2.1 Emesent	23
3.2.2 Near Earth Autonomy	26
3.2.3 Inkonova	29
3.2.4 Flyability	32
3.2.5 Summary	35
4.0 Project Component 2: Photogrammetric Modeling	38
4.1 PC-2 Proof-of-Concept (Prototype) Technology Components	39
4.2 PC-2 Proof-of-Concept (Prototype) Evaluation	41
4.2.1 Quantitative study on the surface (Notchbottom)	41
4.2.2 Creation of 3D models to be used for geological/geotechnical mapping	44
4.2.3 Comparison of software using underground trial imagery (GSM)	46
5.0 Project Component 2B: Thermal and Multispectral Image Acquisition and Modeling	50
5.1 PC-2B Proof-of-Concept (Prototype) Technology Components	50
5.2 PC-2B Proof-of-Concept (Prototype) Evaluation	51
5.2.1 Thermal imagery acquisition and modeling	51
5.2.2 Multispectral imagery acquisition and modeling	57
6.0 Technology Readiness Assessments	60
6.1 Project Component 1: Basic UAV Systems and Imagery Acquisition	61
6.2 Project Component 1B: Systems for Enhanced Navigation	64
6.3 Project Component 2: Photogrammetric Modeling	70
6.4 Project Component 2B: Thermal and Multispectral Image Acquisition & Modeling	71
References & Acknowledgements	73
Appendices	75

1.0 CONCEPT FORMULATION AND MISSION STATEMENT

The overall goal of this research was to contribute to development of a new geosensing tool that allows engineers and geologists to identify and quantify geological features and loose ground that may adversely affect the safety and production of an underground mine in areas that are inaccessible to mine personnel. Adverse geological structures and loose ground within unsupported openings (stopes, raises, drifts, etc.) are the source of ground falls that can endanger miners, underground workers, and equipment. Overbreak along geological features can also cause the dilution of ore as well as the deterioration of supporting rock masses (backs, ribs, pillars, crown pillars, etc.). While overbreak can be directly caused by mining and blasting techniques, structural failures along geologic features can also contribute to the problem. Large ground falls can also be the source of air blasts, or high-pressure blasts of air caused by the displacement of the air by falling rock, that can endanger mine personnel and damage utilities.

The traditional process for performing stability analysis of an inaccessible underground opening involves combining rough design drawings of the opening with structural data obtained through hand-mapping of nearby accessible areas and projected to the inaccessible location. Significant improvements in acquiring better geometry data have been achieved with the development of stationary cavity monitoring survey (CMS) laser-based scanners. The CMS scanner, often deployed from a boom into an unsupported excavation (stope, raise, etc.), provides a point cloud delineating the excavation geometry that may be used to create a 3D model, and some scanners are now able to capture visual red/green/blue (RGB) data for enhanced analysis. The drawbacks of the CMS systems include: 1) the process is time-consuming, particularly for unsupported excavations with curves or laterally extensive openings that require several individual scans, 2) the scans are frequently incomplete because the scanner can only be positioned within line-of-sight of the opening, leaving holes in any areas that are hidden around corners or by protruding rock, and 3) the CMS scanner is at high risk of damage due to rock fall because it must remain stationary for several minutes during the scan.

Although some scanners are now able to capture limited RGB data for enhanced structural analysis, 3D photogrammetric models created from RGB imagery have significant advantages, allowing easier identification and quantification of critical features ranging from undiluted structures to mineralization. Above-ground studies have shown that with the use of georeferenced ground control points, the accuracy of photogrammetric models can be equivalent or superior to the accuracy of laser-based LiDAR models. Use of photogrammetry at underground sites has been hampered by the darkness, dust, humidity, and space constraints inherent in the underground environment.

Due to their ability to access unsupported areas and locations with uneven ground while simultaneously collecting imagery for creating photogrammetric point clouds, unmanned aerial vehicles (UAVs) offer an opportunity for mine personnel to view and better understand the geologic structures in areas that are otherwise inaccessible. A georeferenced, photogrammetry-based point cloud of these unsupported openings allows geological structures to be identified and measured. ***Having a more detailed and thorough understanding of these areas allows for geotechnical analyses and risk assessments to be completed more accurately, thoroughly, efficiently, and safely.*** UAVs also have the potential to significantly improve the ability to create high quality 3D models and maps of accessible areas, as well, allowing expeditious collection of imagery data which can then be manipulated in the safety of the office.

The primary challenges of using UAVs to collect imagery in the underground environment include the ability to navigate safely in a GPS-denied hazardous environment, and to provide adequate lighting to allow collection of high-quality RGB imagery along with a mechanism for associating specific coordinates with objects in the imagery (georeferencing). Although recent technology developments have provided the basic components that would be needed, in a package light enough to be carried by a UAV, no systems specifically focused on capturing photogrammetric data in an underground environment are currently commercially available.

The goal of this research project was to fill that technology gap, achieved through design and assembly of UAV-based imagery acquisition systems using off-the-shelf components, comprehensive testing of the performance of the systems, and use of the imagery to generate point clouds and 3D models using available software packages. The specific objective of this research was to test the ability of UAVs for acquiring digital photographs and thermal imagery to collect geological data from an underground opening that is unsafe for people to enter, thereby demonstrating the viability of a new geosensing tool. ***UAVs have the potential to allow high quality geologic mapping and basic geotechnical characterization of large, unsupported underground openings if the challenges associated with flight control, lighting, and image georeferencing can be overcome.***

The original focus of the research described in this report was to assess and quantify:

- *(Project Component 1)* the ability of UAV-based systems developed using modestly priced off-the-shelf components to a) survive flights within an unsupported underground opening, b) capture high-quality georeferenced imagery that is sufficiently lit and georeferenced, c) collect forward looking infrared (FLIR) thermal imagery that can be georeferenced, and
- *(Project Component 2)* the ability of available software packages to generate photogrammetric models from the imagery and FLIR data which allow accurate definition of the geometry of the underground opening and the geological features that control its stability.

Several issues encountered during the project created challenges but also opportunities to expand the research to include two additional components:

- *(Project Component 1B)* The “Guidance” system designed to allow for object detection and collision avoidance for the primary UAV platform selected for use in this project, the DJI Matrice 100 (M100), was difficult to use and did not perform as expected. The suggestion to evaluate more sophisticated (and expensive) UAV-based systems involving LiDAR and SLAM (simultaneous localization and mapping) led to a supplement and schedule extension to allow this component to be added to the project. Since the cost of these systems exceeded the maximum budget allowed, the strategy involved arranging for multiple vendors to demonstrate their systems underground at a nearby mine site and provide imagery datasets that were used to quantitatively evaluate and compare the performance of the systems.
- *(Project Component 2B)* Generating 3D models from the thermal imagery was more difficult than anticipated, so the project was expanded to include multispectral imagery. The thermal and multispectral equipment, imagery, and models are all described in the section describing Project Component 2B.

The project involved a partnership with Barrick's Golden Sunlight Mine (GSM) near Whitehall, Montana, facilitated by Barrick Geotechnical Engineer and Montana Tech master's candidate Ryan Turner. Mr. Turner also contributed to the proposal that was submitted to the Alpha Foundation. The partnership provided a win-win situation, with Montana Tech benefitting from access to an ideal underground field site located near campus, and GSM benefitting from the data acquired during the course of the research.

The project was initiated in summer, 2017, and spanned 18 months. The first 6-month period was dedicated to selection of equipment, design and assembly of the initial systems, review of available software, acquisition of equipment operation and flight skills, mine safety training, etc. The second 6-month period was focused on acquisition of imagery in accessible and inaccessible underground sites, and use of the imagery to generate 3D models. The final 6-month period was largely dedicated to evaluation of the systems incorporating enhanced navigation, in terms of their performance and the quality of the models produced from the imagery. The thermal imagery research extended throughout the entire project duration.

This report is organized by project component, with the proof-of-concept technology components and evaluation discussed for each of the following components: 1) Basic UAV Systems and Imagery Acquisition, 1B) Systems for Enhanced Navigation, 2) Photogrammetric Modeling, and 2B) Thermal and Multispectral Modeling. ***Since this project involved assembly and evaluation of a system built from components that were already available, the research went beyond proof-of-concept to include investigation of the performance of the working prototype systems in field studies.*** The technology readiness assessment of each component, evaluated in terms of what is needed for adoption by the mining industry, is summarized in a separate section. Accompanying files contain 3D pdfs of the models and one flight video.

Preliminary results were summarized in two interim reports, submitted on 31 December 2017 and 30 June 2018. Additional details are available in the following papers and master's thesis:

- Becker, R.E., L.J. Galayda, and M.M. MacLaughlin (2018). Digital Photogrammetry Software Comparison for Rock Mass Characterization, *Proceedings of the 52nd U.S. Rock Mechanics Symposium*, Seattle, WA, Paper 18-1211 (7 pp).
- Russell, E.A. (2018). *UAV-based Geotechnical Modeling and Mapping of an Inaccessible Underground Site*, Montana Tech master's thesis (95 pp), available via Montana Tech's Digital Commons https://digitalcommons.mtech.edu/grad_rsch/.
- Russell, E.A., M.M. MacLaughlin, and R.M. Turner (2018). UAV-based Geotechnical Modeling and Mapping of an Inaccessible Underground Site, *Proceedings of the 52nd U.S. Rock Mechanics Symposium*, Seattle, WA, Paper 18-516 (9 pp).
- Turner, R.M., N.P. Bhagwat, L.J. Galayda, C.S. Knoll, E.A. Russell, and M.M. MacLaughlin (2018). Geotechnical Characterization of Underground Mine Excavations from UAV-Captured Photogrammetric & Thermal Imagery, *Proceedings of the 52nd U.S. Rock Mechanics Symposium*, Seattle, WA, Paper 18-508 (11 pp).

The most recent results will be presented to the mining community at the 2019 Annual Meeting of the Society of Mining Engineers, to be held in Denver, Colorado, in February. The titles of the presentations are:

- Comparison of UAV Systems Equipped with LiDAR and Photogrammetry for Geotechnical Investigation in Underground Mining Environments* (to be presented by R. Becker)
- Identifying Loose Ground and Unfavorable Structures in Underground Workings Using Thermal and Multispectral Imagery* (to be presented by R. Turner)

2.0 PROJECT COMPONENT #1: Basic UAV Systems and Imagery Acquisition

As mentioned in the previous section, the primary challenges of using UAVs to collect imagery in the underground environment are the ability to navigate safely in a GPS-denied hazardous environment, and to provide adequate lighting to allow collection of high-quality RGB imagery along with a mechanism for associating specific coordinates with objects in the imagery (georeferencing). Several companies have developed UAVs for flying in confined spaces, including underground environments. Flyability's Elios UAV (Flyability, 2018) is enclosed within a rotating cage that absorbs and transfers energy during a collision, allowing the UAV to stay upright after contacting an object; unfortunately, the cage interferes with its usefulness for photogrammetry because of its presence in the imagery. Inkonova's TILT Ranger UAV (Inkonova, 2018) is a custom drone platform dedicated to underground mine mapping with a LiDAR, but cannot be considered an "off the shelf" UAV-based photogrammetry system.

With no modestly priced UAV systems commercially available at the current time, the goal of this research project was to design and assemble one or more UAV-based imagery acquisition systems using off-the-shelf components, conduct comprehensive tests to evaluate the performance of the systems, and to demonstrate that the imagery can be used to generate point clouds and 3D models using available software packages. The first component of this project involved the design and assembly of the systems and evaluation of their performance. Specifically, the focus of Project Component #1 was to assess and quantify the ability of UAV-based systems developed using modestly priced off-the-shelf components to

- a) survive flights within an unsupported underground opening, and
- b) capture high-quality georeferenced imagery that is sufficiently lit and georeferenced.

The use of off-the-shelf components allowed this project to continue beyond proof-of-concept and include field testing of the prototype equipment.

2.1 PC-1 Proof-of-Concept (Prototype) Technology Components

In general, UAV systems consist of the main UAV platform, a flight controller, a battery, and, if desired, an imaging device (camera). A remote controller is commonly used with the system to communicate with its respective flight controller on board the UAV, allowing it to be operated manually. For this underground research, an on-board lighting system was required and an on-board obstacle detection system was used.

After evaluating a number of potential UAV platforms, the DJI Matrice 100 (M100) was chosen to be the primary platform for this study because of its affordability, size, payload capacity, sensing system compatibility, and customization capabilities. Appendix A contains detailed list of specific components described in the following paragraphs, showing cost and mass of each.

The M100 (Figure 1) measures about 650 mm (25.6 in.) diagonally across the top of the frame (DJI, 2019). It is available as a kit that must be assembled by connecting the parts, although soldering is not required. The kit contains all of the necessary parts: the carbon fiber body and arms, legs, flight controller with an internal measurement unit (IMU), a propulsion system, a battery and battery compartment, propellers, a global positioning system (GPS) for enhanced outdoor navigation, plus a separate remote controller. Other smaller parts like the camera gimbal mount and an expansion bay are also included in the M100 kit, but are not necessary for the UAV to function. (Note that some of the citations below refer to the DJI Inspire documentation because the DJI M100 and Inspire 1 UAVs have some identical components and accessories.)



Figure 1. Photo of the M100.

According to DJI, the M100's propulsion system has a capacity of 3600 grams, allowing it to lift the mass of the basic unit (1755 g) and single battery (600 g), with an excess payload capacity of approximately 1245 g. (The GPS unit was attached even for GPS-denied flights.) Off-the-shelf customizations available for the M100 include propeller guards, a second battery, the DJI "Guidance" system for obstacle detection and avoidance, and several digital cameras. The system is designed so that other non-DJI items can be mounted to the UAV as well, although the M100 N1 flight controller is designed to only communicate with DJI products.

The real-time data feed is sent through a 2.4 GHz connection between the UAV and the remote controller. The DJI GO application (app) is necessary for capturing photos or video during operation of the aircraft when a camera is connected. In addition, an iPad (or other mobile device) was connected to each remote controller, so that the live camera point-of view could be viewed by the operator via the DJI GO app. The imagery is reduced to a size that can be quickly transferred to the remote controller and is saved onto the mobile device; the primary devices used for this research included an iPad Air 2 and an iPad Mini 4

The imaging device used for this research was a DJI Zenmuse X3 digital camera, which has the capabilities of recording video or taking still photographs, both with adjustable settings. The Zenmuse X3, X5 and Z3 from DJI are compatible with the M100, but the Zenmuse X3 was found to have a sufficient sensor size (1/2.3" CMOS, which is 6.17 mm x 4.55 mm), a larger FOV (field of view) and is the least expensive (list price \$459, vs. \$1659 for the X5 and \$899 for the z3). It has a fixed lens at 3.6 mm (35 mm format equivalent of 20 mm), and an f-stop of 2.8 at a focal length of infinity. The camera is connected to a 3-axis gimbal that allows for the camera to be tilted up to 120-degrees and rotated 360-degrees (DJI, 2017). A micro-SD card inserted into the camera is used to store the full-sized formatted imagery data and other flight details, while a live feed from the camera is shown in the DJI Go app at 720p (DJI, 2016a).

Additionally, when the M100 was chosen, it was one of the only customizable UAVs that had an off-the-shelf sensor system package that could be added onto the platform for obstacle sensing and avoidance, allowing the M100 to fly indoors and in GPS-denied areas. The M100 utilizes the DJI "Guidance" obstacle sensing system, which works in tandem with the built-in flight controller to aid in the avoidance of obstacles detected at a user-defined distance. Stereo cameras (referred to as the visual positioning system, or VPS) mounted to point ahead, behind, on both sides, and below the UAV are used in conjunction with ultrasonic sensors to detect obstacles (DJI, 2015). One drawback of this system in terms of its use underground is the lack of obstacle detection *above* the UAV which is not needed for traditional above-ground scenarios. Blind spots also exist around the legs of the UAV, because of the camera's 60-degree horizontal and 56-degree vertical field-of-view (FOV), as shown in Figure 2.

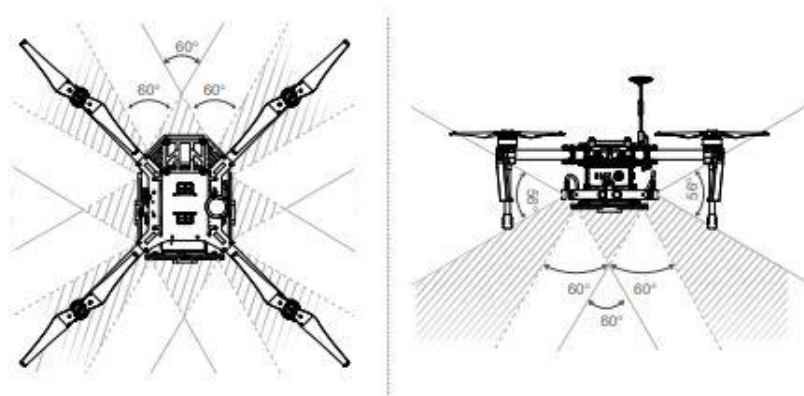


Figure 2. DJI Guidance system cameras FOV (DJI, 2015). Top view (left) showing horizontal blind spots and side view (right) showing vertical blind spots.

With the “Guidance” documentation stating that obstacles may be detected with lux (measured in lumen/m^2) values ranging from 10 to 10,000, it was anticipated that the lighting requirements would be dictated by the imagery. Three light-weight LED lighting systems were investigated:

- LumeCubes (<https://lumecube.com/>) – self-contained
- FireHouse Technology LEDs (<https://www.firehousetechnology.com/>) – self-contained
- Stratus LEDs Arm modules (<https://www.stratusleds.com/>) – consist of a 100 Watt 13,000 lumen 5600K CRI LED emitter, a heat sink, an LED driver, and a LiPO battery

Table 1 summarizes the advertised details of these lighting systems, two of which are shown in Figure 3. The systems were evaluated in terms of mass (LEDs + battery), lumens, beam width, and mounting options. Interestingly, it was determined through trial and error during the experiments (described in the following section) that the “Guidance” system’s lower limit of 10 lux was not accurate and that significantly higher lux was required for obstacle detection. Consequently, the lighting required for the “Guidance” system, rather than the imagery, was the controlling factor in the design of the lighting system.

Table 1. Comparison of different LED lights used.

Lighting System	Mass per light (g)	Lumen output per light	Beam Width (degrees)	Cost
Lume Cubes	99	1500	60	\$149.99 (pair)
Fire House Technology	71	1600	100	\$49.99 (each)
Stratus LEDS	135	13,000	60-160	\$199 (pair)



Figure 3. Two of the lighting systems used for this project. Left: Firehouse lights on the M100. Right: Stratus Arm LED module.

2.2 PC-1 Proof-of-Concept (Prototype) Evaluation

Over the course of approximately six months during the 2017-18 academic year, experiments were conducted to evaluate the LED lighting systems and to investigate the M100's available flight modes, establish its limits in terms of payload and wireless connection to the remote controller, and determine the capabilities of the DJI "Guidance" system. These experiments were conducted indoors on campus and underground at Barrick's Golden Sunlight Mine (GSM). Additional experiments were conducted at GSM during spring and summer 2018 to establish the ability of the system to survive flights in inaccessible underground locations and to provide adequately lit, georeferenced imagery. Although indoor and underground airspace is not regulated by the FAA and FAA Part 107 (drone pilot) certification was technically not required, several project participants (2 graduate students and 1 undergraduate) did acquire FAA Part 107 certification to allow flights out-of-doors when necessary.

2.2.1 Experiments to investigate lighting, payload, Guidance system, etc.

Initial tests of the flight capabilities of the DJI M100 and the proximity sensing capabilities of the DJI Guidance were conducted at the Montana Tech campus. To simulate the underground mining environment, indoor facilities that had low-light conditions, high magnetic interference, and no GPS coverage were selected for test flights. Maintenance bays and racquetball courts, being very tall but not relatively wide, make ideal analogs for stopes; other flights were conducted in secured hallways and in the gymnasium (Figure 4).

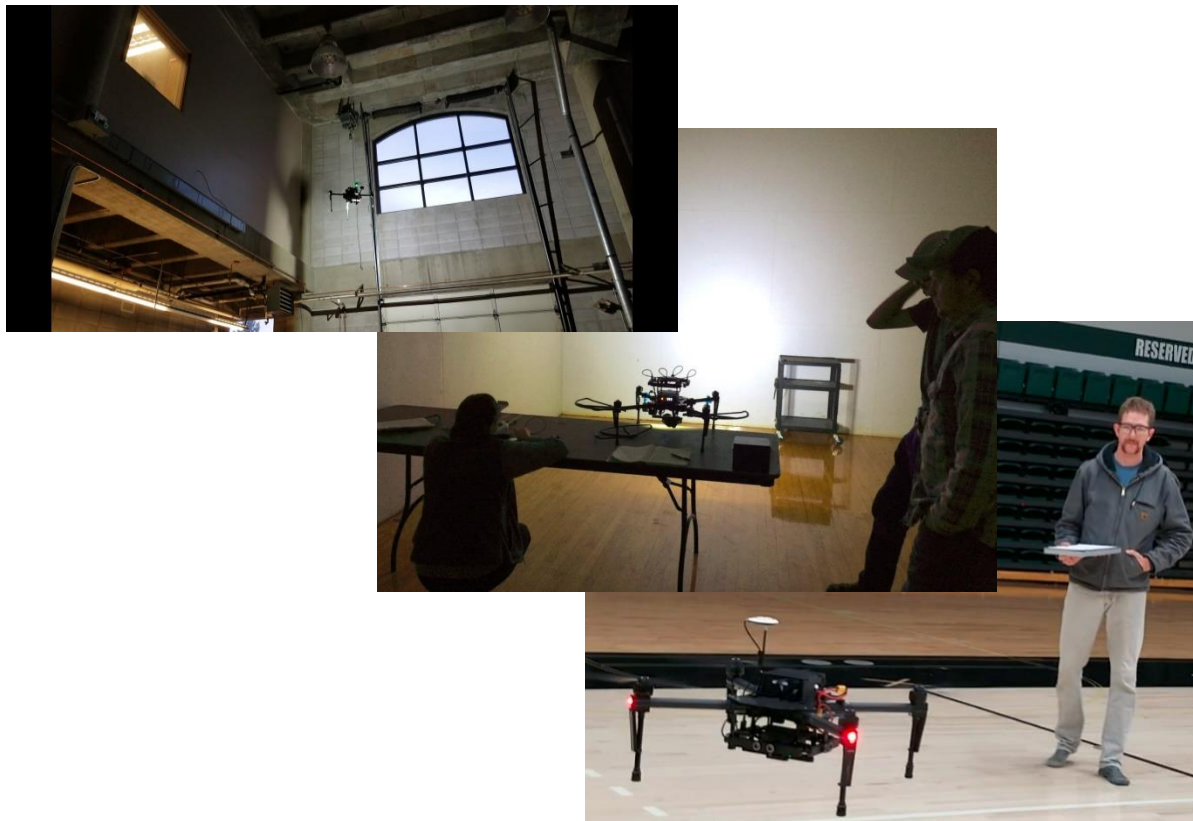


Figure 4. Top: Test of the Guidance system's ability to detect obstacles in a maintenance bay. Middle: Test of the M100's on-board lighting and camera systems in a racquetball court. Bottom: Initial test of the M100's performance in the gymnasium (a GPS-denied environment).

Among the early lessons learned during the dozens of initial flights on campus were the importance of proper positioning of UAV components, of IMU and compass calibrations, and of applying all firmware and software updates in order. It was also learned that the performance of iPad mobile devices was superior to that of smartphones. Learning to fly the M100 in a GPS-denied environment was reasonably straight-forward. The M100 can be flown in three different flight modes: P-mode (positioning); A-mode (attitude); and K-mode (function). P-mode utilizes both GPS (when available) and the Guidance system to allow the M100 to hover stably and detect obstacles. A-mode is a free-flight mode that only accepts inputs from the pilot, and it disregards any on-board instruments. K-mode only uses on-board instruments, such as the Guidance. Of the modes tested, P-mode allowed the M100 to be more stable and fly without drifting, proving it to be the best choice for use with the Guidance system (DJI, 2016a).

The most critical challenge encountered during this research project was learning how to configure and use the DJI “Guidance” system properly. The role of the “Guidance” system is to detect obstacles and prevent the UAV from flying within a specified distance of the obstacles. The documentation provided for the Guidance system is sparse and trial and error are required to achieve proper configuration. Individual sensors on the system are calibrated using a computer monitor and the DJI Guidance Assistant software (DJI, 2015). It was found that if the computer monitor was too small or the resolution was too low, the calibration would fail. When not configured correctly, the Guidance system failed to detect obstacles, allowing the M100 to contact the obstacles and potentially crash. According to the available documentation, the Guidance can be mounted above or below the main platform of the M100, but in tests conducted for this project, it only functioned properly when positioned below. The suspected reason for this is that when the Guidance sensors are positioned on top of the aircraft, the movement of the propellers (which are also positioned above the main platform) interferes with the operation of the sensors. Additionally, two undocumented features of the Guidance were determined during the experimentation: 1) The distance to obstacles was displayed in the DJI Go app as described in the documentation only when an advanced flight battery (TB48D) is used; when a standard flight battery (TB47D) was used, the Guidance functioned as intended but did not interact with the DJI Go app as described. 2) Even though the imaging camera did not have any contribution to the Guidance system, the Guidance only worked properly when the Zenmuse X3 camera was attached to the M100 and did not work at all when the camera was not attached.

The M100 was required to have on-board lighting to support the use of both the digital camera used for capturing imagery and the DJI Guidance proximity sensing system. It was necessary that the on-board lighting provided sufficient illumination for photogrammetry, but not so much that photos were overexposed. The lighting system also had to provide at least 10 lux for the Guidance visual positioning system (VPS) to detect obstacles underground. LED lighting systems from Lume Cube, Fire House Technology, and Stratus LEDs were tested underground in the 895-102 drift at the Barrick Golden Sunlight Mine with no other light sources present. Using a *Dr. Meter LX1330B* light meter, the lux provided by each lighting system was measured at varying distances from the face of an underground drift. A Leica laser distance measuring device was used to record the distance between the lights and the light meter positioned at the rock face. The Lume Cubes and Fire House Technology lights were measured at the highest brightness settings and two at a time to simulate use on the M100. A single Stratus LEDs light was tested with and without its parabolic reflector. The results of the lighting experiment are displayed in Table 2 and Figure 5.

Table 2. Measured lux of each lighting system at various distances underground using a *Dr. Meter LX1330B* light meter.

Distance at which lux was measured [m (ft)]	Lighting System (number of lights) and Measured Lux			
	Lume Cubes (2)	Fire House Tech. (2)	Stratus LEDs w/ reflector (1)	Stratus LEDs w/o reflector (1)
3 m (10 ft)	105	16	4500	550
7.5 m (25 ft)	18	3	1250	75
15 m (50 ft)	4	0.1	300	17
30 m (100 ft)	1	0.1	75	4

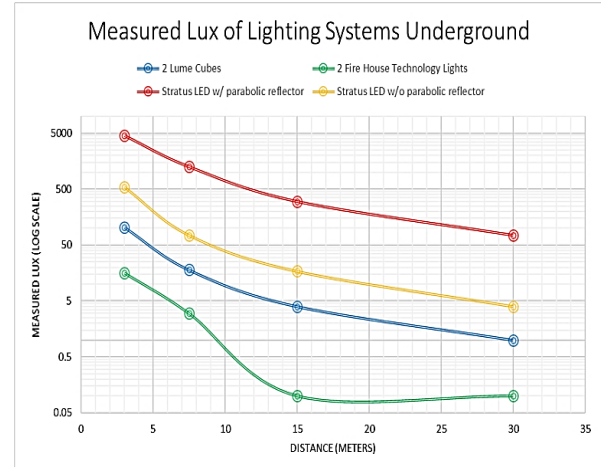


Figure 5. Comparison of the values of lux (lumens/m²) versus distance (m) for each lighting system.

Each of the light systems was tested on board the M100 to determine if the illumination was sufficient for capturing RGB (red, green, blue) imagery and for the Guidance VPS. Payload constraints limited the lighting to two directions: forward (for the benefit of capturing RGB imagery) and downward (for the downward-pointing Guidance VPS system sensor). It was found that the Guidance would not function at less than 105 lux when 3 m (10 ft) away from the rock face. The illumination allowed adequate imagery with the X3 camera.

For frontward illumination, the Lume Cubes and Fire House Technology LEDs were found to have both limited ranges and narrow beam widths when compared to a Stratus LEDs light with the parabolic reflector, as observable in Table 3. In the downward direction, the only system that could illuminate the ground surface sufficiently for the Guidance VPS to work was the Stratus LEDs lighting system used with a parabolic reflector. The parabolic reflector concentrates the beam angle of the light at 60-degrees, versus 170-degrees without the reflector; the smaller beam angle allows the light to be projected over a greater distance, creating a higher lux. When the parabolic reflector was removed, the M100 was able to use the Guidance VPS for positioning, but was limited to a flight ceiling of 6.7 m (22 ft) before the aircraft became unstable. Weight was a limiting factor with all the lighting systems, and the final design involved using a single 6S 3000mAh 25C LIPO battery (weight of 380 g) providing 10 minutes of lighting using the two Stratus LEDs lights and one parabolic reflector. This system provided a) forward illumination of 550 lux at a distance of 3 m (10 ft) from the rock surface and 105 lux at a distance of approximately 6.5 m (21 ft), allowing the forward VPS to operate at a distance of 6.5 m (21 ft) from the rock face with plenty of illumination for the imagery, and b) adequate illumination for the downward-pointing VPS to operate at a distance of 15 m (50 ft).

In order for the parabolic reflector to face downward from the arm of the UAV, longer legs were necessary, slightly increasing the mass of the unit. Longer legs can be purchased through DJI with a Zenmuse X5 Gimbal Mounting Kit but are not sold separately. As an alternative, custom carbon fiber legs were designed and constructed using automobile oil drain plugs to create the connectors to attach the legs to the UAV. The shock absorbing devices from the original DJI legs were attached to the bottom of the new legs.

The system designed for this research, shown in Figure 6, consisted of the M100 platform with a payload that included the DJI Guidance system, advanced flight battery (TB48D), the Zenmuse X3 digital camera, two Stratus LEDs ARM lights (one with a parabolic reflector), and a LIPO battery to power the lights. The M100 has a stated maximum takeoff mass of 3600 grams (DJI, 2016a), but the UAV was often flown in excess of this (Table 3) for flight times of up to 10 minutes. This was necessary due to the weight of the Stratus LEDs, the only tested lighting system able to provide sufficient illumination for photography and the Guidance system.



The following observations were made regarding the functioning of the DJI “Guidance” system:

- When lighting is sufficient and the Guidance system senses an object, a warning of the approximate distance from the object is transmitted to the UAV’s remote controller. The warnings display on top of the real-time imagery. When the UAV senses an obstacle at (or within) the minimum user-defined distance, the UAV stops and may even slightly drift away from the obstacle in the opposite direction of detection. The UAV will no longer allow the pilot to control *forward or backward* movement in the direction of the obstacle, until it is at the minimum distance from the obstacle. *This means that the pilot must back away at an angle.*
- If the visual sensing system is not able to detect an object due to darkness, it will drift toward that direction to avoid other obstacles. Since lux decreases with an increase in distance between the UAV-mounted light source and lit objects in a completely dark area, less lux is available for obstacle avoidance. In an attempt to avoid issues with uncontrollable drifting due to darkness, lights that greatly exceed the minimum lux requirements were chosen. As long as the UAV can sense the ground surface, it remains stable when hovering.

Figure 7 contains a photo of the M100 hovering with control underground. With the aid of on-board lighting, the Guidance system is detecting the ground surface and using it as a reference for remaining stationary in mid-air. Without illumination, the Guidance would not detect the ground, and the M100 would drift if not controlled by the pilot.

Table 3. Masses of the equipment used in this study.

Instrument (quantity)	Mass (g)
M100	1754
TB48D Battery (1)	677
Propellers (4)	72
Guidance	337
Zenmuse X3 Camera	221
Stratus LED ARM LEDs (2)	323
6S 3000mAh 25C LIPO Battery	380
Total mass of the UAV system	3764

Figure 7. The M100 hovering within the 895-102 intersection at GSM. The UAV is approximately 2.75 m (9 ft) above ground level. The blue light indicates that the downward-facing Guidance sensor is functioning properly and positioning the UAV.



2.2.2 Experiments to establish UAV's ability to provide adequate georeferenced underground imagery

After successfully assembling a UAV system with the lighting required for the DJI Guidance to function properly, several sets of experiments were conducted at GSM during spring and summer 2018 to establish the ability of the system to survive flights in inaccessible underground locations and to provide adequately lit, georeferenced imagery.

In terms of photogrammetry, georeferencing refers to assigning coordinates to points in images that have been surveyed on a specified coordinate system. By assigning the actual positions of the points on a coordinate system, the imagery is scaled to the actual life-size scale and oriented correctly in space. With a correctly-oriented life-size scaled 3D model, measurements can be taken on the 3D model and will represent the actual measurement, as if it were taken in the field.

Typically, surveyed control point markers or spray painted points (Figure 8, left) are used for assigning coordinates to points for creating absolute underground 3D models. It is good practice to spread the control points across different areas of the model. When control points are distributed throughout the model, distortion is reduced, providing a truer representation of the area being modeled. Spreading control points across an area that cannot be accessed is challenging, however, and may not be possible. In this project, a paintball gun (Figure 8, right) was used to make paint marks on the rock faces that were within the area to be modeled and also within line-of-sight (LOS) of the surveying equipment.



Figure 8. Left: Control points marked on the rib of the mine drift marked with spray paint (in red) and marked using a paintball gun (in yellow). Right: Graduate student Elizabeth Russell using the paintball gun to mark control points in areas that are out of reach.

The first set of experiments was conducted between January and March, 2018, with the ultimate goal of capturing imagery within an inaccessible stope. The imagery would be used to construct 3D models and allow geologic structures to be mapped, as described in Section 2. Ten underground flights were conducted at Barrick's Golden Sunlight Mine (GSM). Flights conducted underground at GSM followed these steps:

- A heading inspection was completed, and 5-point safety cards were reviewed. Scaling bars were used to remove any hazardous loose material around the draw point. Loose rocks on the sill were removed to create a level landing area.
- A paintball marker was used to establish ground control points in the stope and around the draw point (Figure 8, right). After using two survey control points to resection a total

station, the coordinates of the paintball marks were captured using reflectorless measurements. Figure 9 shows a total station set up at the entrance to a stope; it had to be positioned within line-of-sight of the survey control points and paintball marks within the stope. It was helpful to have one person illuminate the paintball marks with a powerful flashlight while another person measured them using the total station.

- The drone and lights were assembled and tested before flight.



Figure 9. Total station set up at the entrance to a stope.

Important lessons learned through experience included 1) allowing the equipment to equilibrate with ambient temperature before flying, as condensation can develop on the camera lenses, surveying equipment, and other gear due to temperature contrasts and/or high humidity, and 2) conducting short flights in accessible areas to ensure that everything is working properly before flying in inaccessible areas.

Initial flights in drifts and intersections tested the abilities of the Guidance and various lighting systems, as well as the ability of the captured imagery to be used for generating models. Prior to capturing data in an inaccessible underground stope, imagery was captured while flying the UAV in and out of line-of-sight (LOS). These flights were performed to confirm that the DJI Guidance system was functioning properly and to delineate the range of safe operations for collecting structural data on a UAV-based platform in the underground environment. Additionally, a handheld UAV imaging experiment was conducted in a drift at GSM to determine the preferred frame rate of image capture, file format in which the imagery is captured, and resolution at which the imagery is captured. It was concluded that for the underground imaging and in order to accomplish the project goals, a frame rate of 60 frames-per-second (fps), and a 1920 x 1080 resolution were appropriate. When flying out of LOS around the corner of an intersection of connecting drifts, the UAV reached a distance of about 38 m (125 ft.) out of the pilot's LOS with no observed communication errors between the UAV and the remote controller or the live-feed imagery. The 38 m distance was controlled by the space constraints (the end of the drift in which the UAV was flown) and not necessarily the maximum distance that could have been reached before the remote controller lost signal to the UAV.

After a number of successful flights had been logged underground and the preferred imaging format was determined, the UAV was flown in the "815-102" drift at GSM. The UAV was not flown out of LOS in this particular drift. The main goal of this flight was to capture overlapping imagery in an environment similar to the planned stope flight. The imagery was captured successfully, but there was one incident in which the behavior of the UAV did not correspond with the remote controller commands being given. The UAV was being drawn closer toward the rib, and it would not respond to attempts to direct it away from the rib for 15 seconds or so. The problem was not diagnosed, and was dismissed once the UAV responded to the remote controller again.

The overlapping imagery was used to create a model of the 815-102 drift to verify that underground UAV imagery can be used to create an adequate model that can be mapped; details are provided in Section 2. Other reasons for demonstrating the ability to successfully fly and collect data in drifts are a) the ability to inspect a drift after a blast where the ground is unsupported can be advantageous, and b) progressive models can be made with each new blasted portion of the advancing drift, serving as a record of the blasts and a tool to allow mapping of the geological and geotechnical features of the face.

After multiple flights indicated that payload and lighting systems were sufficient, the capabilities of the M100 were tested in a stope. The “NEV” stope was selected because it was available between blast and muck cycles, had three draw points to choose from, and contained muck piles angled toward the draw points that could potentially allow for recovery of the UAV if it crashed. The stope was 6 m (20 ft.) wide, 50 m (150 ft.) tall, and 120 m (400 ft.) long with its long axis oriented primarily east/west. Figure 10 shows the geometry of the stope as captured by multiple overlapping stationary LiDAR scans.

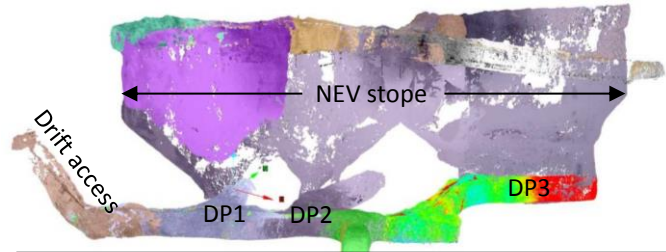


Figure 10. Side view of the NEV stope, including the access drift and the three draw point locations that can be used for access to the stope (B. Dale, GSM, modified).

The UAV was configured to collect video imagery in the stope in 1920 x 1080 resolution at 60 fps. The intended flight path was to enter the stope through draw point 1, cover the lower portion of the stope in an elliptical motion, and then to move up vertically to capture overlapping data with the same elliptical pattern. The initial portion of this spiral flight path worked well, but once the UAV was out of LOS, it became difficult to keep track of its position and orientation. Significant amounts of water dripping from above, along with a large amount of dust in one portion of the stope, contributed the difficulties. When the UAV flew east beyond LOS of the remote controller, contact with the aircraft and flight control was lost, confirming that flying outside LOS with the M100 was not an option with the current equipment. Fortunately, the pilot was able to move to a better vantage point at the draw point and after approximately 30 seconds, the UAV was located by using the downward facing light as a visual reference. The pilot regained control and continued to operate the UAV, occasionally moving the camera to capture more imagery while hovering. The M100 was then flown above the draw point, where its propellers displaced a large amount of dust. The dust blinded the forward-facing VPS on the Guidance, which resulted in the UAV flying towards the rib. The UAV failed to respond to the pilot's commands to direct it away from the rock face, and it impacted the rock and crashed. Fortunately, the M100 was recovered and repaired after the crash. Enough imagery was captured to the east, west, and above the first draw point to build an incomplete model of the western portion of the NEV stope, described in Section 2.

The first stope flight established the limitation of flying within LOS of the remote controller. Additional lessons learned included: 1) the need for redundant ground control points in the event that some of them are not captured in the imagery, 2) the difficulty in maintaining the position and orientation of the UAV while flying in a spiral path, 3) the difficulty in concentrating on capturing quality imagery while exploring and navigating, and 4) the need for a system to protect and recover the UAV in the event of a crash. Immediately implementable mitigations included adjusting the flight paths and acquiring a second remote control unit to allow a second operator to control the camera and collect imagery while the pilot navigates.

Adding electrical engineering undergraduate student Charlie Linney to the team allowed additional strides to be made. In addition to his technical background in electrical engineering and controls, Charlie is an avid and experienced drone pilot. He designed and constructed a custom drone using off-the-shelf components compatible with DJI controllers, to ease payload constraints. Appendix A contains a table listing the components and cost. This UAV, shown in Figure 11, is considered a quadcopter but has 8 motors and sets of propellers. Its payload capacity is huge for its size: it can lift 22 lb in addition to its own weight. To date, its use underground has been limited because the Black Widow UAV frame was larger than anticipated (1.2 m) so it does not fit into tight spaces, the relatively large cost of the propellers (nearly \$900 per set) makes crashing it expensive, and it does not have a built-in collision avoidance system. Electrical engineering graduate student Tyler Holliday has been working on developing a collision avoidance system under the direction of electrical engineering professor Bryce Hill. They have a working prototype that uses visual cameras and are very close to a system that also integrates ultrasonic sensors to provide a supplemental means of detecting and avoiding objects.



Figure 11. Left: Graduate student researcher Rachel Becker stands next to the DJI M100, while electrical engineering student Charles Linney stands by the custom drone he built for the project. Right: Black widow UAV. in flight underground at GSM.

The most significant resources that Charlie Linney brought to the team are his piloting skills. One of the basic things learned during this project is that, for almost every platform evaluated, having a skilled pilot is absolutely critical. With Charlie on board as a pilot, multiple successful underground flights were conducted at the Barrick Golden Sunlight Mine (GSM) between June and September, 2018. Video data were collected in mine drifts, stopes, and raises using various UAV platforms and piloting methods, described in detail elsewhere in this report. The majority of these flights used the M100 platform with on-board lighting systems for illumination, and were manually piloted. Charlie Linney has since graduated and was hired by Unmanned Aerial Systems, a Canadian company specializing in UAV-based underground inspections, one of the subcontractors who participated in the underground trials of the systems with enhanced navigation described in the Section 1B.

Due to the space constraints associated with UAV operation in an underground environment, no specific flight protocols (speed, elevation, flight path, etc.) were followed, and video data collection methods varied significantly depending on the flight location, UAV platform, and pilot preference. However, the invaluable experience gained during the underground flights resulted in the development of “best practices” recommendations for optimizing photogrammetric data collection underground; as Nicholas Rey of Flyability contributed to, compiled, and summarized these findings, they are discussed in the Flyability portion of Section 1B.

3.0 PROJECT COMPONENT #1B: Systems for Enhanced Navigation

Due to the difficulties of manually piloting a UAV underground and beyond visual line-of-sight, there is a need for UAVs with enhanced obstacle detection and avoidance capabilities. Some of the systems being developed utilize LiDAR-enabled simultaneous localization and mapping (SLAM) to navigate through confined, unknown environments. SLAM uses a LiDAR scanner to create a point cloud of the surrounding environment while also locating the position of the UAV within the point cloud. As the UAV travels through an area, the point cloud is updated and obstacles can often be detected on the fly.

Because of the high cost of SLAM-enabled UAV systems, a set of trials was designed for this investigation to test and compare different systems in an underground mine to determine the current state of technology. The purpose of the trials was also to collect photogrammetric data within inaccessible areas by utilizing a UAV platform that could safely navigate through the environment and return with useable data.

3.1 PC-1B Proof-of-Concept (Prototype) Technology Components

Four teams accepted the invitation to participate in the system demonstrations, designed to evaluate the performance of the UAV systems in inaccessible, underground environments: Emesent, Near Earth Autonomy, Inkonova, and Flyability.

3.1.1 Emesent

The team that formed Emesent originally worked with the CSIRO (Commonwealth Scientific and Industrial Research Organization) Data61 program of Australia to create and enhance autonomous robotic systems. They formed Emesent to continue with the development and commercialization of the Hovermap platform, a UAV with SLAM enabled obstacle sensing and avoidance capabilities designed to fly in inaccessible environments.

The Hovermap system includes an on-board, rotating Velodyne Puck Lite (VLP-16) LiDAR scanner that identifies when the UAV approaches obstacles without the need for additional lighting or cameras. The Hovermap payload is mounted on a DJI Wind 2 platform. The system can carry a payload of approximately 3 pounds, allowing for the addition of LED lights and cameras for obtaining photogrammetry imagery. The Hovermap platform utilizes SLAM for obstacle detection and avoidance using the on-board LiDAR scanner.

Emesent demonstrated two versions of the Hovermap platform - the *Standard* payload and the *Mining* payload (Figure 12). On the *Standard* payload, the Velodyne Puck Lite LiDAR scanner (VLP-16) is mounted beneath the center of the UAV, near the center of gravity. The VLP-16 has a range of 330 feet, and at that distance has an accuracy of +/- 1.2 inches. On the *Mining* payload, the scanner is still mounted beneath the UAV but it is oriented toward the front of the UAV rather than beneath the center. The orientation of the *Mining* payload allows the scanner to obtain a wider field of view and



Figure 12: Emesent's Hovermap *Mining* Payload (left) and *Standard* Payload (right).

detect the environment above the UAV. Compared to other systems, both payloads are unique in that the Velodyne is mounted to a detachable gimbal that rotates the LiDAR around a fixed axis. In combination with the rotation of the LiDAR within the Puck Lite housing, the rotating gimbal allows for Hovermap to capture data in all directions. Traditional fixed mounting of the Velodyne Puck Lite, as other teams utilized, only allows the LiDAR to capture 360° horizontal by 15° vertical fields of view (Velodyne, 2018).

The Hovermap is capable of flying using various flight modes. “Assisted Flight with Collision Avoidance” allows the pilot to manually fly the UAV with SLAM enabled obstacle detection activated. In this mode, the pilot is receiving live updates of how far the UAV is from an obstacle in all directions. The pilot can define an obstacle detection radius that actively prevents the UAV from colliding with any obstacles. The Hovermap can also be flown using “Waypoint Guided Mode”, in which the pilot defines waypoints based upon a point cloud and the Hovermap autonomously generates a flight path between points. There are two options within this mode—“Posemap” and “Tap-to-Fly”. In the “Posemap” option, a previously collected point cloud is used to plan the flight waypoints before the UAV takes off. This point cloud could be one that was collected on a previously flown assisted flight or from a stationary LiDAR scanner. In the “Tap-to-Fly” option, the waypoints are defined while the UAV is in flight based on the point cloud that is actively being generated. The point cloud is updated as the UAV progresses through the environment and is transmitted to the operator. Lastly, the team is working on developing a “Free Exploration Mode”, which would allow the UAV to explore an environment fully autonomously without a previous point cloud and without defined waypoints.

3.1.2 Near Earth Autonomy

Near Earth Autonomy, based in Pittsburgh, Pennsylvania, is focused on expanding the capabilities of autonomous flight of unmanned vehicles. Without specifically focusing on underground mining environments, Near Earth Autonomy has developed systems equipped for exploring caves, inspecting tunnels, mapping in GPS-denied environments, and more. They also have multiple contracts with the US military for developing autonomous aircraft.

The platform demonstrated by Near Earth Autonomy (Figure 13) includes an on-board, stationary Velodyne Puck Lite (VLP-16) LiDAR scanner mounted on the top of a DJI Matrice 100 with propeller guards. Because the LiDAR scanner is mounted to be stationary, the system builds a 2D map of the environment and is not equipped for vertical exploration.



Figure 13: Near Earth Autonomy’s UAV platform.

The platform is capable of two different flight modes including Piloted mode (P-mode) and Autonomous mode (F-mode). In P-mode, the pilot has full control of the UAV without the assistance of the obstacle detection and avoidance system. This mode is dominantly used for take-off and landing. In F-mode, the UAV explores an environment freely without a previously collected map and determines where to travel based on the location of holes in the map. Once an area is fully explored and there are no more holes, it will explore other areas that still need to be filled in.

3.1.3 Inkonova

Inkonova was founded in 2015 in Stockholm, Sweden, to build racing drones. The company is now focused on developing UAV technology for underground mining environments.

Inkonova's fleet of UAVs includes the Ranger (Figure 14, top), a commercially available and custom-built UAV designed for underground flights. The Ranger has the capacity to carry custom payloads such as a LiDAR scanner or camera. Time-of-flight sensors are located on the four sides and top of the UAV to aid in obstacle detection and avoidance. There are forward-facing, onboard LEDs that are sufficient for capturing imagery. FPV cameras are mounted to face forward, above, and below the UAV for the pilot to use in the case of flying with FPV goggles. The Ranger is designed to be flown manually by the pilot and does not have autonomous flight capabilities. The Batonomous unit (Figure 14, bottom) is a custom-built, semi-autonomous UAV with a stationary Velodyne Puck Lite (VLP-16) LiDAR scanner mounted on top. Similar to the Ranger, the Batonomous has time-of-flight sensors located on all four sides and the top of the UAV with forward-facing LEDs that are sufficient for capturing imagery.

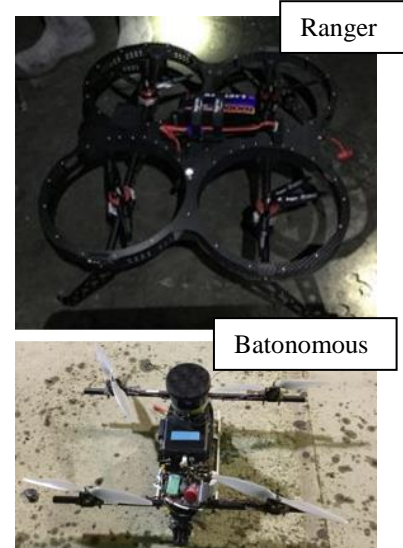


Figure 14: Inkonova's UAVs.

Both the Tilt Ranger and the Batonomous have a manual flight mode where the pilot is entirely in control of the UAV without the assistance of obstacle detection and avoidance. Both units can also be flown manually by the pilot with the obstacle detection and avoidance system enabled. The semi-autonomous capabilities of the Batonomous are displayed in Waypoint Navigation Mode, where the pilot uses a laptop to place waypoints based on the point cloud being generated by the LiDAR scanner on the UAV. The UAV builds a path based on the defined waypoints and the geometry of the region captured on the point cloud.

3.1.4 Flyability

Flyability, founded in Switzerland in 2014, develops inspection-oriented UAVs designed to safely operate in confined spaces and around people. Flyability's primary product, the Elios (Fig. 15), is a commercially-available UAV that is contained entirely within a spherical, carbon fiber cage. The drone and camera are mounted on a gimbal and are de-coupled from the cage. These components work in conjunction to help minimize the impact of a collision on the flight pattern and imagery of the UAV. The Elios is operated entirely manually by the pilot, but the durability and robustness of the platform allow for a less-experienced pilot to successfully fly the UAV without damage. Although there is no LiDAR system integrated for obstacle avoidance, there are two cameras mounted on-board including a 1080 HD camera and a non-radiometric FLIR thermal camera. The live video feed is transmitted back to the pilot for easier beyond visible line-of-sight (BVLOS) flight and is also recorded on an on-board SD memory card. The system contains adjustable LED lights that face forward, upward, and downward, and allows the pilot to adjust the lighting and camera parameters on the fly to achieve the appropriate exposure in the imagery based on the distance of the UAV away from the rock face.



Figure 15: Flyability's Elios.

3.2 PC-1B Proof-of-Concept (Prototype) Evaluation

Four teams accepted the invitation to participate in a demonstration of the abilities of their UAVs in inaccessible, underground environments. Each team visited Barrick's Golden Sunlight Mine near Whitehall, Montana, to test the capabilities of their systems in underground drifts, long hole stopes, and in some cases, ventilation raises. Teams were briefed on the flight conditions that could be expected underground beforehand and were given the prerogative to opt out of any trials deemed too risky for their technologies. There were several types of flights that each group was challenged to accomplish. The UAV trials were designed to start with the lowest risk and simplest scenarios and work up to the more risky and complex challenges. The trials included:

- Flights in the surface wash bay as a stope simulation
- Underground drift flights to test repeatability and precision
- Underground drift flight with obstacles for change detection analysis
- Underground drift flight out of line-of-sight
- Underground stope flights within and out of line-of-sight

The initial flights took place in the wash bay, a large surface facility used for washing heavy equipment (Figure 16, top left), providing a GPS-denied environment where the UAV could be recovered easily in the case of a crash. With the garage door lowered to a height that simulated a draw point, the UAVs could fly from outside the bay, through the opening made by the door, and into the bay. This trial simulated the flight pattern that would be used to fly into a stope underground.

Once underground, the team would complete multiple flights along the same section of a drift (Figure 16, top right), within line-of-sight (LOS). The duplicate flights were completed to demonstrate the repeatability of the flight and to allow for a comparison of the precision of the collected data, including visual imagery, thermal imagery, and LiDAR point clouds. Obstacles such as rocks, scaling bars, and cones were then placed throughout the drift. These flights were performed for comparison to the original flights and for using the resulting point clouds for change-detection analyses. The teams were then tasked with flying the UAV beyond visual line-of-sight (BVLOS), testing the ability of the UAV to detect and avoid obstacles as well as the ease of use of the system for the pilot when the UAV could not be seen.

If the team was satisfied with the performance of their systems, the next challenge was to fly the UAV in a stope (Figure 16, bottom left). These trials were significantly riskier because if the UAV crashed inside of the stope, there was a chance it would not be retrievable. The first flights within the stopes were kept within LOS. Not all teams chose to demonstrate their UAV in a stope. Finally, the teams were tasked with flying the UAV within a stope and BVLOS. Once again, this tested the obstacle detection and avoidance capabilities of the UAV and provided an opportunity to evaluate the quality of data that was returned from the flight. The ultimate goal of these trials is for the UAV to be flown with ease in underground environments such as stopes, so the successful completion of this step was a strong indicator of the technology readiness. If a team successfully completed all the previous trials, they had the option of attempting additional flights in other challenging areas of the mine including in a ventilation raise.

Survey control of the LiDAR and photogrammetry point clouds produced using data from these flights was achieved by two methods: co-registration with existing georeferenced point clouds or georeferencing ground control points (GCPs) in the form of 6" diameter foam balls (Figure 16,

bottom right) covered in 3M retro reflective tape that are surveyed in using a total station. Co-registration can be completed in commercial point cloud software such as Maptek I-Site Studio or 3DRecapture, or in freeware such as CloudCompare. Wooden dowels were used to place the reflective survey balls adjacent to the UAV's flight path in survey collars in the ribs that had been made for standard mine survey reflectors or that were created specifically for this project using a hammer drill. The positions were surveyed using a total station, providing the coordinates of these points. The reflective balls appear in the survey data as points that reflect 100% of the LiDAR's beams.



Figure 16. Top left: Surface wash bay flight. Top right: drift flight. Bottom left: stope flight. Bottom right: reflective ball.



3.2.1 Emesent Demonstration

The Emesent demonstration took place from 16-19 July 2018. The trial participants included Matt McKinnon, Stefan Hrabar, Farid Kendou, and Glenn Wagner along with Barrick and Montana Tech representatives Gerald Rosas, Mary MacLaughlin, Ryan Turner, and Rachel Becker. Observers during the trials included Beverly Hartline, Fred Hartline, Jennifer Fowler, Sam Kraha, Jeremy Crowley, Jesse Bunker, and Charlie Linney. Additional data were collected using Emesent's Hovermap payload on 10-11 September 2018.

The first flights occurred on the lawn above ground to test the equipment after shipment. The obstacle detection and collision avoidance system was initially demonstrated by flying around a large tree. The surface wash bay flights (Figure 17) were also completed successfully.

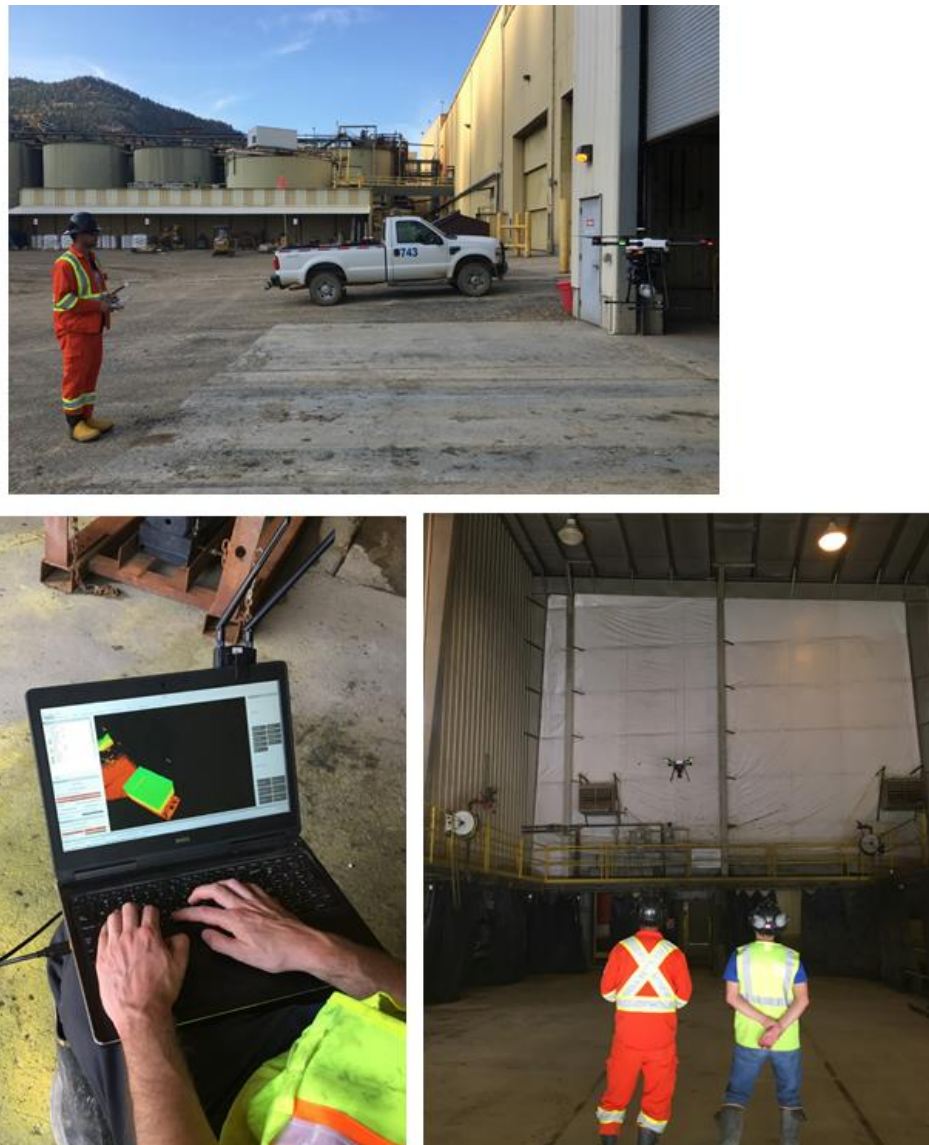


Figure 17. Top: Flying through the wash bay doors with the Emesent Standard payload to simulate entering a stope from a draw point. Bottom left: live view of the point cloud generated by the Hovermap system during a flight in the wash bay. Bottom right: looking into the wash bay while the Emesent Standard conducts its mission to explore the space.

The first flights underground were completed in the Lower SAM drift using the SLAM-assisted flight and tap-to-fly modes. As shown in Figure 18, the Lower SAM is a straight extent of the drift that approaches an intersection and curve at one end. These trials also demonstrated the obstacle detection and collision avoidance system by identifying and altering the flight path around a rope barricade across the end of the drift and a 0.5-inch diameter rope hanging from the back. Several flights were repeated along the same extent of the drift in order to complete a change detection analysis of the consistency of the data. These drift flights also included flights BVLOS, with a safety pilot following behind the UAV to take control if it started to fly off course. Additional drift flights were completed in the nearby 995-480 drift (Figure 18) where the team was not given a preview of the drift. The task was to explore the drift using just the UAV. This drift included flying past the inlet for a ventilation bag, where the air became turbulent. The majority of these flights were completed using the Hovermap *Mining* Payload, and each trial was completed successfully.

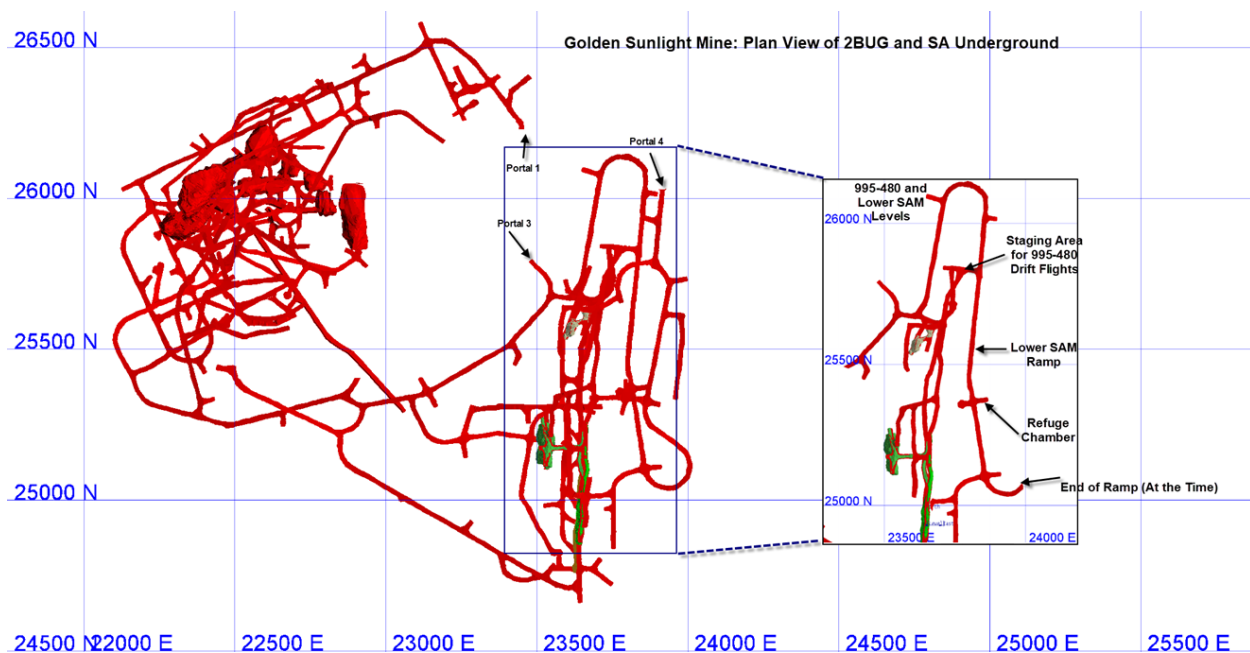


Figure 18. Plan map of the underground workings at the Barrick Golden Sunlight Mine, and the individual locations of flights conducted during the Emesent trials: the Lower SAM and 995-480 drifts. The mine grid units are in feet.

After several successful drift trials, the team confidently chose to fly from the draw point of the 102 stope, a large narrow-vein stope with entry-points at multiple levels, as seen in Figure 19. The flights were initially completed using the SLAM-assist and tap-to-fly flight modes. During one of the tap-to-fly flights, the flight controller malfunctioned on the Hovermap *Mining* Payload and the UAV crashed into the muckpile within the stope. Mine personnel are prohibited from entering the stope because the rock is not supported by rock bolts, however the UAV was able to be retrieved using blast pipe. The cause of the crash was determined to be from a lapse in communication from the DJI A3 flight controller on the UAV, and the team made adjustments so that error would not occur again, and multiple successful flights were conducted after the incident. In total, 28 successful flights were completed using the *Standard* Payload and 12 successful flights were made using the *Mining* Payload before the stope crash rendered it inoperable. The team successfully demonstrated the capabilities of the UAV in drifts and stopes beyond line of sight. Figure 20 contains additional photos taken during the Emesent trials.

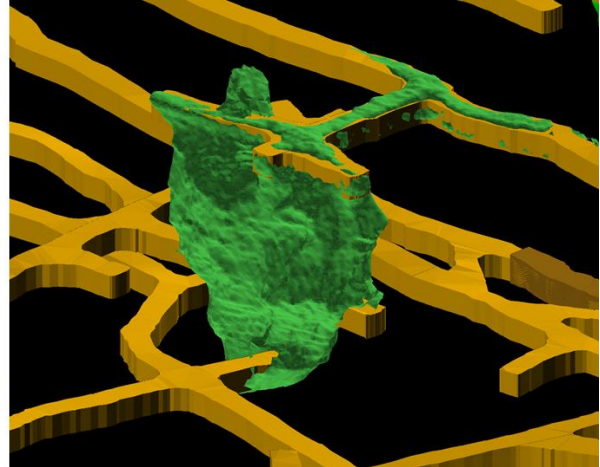
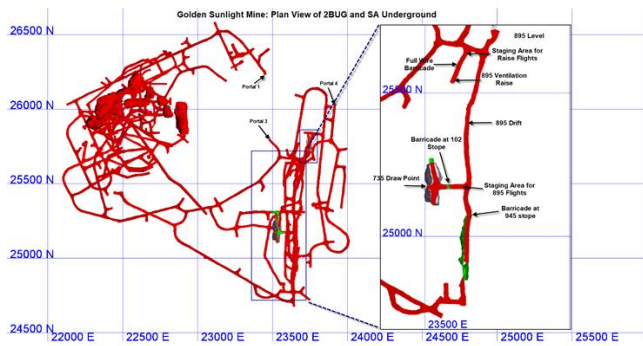


Figure 19: Left: plan map of underground workings at the Barrick Golden Sunlight Mine, highlighting the 895-level which was used for the 102 stope and 945 stope flights. Right: oblique view of a CMS scan of the 102 stope looking NE. The stope was accessed from the 895 level at the top and the 735 level at the bottom draw point (right).



Figure 20. Additional photos from the Emesent trials.

3.2.2 Near Earth Autonomy Demonstration

The Near Earth Autonomy demonstrations took place from 1-2 August 2018. The trial participants included Patrick DeFranco, David Murphy, and Ji Zhang along with Barrick and Montana Tech representatives Gerald Rosas, Mary MacLaughlin, Ryan Turner, and Rachel Becker. Observers during the trials included Steve Iverson, Bryce Hill, and Tyler Holliday.

With the team declining to fly above ground beforehand, the demonstrations began in the underground drift with a demonstration of the autonomous mode and LiDAR scan. Upon take-off, however, the UAV immediately began showing signs of malfunctioning: it entered into an uncontrolled yaw-spin in which it would start to rotate in place, accelerating until the UAV was manually landed. This problem has been observed in the past with Montana Tech's M100 and is attributed to the UAV approaching its maximum payload. At this point, one of the propeller motors stops receiving enough power to keep the UAV in flight and it begins to spin. To address the issue, the Near Earth Autonomy personnel removed all non-essential components of the payload including the small LED lights and the DJI Zenmuse X3, retaining a GoPro that could be used to collect imagery. Because no lights could be carried on the UAV, all lighting came from an external, handheld LED flashlight with a brightness of 13,000 lumens. Although several flights were successfully completed along the same drift segment, the UAV had repeated problems with clipping the rib near one specific location that coincided with a curve in the drift. The navigation problems could have been caused by a T2 electrical power box (Figure 21) located on the rib nearby, which may have been introducing magnetic interference to Near Earth Autonomy's onboard compass. Because of the repeated collisions in this area, most of the flights lasted between 1-3 minutes. Though the source of the issues was never verified, the team moved to a different drift that did not contain a power box to continue with the remaining trials.



Figure 21. T2 electrical power box (left) that may have been creating magnetic interference in the UAV compass (right).

The trials continued in the nearby 995-480 drift. The challenge in this location was to have the team fly the UAV down the drift without having any knowledge about the conditions beyond line of sight. The air inlet for a ventilation fan also created air turbulence near the take-off location, and the noise from the fan made audible communication difficult. The UAV was able to fly past the ventilation fan with only slight instability. The flights in this location lasted between

2-4 minutes and focused on the ability of the UAV to autonomously travel through unknown areas in exploration mode, shown in Figure 22. This flight would also demonstrate the flight BVLOS, because the safety pilot would only follow to intervene if the UAV went off course. The UAV flew down the center of the drift until it reached an intersection. It entered and scanned an unexplored area until the data collection was complete, upon which it retreated to the original drift and continued until the next intersection. When it reached the location in the drift that was blocked by active mining operations, it turned around and attempted to return to the take-off location. The UAV did have to be quickly landed after clipping the rib and was manually flown back to the starting location.

There continued to be some problems with the uncontrolled yaw spin and the UAV clipping the rib at corners, indicating that adjustments needed to be made for the distance of the obstacle avoidance bounding box. The battery also needed to be closely monitored to ensure that there was enough power to keep the UAV in flight without entering the yaw spin.

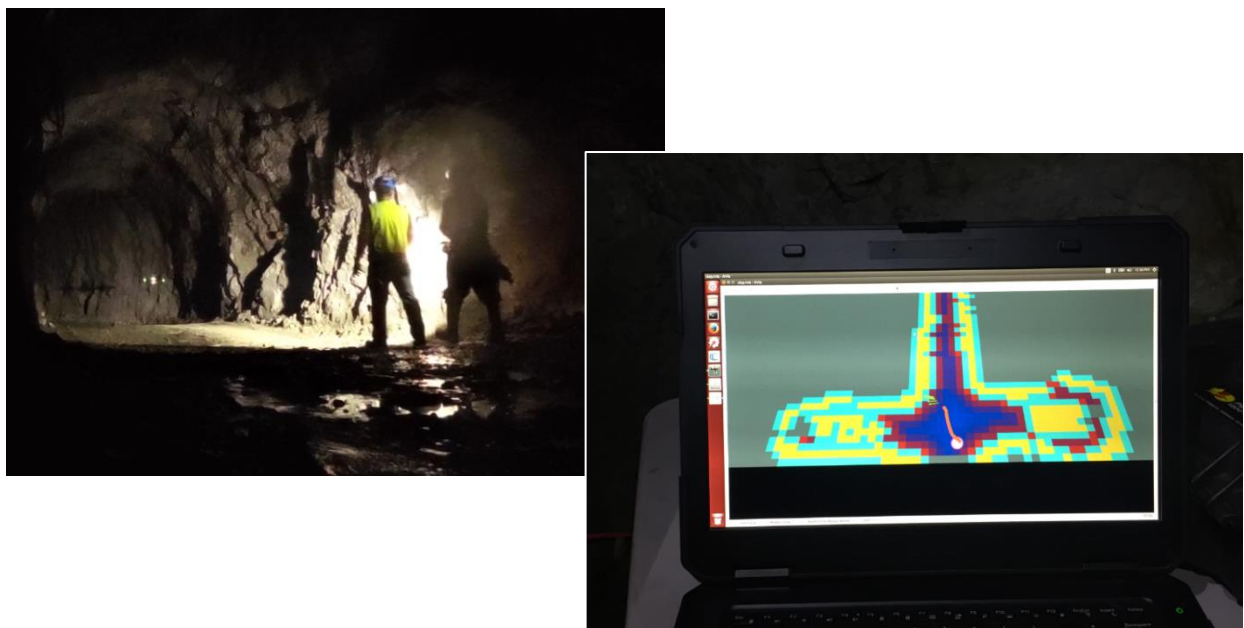


Figure 22. Left: UAV in exploration mode in 995-480 drift with safety pilot. Right: computer display during autonomous flight in exploration mode.

After facing numerous problems with flights in the underground, the team chose to attempt a demonstration of the exploration mode in the surface wash bay. The wash bay was used to simulate the stope environment by lowering the garage door, and in this instance, a truck was positioned inside the bay to serve as an added obstacle. Even with this obstacle, the UAV was able to immediately scan the entire wash bay from the entrance and did not enter the wash bay to attempt any further exploration because it had satisfied its task. The free exploration mode is entirely autonomous and does not allow the pilot to direct the UAV's flight path.

No further flights were completed but the UAV was used to gather more LiDAR point cloud scans underground. The UAV was carried from the 995 drift to the 895 drift on another level to test its ability to create maps with three dimensions. The UAV was also held near the 895-level entrance of the 945 stope to determine how much of the stope could be measured from the opening. Based on the results of the previous trials, the team opted to not participate in the stope or raise flight trials. There were 14 flights completed in underground drifts, however all but 5

flights ended in a collision or uncontrolled yaw spin. The team demonstrated flight beyond line of sight in a drift, however due to the high rate of collision, a safety pilot was always present.

Figure 23 contains additional photos from Near Earth Autonomy trials.



Figure 23. Top left: Flight in wash bay with pickup truck as obstacle. Top right: Flight in the Lower SAM near the T2 electrical box that was thought to cause issues with the UAVs compass. Bottom: Attendees of the Near Earth Autonomy trial.

3.2.3 Inkonova Demonstration

The Inkonova demonstrations took place from 26-27 August 2018. The trial participants included Alexandru Camil Muresan, José Manuel Castaño Dominguez, and José Maria Navarro along with Barrick and Montana Tech representatives Gerald Rosas, Mary MacLaughlin, Ryan Turner, and Rachel Becker. Observers during the trials included Iain Allen, Sean Warren, Charlie Linney, Joseph Bailey, and Deb Ross.

The first flights were completed in the surface wash bay to test the equipment after shipment. The demonstrations continued in the 895 drift, beginning with a demonstration of the semi-autonomous flight mode using the Batonomous. These flights accomplished several objectives including collecting LiDAR point clouds and photogrammetry data that could be used for change detection analysis, demonstrating obstacle avoidance, and flying BVLOS. The tap-to-fly mode was demonstrated in which the pilot would create waypoints on a laptop displaying the scan of the environment and the Batonomous would fly to the defined points. The Batonomous was manually flown during take-off until the connection with the laptop was verified and the point cloud was created. The pilot would then switch to the semi-autonomous tap-to-fly mode and control the horizontal position from the laptop. During the second flight with the Batonomous, the UAV briefly lost connection with the controller and landed beyond line-of-sight in the drift after successfully flying to the end of the drift. The UAV landed in a muddy puddle, and the electrical system was compromised. This was due to an error in the UAV's protocol for the situation in which connection with the controller is lost, and Inkonova has since corrected this issue. The damage to the Batonomous is shown in Figure 24. The Batonomous flights lasted between 2-3 minutes. The flights in the 895 drift were continued with the TILT Ranger. The objective of these flights was to collect repeated sets of photogrammetry imagery of the ribs for comparison. The obstacle detection and avoidance system was also demonstrated by holding obstacles in front of the UAV in each direction. The UAV would move away from the obstacles as they approached.

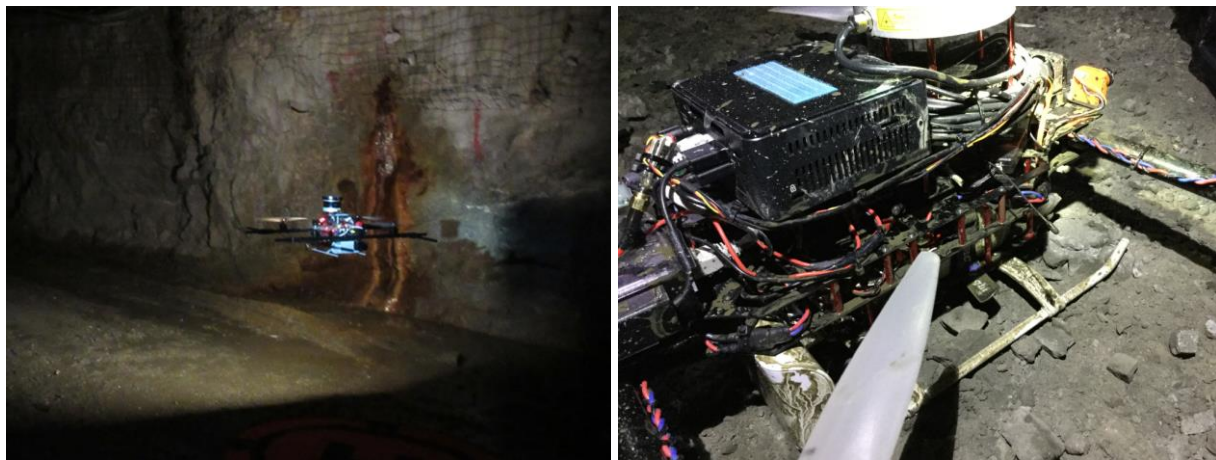


Figure 24. Left: Batonomous in flight underground. Right: Damage to the Batonomous after unexpectedly landing in a muddy puddle.

Due to the repeated success of the drift flights, the TILT Ranger was flown from the 750-level drawpoint of the 735 stope to collect photogrammetry data. These flights were also completed repeatedly to allow for full coverage of the stope. The flights started outside the drawpoint and captured the control points in the imagery before entering the stope. Each flight would focus on a

section of the rib at a time for the allotted flight time. No crashes occurred within the stope. There was some wear and tear noted on the propellers, shown in Figure 25, that was attributed to the amount of dust in the air during flight, however the propellers could quickly be replaced with new propellers. Where possible, the flight area was wetted down with a hose to minimize dust in the air that could limit the visibility on the imagery or damage the UAV. An additional flight was completed where the UAV was flown from the drawpoint of the 735 stope and around the corner opposite the stope into a drift. One rib was captured during the advance of the flight and the opposite rib was captured during the retreat.



Figure 25. Left: Flight conditions of the 735 stope. Right: damaged propellers from dust in the 735 stope.

The pilot flew both the Batonomous and TILT Ranger using first-person view (FPV) goggles (Figure 26) that showed live video footage from the UAV, so there was no safety pilot following the UAV. The UAVs maintained a less stable flight behavior, however the pilot indicated that the stability could be adjusted based on the preference of the user. With a history in drone racing, the pilot preferred the UAVs to fly differently than most less experienced users. This feature was not demonstrated.

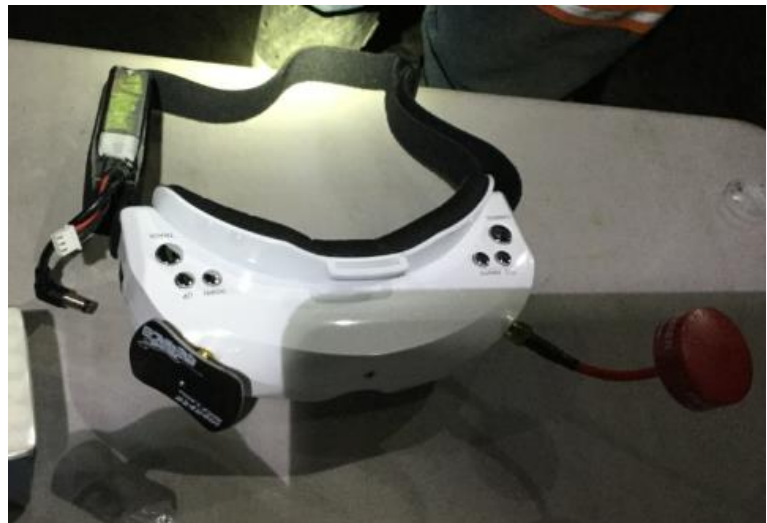


Figure 26. First-person view (FPV) goggles used by the pilot to fly the Batonomous and TILT Ranger beyond line-of-sight.

A total of 5 flights were completed with the Batonomous and 12 flights were completed with the TILT Ranger. In total, 12 flights were completed in underground drifts and 4 flights were completed in underground stopes. The unexpected landing of the Batonomous in a puddle was

the only crash that caused any damage to the UAVs. The team successfully demonstrated flight beyond line of sight in both drifts and stopes. Figure 27 contains photos from these trials.



Figure 27. Top: The Ranger in flight in the 735 stope. During this flight, the UAV was purposefully landed in the stope and then it continued its mission. Middle: The group in attendance during the Inkonova trial. Bottom left: Camil monitoring the Batonomous during “waypoint navigation” mode. Bottom right: screenshot of the Batonomous in flight during “waypoint navigation” mode.

3.2.4 Flyability Demonstration

The Flyability demonstrations took place from 13-14 September 2018. The trial participants included Matt McKinnon and Nicholas Rey, along with Barrick and Montana Tech representatives Mary MacLaughlin, Ryan Turner, and Rachel Becker. Observers during the trials included Steve Iverson and Charlie Linney.

Because the Elios was tested as a more affordable non-LiDAR based option, the trials were completed differently than for the other groups. The first flights were completed in the 895 underground drift, where it demonstrated its ease of flight, durability, and safety when bumping into objects. A camera located on the front of the Elios transmits video to the pilot during flight and records video for later use. The drift flights were completed to test different camera positions with relation to the ribs for obtaining the best photogrammetry imagery. The Elios was then flown from the 895 level of the 102 stope to investigate the drop raise and sill of the stope. The same stope was flown the next day after the drop raise was blasted on the night shift to collect video imagery of the results of the shot. Multiple flights were also completed in the 750 drift and the 735 stope in which the Elios was flown BVLOS to investigate the back, ribs, and around a corner within the stope. The stope flights were all completed successfully with no technical difficulties.

Based on the success of the stope flights, the team agreed to attempt to fly the Elios in a ventilation raise, where the strong and turbulent air and confined space would make it difficult for most UAVs to travel. The 895 ventilation raise extends approximately 115 feet, connecting two levels of the mine. The carbon fiber cage gave the Elios the unique ability to fly in such a tight space without the concerns for damaging the propellers or crashing that most UAVs would have. Figure 28 shows the Elios approaching the 895 ventilation raise.



Figure 28. Elios approaching 895 ventilation raise.

The Elios was also used to demonstrate its usefulness for reconnaissance in a mine rescue scenario. A “victim” sat against a rib out of line-of-sight of the starting location, as shown in Figure 29, and the pilot utilized the visual and thermal cameras to locate the “victim.” The pilot relied on the video transmitted from the UAV to manually identify the location of the mine personnel in an area that was hypothetically unsafe to travel on foot.

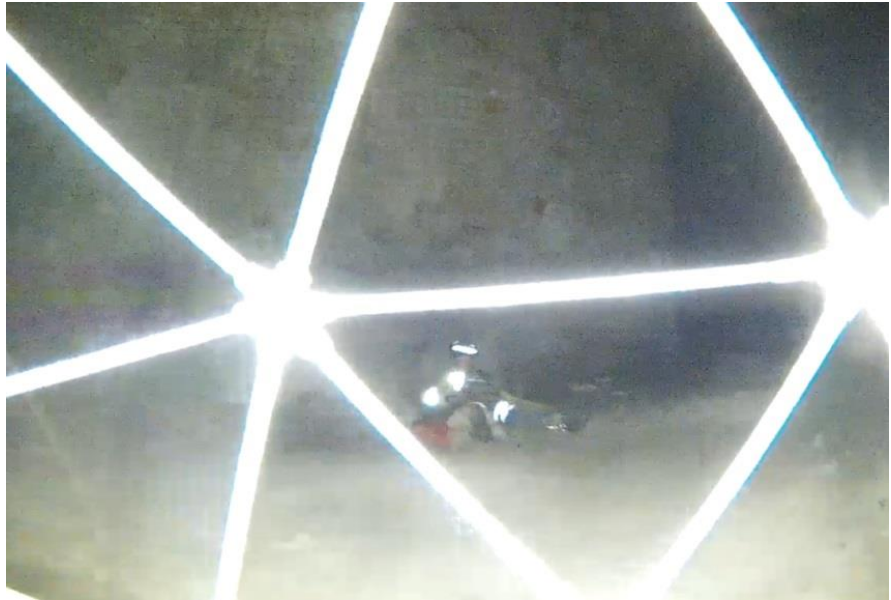


Figure 29: Elios in reconnaissance flight during mine rescue scenario.

A total of 18 flights were completed with the Elios including 6 underground drift flights, 10 underground stope flights, and 1 ventilation raise flight. There were no crashes that caused damage to the UAV. The team successfully flew beyond line of sight in the drift, stope, and ventilation raise. Figure 30 contains additional photos from these trials.

As mentioned at the end of Section 1, Nicholas Rey of Flyability contributed to, compiled, and summarized a set of “best practices” recommendations for optimizing photogrammetric data collection underground. These best practices are paraphrased as follows:

- 1) Use the UAV’s lighting system at its maximum available intensity.
- 2) Set the camera to auto-exposure mode. Correct the exposure in-flight as necessary using the “EV compensation” setting.
- 3) Avoid collisions; if a collision occurs, return to original flight path if possible.
- 4) Make *very slow* rotations and control camera pitch and drone yaw throughout.
- 5) Limit the camera pitch to avoid obstructions in the images.
- 6) Maintain visual continuity and avoid rapid, dramatic image changes. Enter confined spaces, raises, and stopes slowly to ensure adequate image overlap; if possible, orient the camera to capture continuous features (ceiling or floor).
- 7) If possible, maintain a consistent distance between the UAV and the imaging surface.
- 8) Orient UAV perpendicular to imaging surface during data collection.
- 9) “Close the loop” by following the same flight path/trajectory and maintaining the same camera orientation when revisiting previously imaged areas.
- 10) When mapping larger areas, “close the loop” by flying several lines in a grid pattern with at least 50% overlap.
- 11) If an area cannot be imaged in a single flight, connect multiple flights by obtaining repeat images of at least 3 locations captured in the previous flight; attempt to replicate the same flight path/trajectory and camera orientation used in the previous flight during subsequent flights (see No. 9 above).

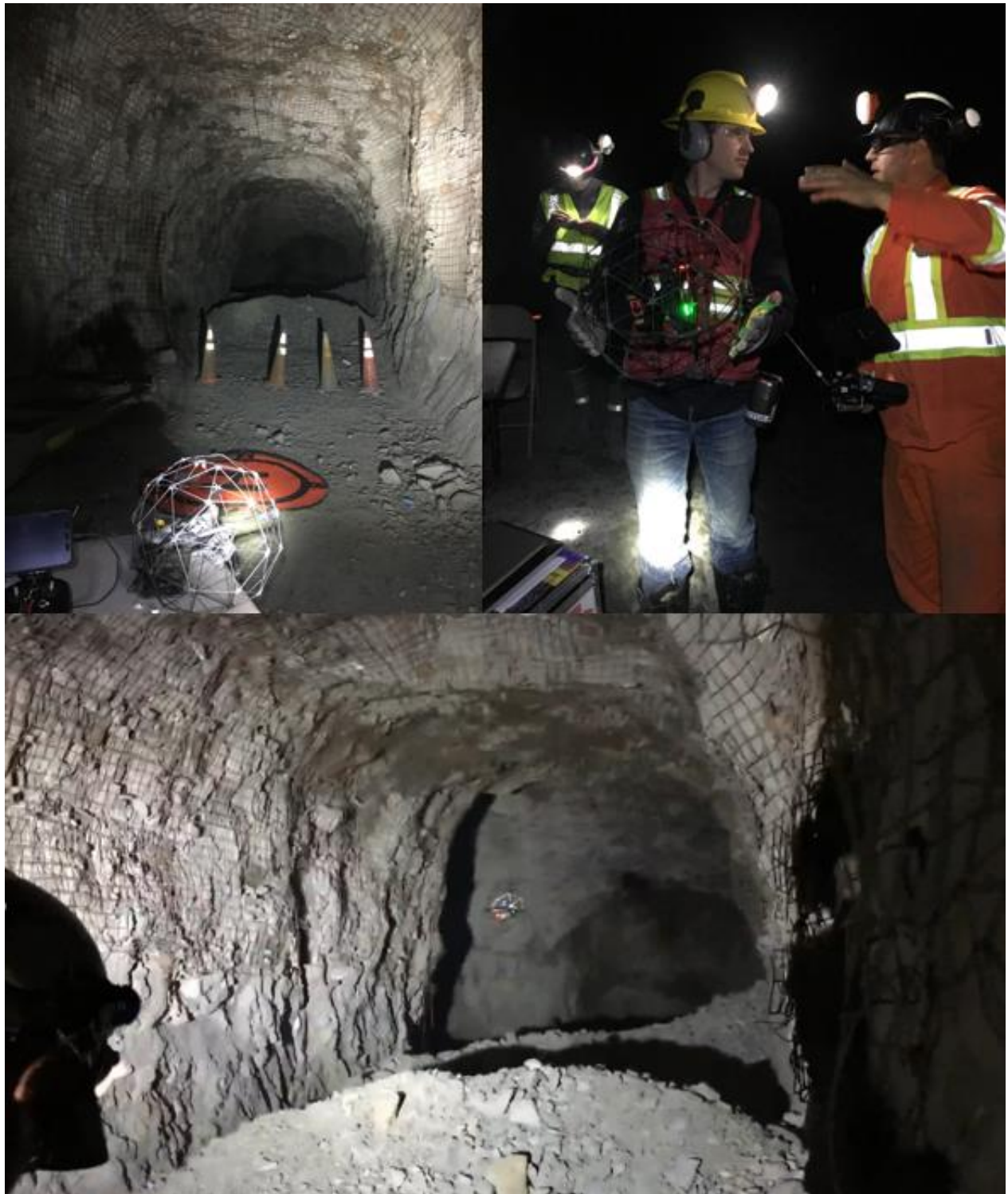


Figure 30. Top left: Elios before flying the top of the 102 stope. Top right: Pilots Matt MacKinnon (right) and Charles Linney (left) discuss flying the Elios. Bottom: The Elios in flight at the top of the 102 stope.

3.2.5 Summary of the Flights Associated with the Underground Trials

Throughout the underground UAV flight demonstrations, over 65 flights were completed in drifts, stopes, and raises. A summary table of the type of flights that were completed by each team is shown in Table 4. For a complete record containing details of each flight, refer to Appendix B. Emesent completed the most flights, attempting to fly in drifts and stopes both within and beyond line-of-sight. Inkonova mainly focused on completing drift flights, but several stope flights were successfully attempted beyond line-of-sight. The Elios was flown mostly within stopes, with an additional flight completed to explore a ventilation raise. The flights completed by Near Earth Autonomy were all located along a drift, and no stope flights were attempted. Emesent compiled a video summary of their experience at GSM and has posted it on the web: <https://www.youtube.com/watch?v=7c0wBgM2WU8&t=0s>.

Table 4: Summary of Flight Types for UAV Demonstrations.

	Emesent		Near Earth Autonomy	Inkonova		Flyability
	Standard Payload	Mining Payload	M2	Batomous	TILT Ranger	Elios
Surface Flights	3	0	0	1	0	0
Drift Flights	2	7	14	4	8	6
Stope Flights	7	2	0	0	4	10
Raise Flights	0	0	0	0	0	1

Each of the four teams successfully demonstrated UAV flight beyond visual line-of-sight (BVLOS) of the pilot. This was a critical task for the teams to complete because the main purpose of the enhanced navigation and obstacle avoidance systems is to allow for flight beyond where a pilot can easily fly the UAV manually. The systems are also designed to allow a less proficient pilot to successfully collect data in the difficult flight environment. Flying BVLOS is difficult due to numerous factors. The pilot is wholly dependent upon the onboard technology of the drone (obstacle detection, radio communication, live view from cameras, reliable battery life) and must navigate using the live view from the remote control only. Navigation using only the live view is a challenge for even experienced pilots because of the numerous obstacles underground that can be obscured by the darkness or from the limited field-of-view possessed by the onboard camera(s). The sharp corners and rapid changes in elevation underground make navigating BVLOS more difficult because radio communication and live video (analog or digital) between the remote control (RC) and UAV can quickly lapse or weaken. Operating BVLOS is a significant risk to the UAV and its payload, and is considered a technological hurdle in terms of UAV development as well as a significant challenge for pilots.

The results of these trials included a great wealth of knowledge gained by the trial hosts, participants, and observers. One of the positive side effects of inviting the four teams to participate in the demonstrations was creating an open channel of communication for discussing the needs of underground mines for UAV platforms directly with the system developers. Many of the teams had not had many previous opportunities to test their technology in the intended

operational environment. The teams acknowledged that they garnered a clearer understanding of the improvements that they need to continue making on the UAV platforms.

Despite some initial resistance to the new technology, the mine shifters quickly became interested in the potential applications for using the UAVs to collect data that they typically cannot obtain. There were several instances of the mine shifters actively seeking out the underground flight participants to conduct flights in specific areas where they needed to better understand the conditions for normal mine operations. The UAVs were not only used for the LiDAR point cloud data or photogrammetry applications; the video footage also provided invaluable information for the mine engineers to get a better view of the rock behavior within the stopes.

A variety of observers attended the underground trials, allowing new connections to be made and established connections to be deepened. Montana Tech observers included representatives from the departments of Electrical Engineering and Environmental Engineering, and the Montana Bureau of Mines and Geology, along with the Vice Chancellor for Research and Graduate Studies. Personnel representing the NIOSH Spokane Research Center observed most of the trials, as did personnel from the Montana Space Grant Consortium. Barrick personnel organized a workshop held in Winnemucca, Nevada, on 25-26 October 2018 to share results of the research.

- On Wednesday, 24 October 2018, Barrick employees from Turquoise Ridge Mine and Golden Sunlight Mine, MT, in conjunction with University of Nevada, Reno (UNR) and Montana Tech STEM students, met at the Boys and Girls Club in Winnemucca, Nevada, to discuss the current state of autonomous UAV technology available for use underground. Ryan Turner and Rachel Becker, respectively from Barrick Golden Sunlight Mine and Montana Tech presented on the results of the drone trials conducted during the summer months of 2018. Drone researchers from UNR presented on their research, and vendors from Unmanned Aerial Services and Robotics Centre were available to answer questions from Barrick mine personnel. Following the meeting, Andy Sholty from Barrick's Turquoise Ridge Mine organized a hands-on learning experience for students attending the Winnemucca Boys & Girls Club with drones and thermal cameras. Pilots Matt MacKinnon and Charles Linney from Unmanned Aerial Services flew their professional drones for the students, and helped them to learn how operate hobby-scale drones.
- On Thursday, 25 October 2018, attendees of the previous day's meeting met at the Turquoise Ridge Mine outside Winnemucca. Mine personnel and guests took a shaft underground and observed as Unmanned Aerial Services demonstrated the use of the Emesent and Flyability UAVs. The first flights were completed in underground haulage ramps and headings using the Emesent Hovermap system (Figure 31, top left) and the Flyability Elios system. Mine personnel were given the opportunity to learn how to fly the Elios for themselves (Figure 31, top right). UNR researchers demonstrated their prototype UAV on the haulage ramp and heading as well. The final flight of the day was completed by the Elios up a 3-ft. diameter, 400 ft. long aggregate raise (Figure 31, bottom). The workshop was considered a success because it demonstrated the current state of technology for autonomous UAVs underground and it created discussion in terms of where the technology is headed in the future.



Figure 31. Top left: Emesent Hovermap in drift flight. Top right: Mine personnel operating Flyability Elios. Bottom: Flyability Elios in aggregate raise.

4.0 PROJECT COMPONENT #2: Photogrammetric Modeling

Photogrammetry is a science that uses two-dimensional (2D) overlapping imagery to resolve three-dimensional (3D) locations of the object(s) being captured (Adam Technology, 2010). Using photogrammetric techniques, two images with significant overlap horizontally and vertically, called stereopairs, can be used to recover 3D data that are lost in 2D images. The imaging device receives light bouncing off of the object through its lens to the sensor (Figure 32, left). At that point the origin of the light reflecting onto the sensor is unknown. When another image is captured from a different location and light is received through the lens and onto the second sensor from the same location, a unique 3D location can be determined. The 3D location is where the light rays from the two different camera positions intersect. In Figure 32 (right), small uncertainty in the position of the image on the sensors translates to an error ellipse created between the two light paths, colored orange in the diagram. The accuracy of photogrammetry is highly configurable, in theory. Higher accuracy can be achieved by increasing the base (distance between images) to distance (distance to the object) ratio, making the error ellipse more circular. Accuracy also increases with smaller ground pixel sizes, reducing the uncertainty in the position on the sensors and consequently reducing the size of the error ellipse. Photogrammetric accuracy is more difficult to configure when using UAV imagery as compared to terrestrial imagery because the imaging device's base-to-distance ratio is not as precisely controllable.

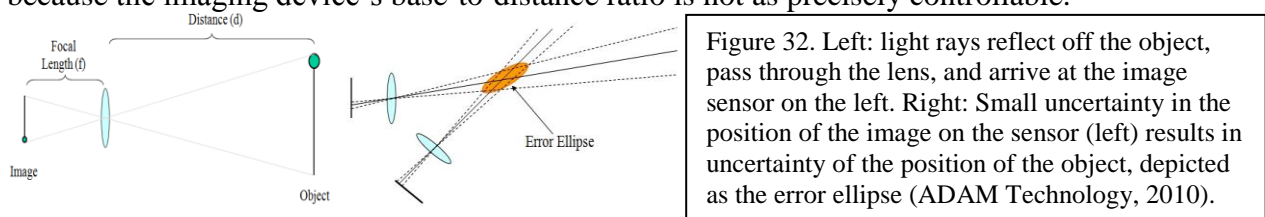


Figure 32. Left: light rays reflect off the object, pass through the lens, and arrive at the image sensor on the left. Right: Small uncertainty in the position of the image on the sensor (left) results in uncertainty of the position of the object, depicted as the error ellipse (ADAM Technology, 2010).

Improvements in photogrammetry modeling software and UAV-based video data acquisition platforms over the past decade have allowed photogrammetric modeling to emerge as an increasingly powerful tool for geotechnical investigations. With surveyed ground control points and a complete digital photo set, most commercially available photogrammetry software packages are capable of generating a georeferenced point cloud and 3D mesh to permit visual inspection of 3D rendered surfaces and accurate post-processing spatial analysis, including volumetric comparisons and software-assisted structural mapping. Digital photogrammetry offers some practical advantages over traditional terrestrial or UAV-based LiDAR scanning, including relatively low implementation costs and the ability to confirm data quality in the field by observing live video feed during imaging. However, the effects of conventional video data collection challenges and processing limitations are amplified in the underground operational environment; UAV-based digital video acquisition requires high-lumen output onboard lighting for illumination, and under/overexposure, camera obstructions, dust, turbulence, prop wash, and water can all adversely affect image quality. Furthermore, overlapping oblique, overhead, and downward-facing camera orientations must be obtained from a spatially-consistent perspective roughly perpendicular to the imaging surface. Poor image quality and/or loss of visual continuity (such as can occur during UAV rotation) can result in holes (void space), artifacts, and/or distortion in the rendered models.

For the purpose of this research, a distinction is made between two terms that are often used interchangeably. The term “modeling” refers to the process of creating a 3D surface of the area being captured. The term “mapping” is reserved for the process of identifying geologic features and assigning 3D quantitative values to geological data present within the model.

4.1 PC-2 Proof-of-Concept (Prototype) Technology Components

The steps involved in creating 3D photogrammetric models include capturing imagery, loading the imagery into a photogrammetry software package, specifying processing parameters within the software, and processing the imagery. The basic outputs across all software packages include a digital point cloud, exportable as interoperable LAS, LAZ, PLY and/or XYZ files, and a textured 3D polygon mesh generated from the point cloud data, exportable as interoperable PLY, FBX, DXF, and/or OBJ files. Proprietary post-processing features – including (but not limited to) point cloud densification and editing tools, orthomosaic or digital surface model (DSM) generation, georeferencing/scale constraint calibration, and quality reporting parameters – differed between software packages.

This section focuses on the photogrammetry software, since almost all of the image-capturing devices were described in other sections of this report and computers available for processing, which can include cloud-based processing with a variety of cost structures, differ greatly. The system requirements for photogrammetry processing vary depending on the computational demands of the project and the performance demands of the user; for example, a large project with high-resolution imagery (ex. 500 – 2000 images at 14 MP) will require greater system resources than a project with fewer images and/or lower resolution imagery, and processing time can vary considerably between different computer systems. It should be noted that, regardless of project size, the computing demands of photogrammetry modeling are significant for most systems; computing resources must be fully dedicated to the software for the duration of processing activities, and multitasking on the system is generally ill-advised for all but the most powerful computer platforms. Appendix C contains the specifications of the computers used for image processing during this study).

When the proposal for this project was submitted, it was anticipated that ADAM Technology's 3DM Analysis Suite software would be used for the digital photogrammetry processing. ADAM Technology (www.adamtech.com.au) is headquartered in Perth, Australia. ADAM Technology's software is widely used in the mining industry for terrestrial photogrammetry and is known for providing high quality submillimeter accuracy with proper imagery and calibration; the software is available at Montana Tech and Barrick's GSM, and the project participants are experienced 3DM users. When initial attempts to create models with the underground imagery were unsuccessful due to space constraints and the difficulty in selecting imagery from ideal positions, alternative software packages were explored. More recently developed photogrammetry software are available that are based on algorithms more suited for drone-based imagery sets containing large numbers of images not necessarily from ideal positions. A number of software packages were evaluated and three were selected for use in this project: Agisoft PhotoScan Professional (v1.4.5), Bentley ContextCapture (v4.4.8.561), and Pix4Dmapper (v4.3.31).

- Agisoft (www.agisoft.com) is a computer vision technology company based in Russia. Founded in 2006, the company developed the standalone PhotoScan software product line dedicated to 3D reconstruction, visualization, surveying and mapping tasks. NIOSH Spokane Research Center researcher Steve Iverson recommended Agisoft PhotoScan based on his observations that it is less-time intensive and more cost-effective than other software, and does not rely upon the use of panoramic tripod heads and multiple camera stations; he also had success using Agisoft PhotoScan to build 3D models with thermal images. The online retail cost for a single node-locked (1 device) Professional Edition license is \$3499 (all costs USD), while an educational license is available to qualified

users for \$549 (January 2019 pricing). A newly released free update for licensed PhotoScan users (Agisoft Metashape) offers improved photogrammetry processing capabilities. Photoscan Professional/Metashape supports cloud-based processing.

- Bentley Systems (www.bentley.com) is a global industry software provider headquartered in Pennsylvania. The company acquires, develops, and licenses software products for a wide range of industrial and commercial applications. The reality modeling software ContextCapture is produced by Acute3D, a French company acquired by Bentley Systems in 2015. The ContextCapture platform emphasizes hybrid processing capabilities, whereby photogrammetry point clouds can be supplemented with laser scanning data. The ContextCapture software is widely used in the mining industry and was specifically recommended by colleagues at Kennecott based on its ability to generate 3D point clouds and meshes from video imagery. Bentley Systems offers a range of Context Capture software licensing options for professional and commercial users. An educational license is available to qualified users for \$200 per licensed device, with a minimum purchase requirement of ten licenses (serves ten individual users). Acute3D viewer (www.acute3d.com), a free downloadable application provided by Bentley Systems/Acute3D, allows non-licensed users to view models generated in ContextCapture.
- Pix4D (www.pix4d.com) is a popular global photogrammetry software company headquartered in Switzerland. The company was formed in 2011 as a spinoff of the École Polytechnique Fédérale de Lausanne (EPFL) Computer Vision Lab. The Pix4Dmapper photogrammetry software platform provides integrated survey-grade photogrammetry, 3D modeling, and DSM/DTM generation capabilities. The online retail cost for a single perpetual license for Pix4dmapper is \$4990; a perpetual (educational) classroom license allowing 25 concurrent uses is available for \$6700, and a variety of other subscription and specialized licensing options are available for qualified users. In addition to Pix4Dmapper, Pix4D produces photogrammetry products specialized for the construction and agricultural industries (Pix4Dbin and Pix4Dfields, respectively) and manufacturers the Sequoia multispectral camera.

These respective software packages rely on proprietary algorithms to process digital images into 3D spatial data (point clouds and textured polygonal models). While the programs differ in user interface, processing methods, and output format, their functional application and rendering capabilities are comparable, enabling qualitative side-by-side comparisons of models between platforms. Each software program was also evaluated independently to gauge the sensitivity of model outputs to parameterization and to optimize processing parameters.

None of the three software packages contain “mapping” features that allow the user to capture and digitize geological structures, but Agisoft PhotoScan does allow the user to export the model in formats that can be read by software packages that do have these features: ADAMTech’s 3DM (<https://www.adamtech.com.au/3dm/Analyst.html>), Split Engineering’s Split-FX (<https://www.spliteng.com/products/split-fx-software/>), and the public domain program CloudCompare (<http://cloudcompare.org/>) with the Compass mapping plugin. The mapping component of this project incorporated use of 3DM and Split-FX, and CloudCompare was used for a variety of tasks throughout the project, including georeferencing, co-registration, transformations, and change detection.

4.2 PC-2 Proof-of-Concept (Prototype) Evaluation

Three sets of experiments were conducted to investigate and evaluate the performance of the different software packages and the quality of the 3D models produced:

- A surface (non-underground) pilot study to quantitatively compare the accuracy of the 3D models produced by the software was conducted using imagery collected at Notchbottom.
- A preliminary study to evaluate the ability of the software to create models that could be used to perform joint mapping was conducted using imagery collected underground at Barrick's Golden Sunlight Mine (GSM).
- Further investigation to evaluate the ability of the software to produce quality models was conducted using imagery collected underground at GSM by the M100/X3 and more sophisticated systems with enhanced navigation capabilities.

For each of these studies, initial model processing work flow required digital still photos (.jpg or .tif format) to be extracted from high-definition (HD) RGB video (4k, 1920x1080 or 1280x720 pixels) in .mp4 or .avi format. This was typically accomplished using the photo extraction utilities included in each of the photogrammetry software programs. Video imagery was acquired at a frame rate of ~30 frames per second using the available onboard UAV camera or accessory camera systems (DJI Zenmuse X3 and GoPro Hero 4), and still images were extracted every 10 to 30 frames (1 to 3 frames per second). The resulting photo set was typically processed without editing; however, severely under- or over-exposed images or excessive duplicate still images were generally removed from the photo set to improve processing speed and quality.

4.2.1 Quantitative study on the surface (Notchbottom)

Based on a study similar to one conducted as part of the GoldenRocks ARMA conference in 2006 (as described in Tonon and Kottenstette, 2006), a trial was completed above ground to compare the quality of three different photogrammetry software packages: Bentley ContextCapture, Agisoft Photoscan, and Pix4Dmapper. An outcrop near the Notchbottom fishing access southeast of Glen, Montana, was selected as the location of the trial (Figure 33). This outcrop is referred to as the 'Notchbottom outcrop' based on its proximity to the fishing access site. The Notchbottom outcrop is composed of Permian to Mississippian-aged Quartzite (USGS, 1993) and is approximately 50 feet tall and 200 feet wide. The rock mass has many overlapping joint sets that create a blocky appearance, providing adequate relief and texture to build a photogrammetry model.

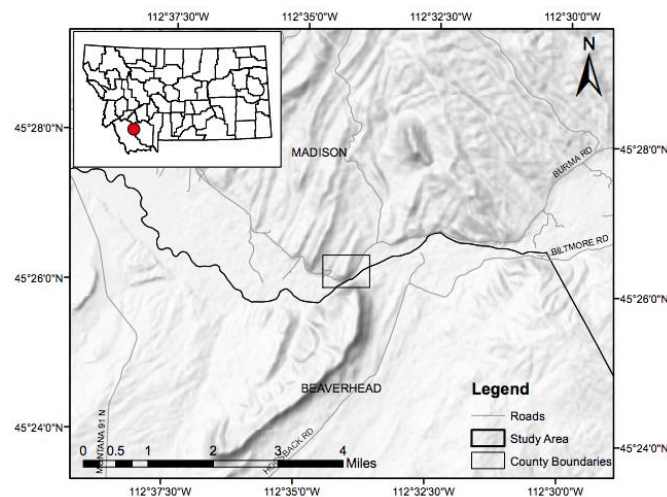


Figure 33: Location map of the study area located southeast of Glen, Montana, near the Notchbottom fishing access site.

The data for this study were collected during two site visits on 15 February 2018 and 1 March 2018. Each of the site visits lasted approximately 4-5 hours and included surveying the control points, taking manual geotechnical measurements including descriptions of discontinuities, and

multiple UAV flights to collect video imagery of the site. The site visits were both made on days with overcast weather so that variation in the imagery caused by shadows could be minimized.

A set of nine control points was marked and surveyed on the outcrop before the UAV flight so that the points would be included in the video imagery. The points were marked for identification using either small targets or spray paint on the rock outcrop. The location of the surveyed points is shown in Figure 34. A Leica TS 11 was used to resection the points using two benchmark locations. The TS 11 located its position in space based on the angles between it and the established benchmarks. Once this resection was complete, the relative coordinates of the nine control points were measured.

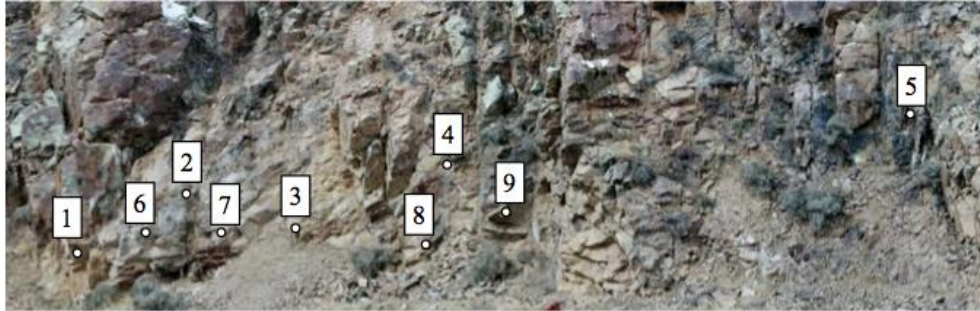


Figure 34: Location of control points and check points marked on the Notchbottom outcrop.

A DJI Phantom 4 Pro UAV was manually flown in horizontal strips across the outcrop to collect video imagery. At the end of a horizontal strip, the UAV was flown upward to reach approximately 50% overlap with the previous strip before being flown in a horizontal strip in the opposite direction. This was repeated from the bottom to the top of the outcrop. A photoset totaling 236 photos was extracted from the flight video using Bentley ContextCapture at a rate of one photo every two seconds. Any images captured before or after the flight were removed from the photoset, however no post-processing was applied to the images.

The photoset was brought in to each of the three photogrammetry software packages. A point cloud and a mesh were generated using each of the software packages, and the resulting meshes are shown in Figure 35 (left). As shown, each of the software packages created a mesh with adequate quality for further analysis. There are some holes in each of the models where the UAV flight did not cover all angles of a feature, however the holes are minimal and generally do not impact the effectiveness of using the model for an analysis.

A close-up view of each of the meshes is provided in Figure 35 (right). The mesh generated by Bentley ContextCapture (Figure 35.A) has the greatest resolution and retains the most detail when viewed closely. The Pix4Dmapper mesh (Figure 35.B) has a moderate resolution, however it begins to lose some of its detail up-close. Lastly, the Agisoft PhotoScan mesh (Figure 35.C) has the lowest resolution and loses its fine detail. The shape and structure of the rock is visible in each of the models, however the level of detail when examined closely widely varies.

Five of the surveyed points (1-5 in Figure 34) were used as control points to build the georeferenced point cloud by locating the point in at least three photos, tagging it, and assigning its measured coordinate values. The remaining four points (6-9 in Figure 34) were used as check points to validate the accuracy of the point cloud. The coordinate values of the check points in the model were compared to the known coordinate values from the survey. The error in the check points was calculated by finding the difference in the X, Y, and Z direction as well as the

3-dimensional distance between the coordinates of each point in the model and the coordinates from the survey. This 3D distance is found by taking the square root of the sum of the squares of the coordinate error values. Table 5 includes a summary of the average 3D distance, the maximum error in any direction, and the minimum error in any direction for both the control points and check points in each of the three software packages.

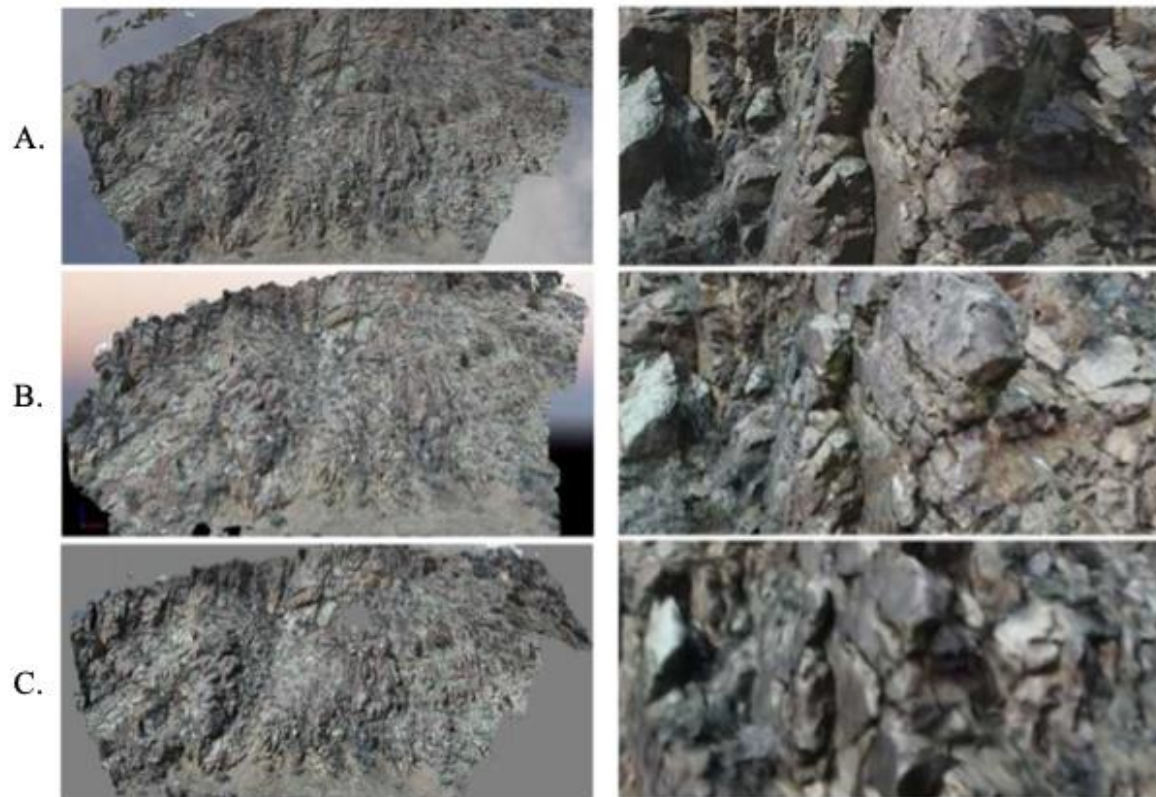


Figure 35: Generated mesh of outcrop using Bentley ContextCapture (A), Pix4Dmapper (B), and Agisoft PhotoScan (C). Left: entire outcrop. Right: magnified view of a portion of the outcrop.

Based on the average 3D distances shown in Table 5, the Bentley ContextCapture model had the smallest error in the control points (0.0089 ft) and the Pix4Dmapper model had the smallest error in the check points (0.0506 ft). Because the control points are used to build the georeferenced model, it was expected that the control points would have less error than the check points. While the models built using ContextCapture and Pix4Dmapper both showed this expected result, the Agisoft PhotoScan model displayed greater error in the control points (0.1056 ft) than the check points (0.0703 ft). Although all three software packages built reasonably accurate and usable models, the Bentley ContextCapture model also retained the highest resolution when viewed up close and was judged to have produced the most effective models for geotechnical analysis.

Table 5: Average, Maximum, and Minimum Error Values for the Notchbottom study.

	Software	Average 3D Distance (ft)	Max. Error (ft)	Min. Error (ft)
Control Points	Bentley CC	0.0089	0.0130	0.0010
	Pix4D	0.0206	0.0250	0.0000
	Agisoft	0.1056	0.1860	0.0030
Check Points	Bentley CC	0.1219	0.1330	0.0040
	Pix4D	0.0506	0.0740	0.0010
	Agisoft	0.0703	0.0840	0.0000

4.2.2 Creation of 3D models to be used for geological/geotechnical mapping (GSM)

One of the goals of this research was to evaluate the ability of the photogrammetry software packages to create models that could be used to perform joint mapping. To investigate this, imagery was collected underground at Barrick's Golden Sunlight Mine (GSM) during February and March, 2018. Using imagery collected during flights in the 815-102 drift and the NEV stope, models were constructed using two different sets of software for comparison:

- Adam Technology's 3DM CalibCam, DTM Generator, and 3DM Analyst
- Bentley's ContextCapture, Agisoft PhotoScan and Split Engineering's Split-FX

Both software packages used for data processing provide the option to run the model as a controlled model, defined by georeferenced or defined control points, or as a relative model, defined by matching points that the software finds in multiple images. For this project, the models of the 815-102 drift were constructed as relative models, while the NEV stope models were constructed with a georeferenced orientation on the local mine coordinate system. Georeferenced models, also referred to as absolute models, are scaled and oriented correctly with respect to the real world.

Models of the 815-102 drift were successfully built and mapped using both sets of software. Figure 36 shows the model produced by the 3DM software along with the mapped structures (rock joints), and Figure 37 contains the mapped joint data presented on a stereonet. In ADAM Technology's software suite, 3DM CalibCam program is used to build 3D point clouds, meshes, and surfaces. The DTM Generator first generates sections of digital terrain models (DTMs) using the point clouds from each image strip, then merges all of the DTM pieces into a single DTM of the entire area. Last, 3DM Analyst is used to map 3D structures on the merged model. As shown in Figure 36a, when the model DTM is merged, the imagery is not projected onto the surface; however, the imagery can be projected onto the surface when loading all of the individual DTMs used to create the merged model (Figure 36b).

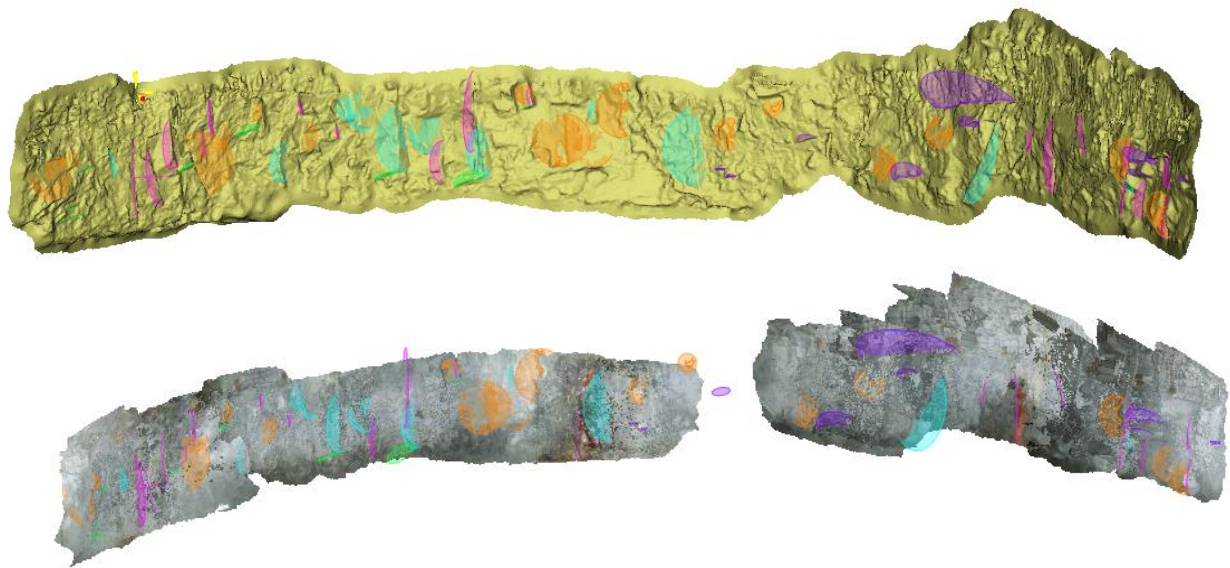


Figure 36. Top: Merged ADAMTech DTM model of the 815-102 drift with mapped structures at GSM that does not show the projected imagery. Bottom: DTM pieces loaded together, so that the imagery is projected onto the surface of the model with mapped structures – seven of the DTM pieces were unable to load, creating a hole in the model.

The merged DTM was created with relative orientation, which resulted in a curved model shape. Without defined ground control points, the model was unable to accurately represent the (straight) drift as it is found underground. Consequently, the joint data for this model presented on the stereonet in Figure 34 do not accurately represent the fractures in the rock mass surrounding the drift due to the fact that the model is not in an absolute orientation. In addition, the curvature of the model causes erroneous variation in orientation of joints that are closely aligned in real space.

A corresponding 3D model was built of the 815-102 drift using Bentley's ContextCapture (Fig. 38) using the same image frames that were used to construct the ADAM Technology model. The images were assigned to generate a model with a relative orientation in the aerotriangulation stage of the model build. The model created with Bentley's ContextCapture was judged to be more successful in capturing the (straight) shape of the 815-102 drift.

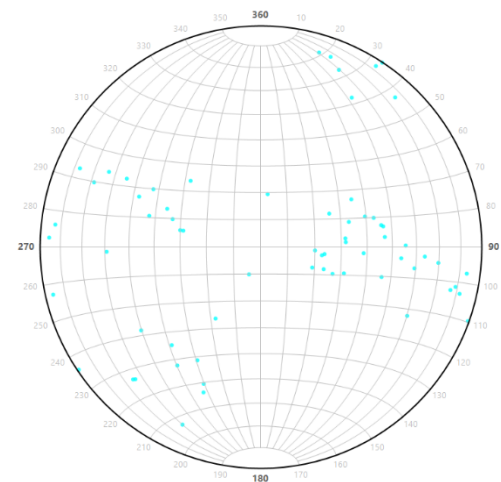


Figure 37. Stereonet of structures (with relative orientation) mapped on the 815-102 drift located at GSM using ADAM Technology's 3DM Analyst.



Figure 38. Model of the 815-102 drift at GSM created using Bentley's ContextCapture.

Built-in features to map geologic structures are not available in ContextCapture, so structure (joint) mapping was accomplished using Split Engineering's Split-FX software. The point clouds created in ContextCapture were exported as .las files, imported into Agisoft Photoscan in order to create ASCII ".pts" files, which were then imported into Split-FX, allowing joints to be mapped using the mapping features available in Split-FX. The joint data from the ContextCapture model do not contain the error associated with the curvature of the 3DM model, but they still fail to correspond to the fractures mapped in the real world because the relative model is not oriented correctly with respect to north. Mapping in Split-FX was found to be more difficult than in 3DM Analyst, because the model is much harder to manipulate than in 3DM Analyst.

Attempts were made to create absolute models of the NEV stope using both software packages, for the purpose of joint mapping. Frames from a four minute flight in the stope were selected and imported into both 3DM CalibCam and ContextCapture. Each model used only three of the four control points measured with the Trimble total station because the fourth point was not clearly visible in the imagery. 3DM CalibCam was not able to produce a model, and although the ContextCapture model was built successfully, it contains holes where either bad data exists or no data exists (Figure 39). Nevertheless, the general shape of the first draw point can be clearly seen in the model. Structures were mapped in the point cloud model using Split-FX, but few visible surfaces were identified (Figure 40). With an adjusted flight plan and better imagery, it is possible that a better model can be created with more visible features that can be mapped.

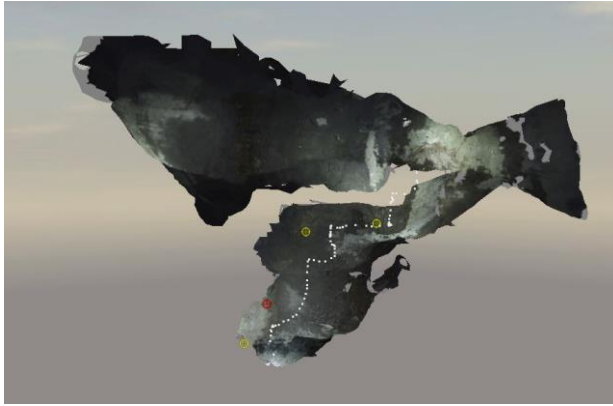


Figure 39. ContextCapture model built from a UAV flight into the first drawpoint of the NEV stope at GSM (three ground control points used shown in yellow; single unused ground control point shown in red; white dots represent the UAV route).

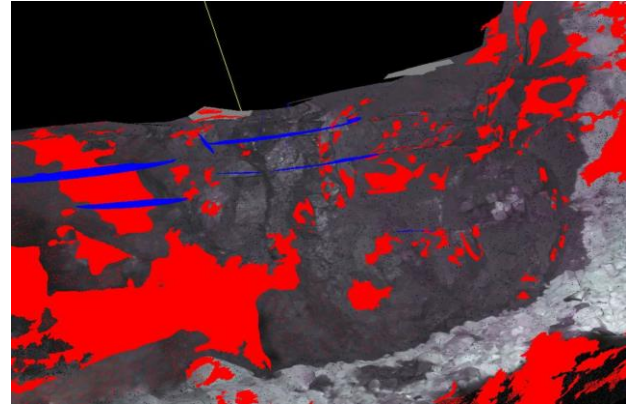


Figure 40. ContextCapture model built from a UAV flight into the first drawpoint of the NEV stope at GSM with mapped structures (created by Ryan Turner).

Working with both software packages, it became apparent that the underground models are more reliably built using Bentley's ContextCapture. The software package is straightforward and generated models can easily be navigated. Adam Technology's suite of software for building the DTM is not as intuitive to use as ContextCapture and is less straightforward on which steps to take. Adam Technology was designed for very precise data modeling, but UAV-based imagery from manual flights does not allow for such precision. It is convenient, though, that Adam Technology has the ability to map structural data within its software. Having to convert the exported Bentley point cloud using a separate software is a hassle and would not be an option if Agisoft PhotoScan was not available. Mapping using Split-FX was much more difficult than it was using 3DM Analyst. In Split-FX, the point cloud was slow to respond to manual rotation and zooming. When trying to pull the model in a certain direction, the model was moved in a different direction. Lack of experience with the Split-FX software is most likely contributable to these issues as well. On the other hand, mapping features in 3DM Analyst was fairly easy to navigate.

One significant result of this aspect of the research is that a single flight conducted in a stope can provide data that are not otherwise available because the location is inaccessible. While a high quality, georeferenced 3D model would be ideal, the imagery alone can provide improved understanding of the conditions.

4.2.3 Comparison of software using underground trial imagery (GSM)

Photogrammetric models were generated from video data collected during underground UAV flights using each of the three software platforms, Pix4Dmapper, Agisoft PhotoScan, and Bentley ContextCapture. The resulting data set included point clouds and 3D textured mesh layers generated from video collected during four Emesent flights (102 stope and 735 stope), three Near Earth Autonomy flights (Lower SAM), four Inkonova flights (735 stope and 895 drift), and four Flyability flights (895 raise, 735 stope, 735 drift, and 102 stope) performed between July and September 2018. Models were also produced using imagery captured by Montana Tech's M100. Appendix D contains graphical summaries of the bulk of the photogrammetric models produced for this study (36 models in total), along with a summary of processing and quality reporting parameters.

In order to compare the models produced by the three different software packages, a blind evaluation was completed assessing components of the completeness and level of detail for the point clouds built in each. One flight video was chosen for each of the four teams that participated in the UAV trials. The selected videos included both drift and stope flights, and were not necessarily the best imagery captured by each team. The flights that were modelled in each of the three software packages include:

- Emesent - Flight 2, 102 stope, 11 September 2018
- Flyability - Flight 5, 102 stope, 14 September 2018
- Inkonova - Flight 5, 895 drift, 26 August 2018
- Near Earth Autonomy - Flight 7b, Lower SAM, 31 July 2018

A photoset was extracted from each flight video and used to build point clouds and models in each of the three software packages. 3D pdfs of the twelve models created for this aspect of the research are contained in the accompanying file. The point clouds were exported (.LAS file type) and opened in CloudCompare, a public domain point cloud processing software. An objective evaluator scored each of the point clouds based on a standardized scoring sheet (Appendix E) without knowing which teams or software packages were associated with each model. The point clouds were evaluated with respect to model completeness and level of detail. The parameters taken into consideration for completeness include: continuous surface, realistic geometry, lack of excessive artifacts, and lack of distortion. The parameters considered for the level of detail include: surface texture, surface resolution, visible discontinuities, and well-defined recognizable features. Point density was not strictly included because this parameter can be easily adjusted by running a higher quality model that is both more time and computationally intensive.

The point clouds produced by Bentley ContextCapture had a high level of detail with nearly complete and continuous surfaces. Many features could be recognized including markings on the ribs and people, and the detail was still adequately defined when viewed closely. Some of the surface texture appears to be smoothed out when represented as the point cloud, and there are some inaccurate geometries created. This may in part be attributed to the quality of the imagery that was used to build the models, but because point clouds produced by the other two software packages from the same imagery did not have the same inaccuracies, the proprietary processing algorithm must be partially to blame. Although the point clouds do include a high level of detail, the large file sizes can limit the storage and manipulation of the models.

Many of the point clouds built with Agisoft PhotoScan have a more complete surface with only some small holes. Represented in the point clouds were many recognizable features including people and bolt plates. However, the point clouds have a lower resolution and do not retain these details when viewed closely. A higher quality model would be needed for additional analysis to be completed. The Agisoft PhotoScan point clouds generally scored comparably well to the Bentley ContextCapture point clouds, and yet had a much more manageable file size.

The point clouds built using Pix4Dmapper generally have a less continuous surface with more small holes throughout the point cloud. Some unrealistic geometries were also represented, including point clouds representing (straight) drifts as curved. The point clouds also had a low resolution and could not be viewed closely without losing much of the detail and texture.

In addition to comparing the quality of the models produced by each software package, an analysis of the precision of the models was planned. In order to measure the repeatability of the photogrammetry results, multiple flights were completed following the same general flight path to collect multiple sets of video imagery. To test the precision of the models, photogrammetry point clouds can be built for two sets of imagery using the same software package. The point clouds can then be imported into CloudCompare, and the *cloud-to-cloud distance tool* is used to detect the quantitative distance between the point clouds.

For this test, point clouds were built using Agisoft PhotoScan for the Inkonova Flight 8 and Flight 9 on 27 August 2018, as shown in Figure 41. The flights were repeated using the same UAV, lighting, and GoPro camera near the 750-level draw point to the 735 stoep. Images were extracted from the video every 15 frames and used to build the corresponding point clouds. The point clouds were exported as .LAS file types and imported into CloudCompare for the analysis. The flights covered slightly different areas, so the areas that did not overlap were approximately cropped using the *segment tool*. Because the point clouds were not initially georeferenced, the two point clouds were then coregistered with each other using the *align tool* and by selecting corresponding match points in each of the point clouds. At this point, the *cloud-to-cloud distance tool* was used to detect differences in the point clouds.

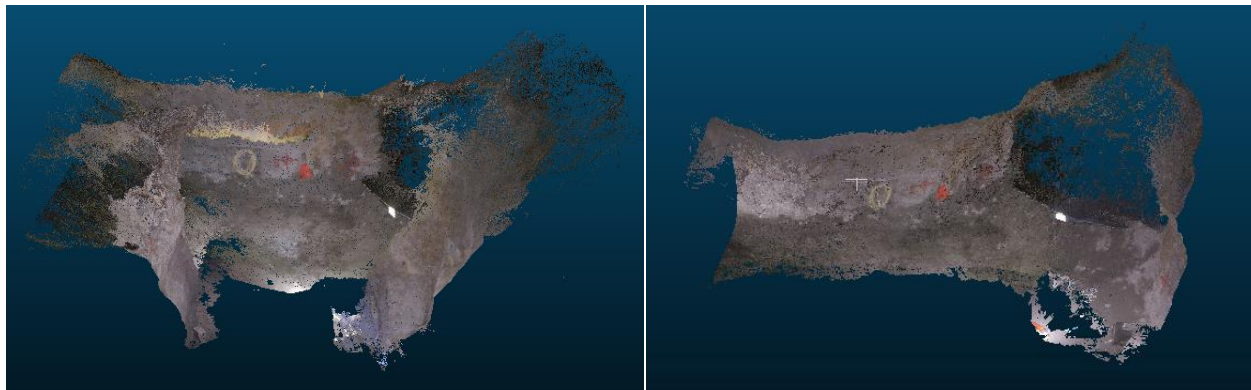
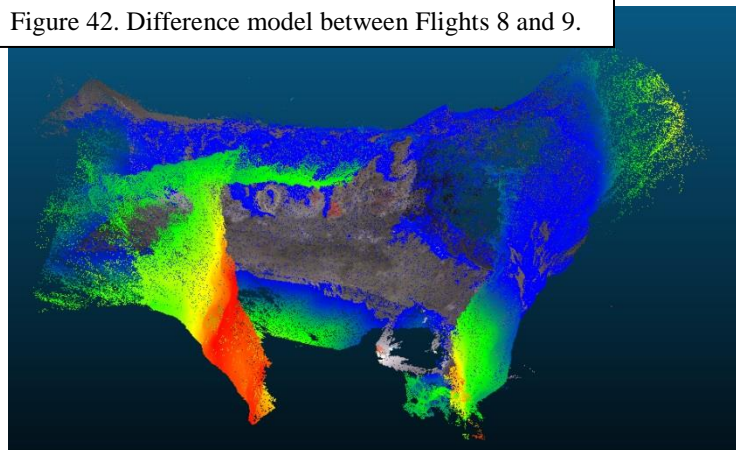


Figure 41. Inkonova point clouds. Left: Flight 8. Right: Flight 9.

Rather than highlighting the details that were expected to vary based on the inherent differences in the flight conditions, a high amount of difference was detected between the two point clouds, as shown in Figure 42. This is partially due to the different coverage of each of the point clouds within the drift. Because the two point clouds were not georeferenced, the *cloud-to-cloud distance tool* also only quantified the accuracy of the *align tool* based on the match points that were manually selected. In order for this analysis to be thoroughly completed in the future, it should be completed with two georeferenced point clouds. A very detailed manual alignment could also be completed, but this process can become time intensive and is also subject to the error introduced by the user.

Figure 42. Difference model between Flights 8 and 9.



A change detection analysis was also completed using the same procedure described previously. During the Emesent trial on 17 July 2018, the pilot was asked to repeat flights up the Lower SAM drift so that changes in the geometry of the resultant point clouds could be detected. The first flight up the Lower SAM with the DJI Wind 2 and Hovermap payload was completed to establish a baseline. After the first flight, three objects (rocks) were placed at random places within the drift. The flight was repeated using the same UAV, payload, lighting, and DJI Zenmuse X3 camera. After the flights were completed, still images from video captured during individual flights were extracted every 8 frames (video captured at 29 frames/second), and individual 3D point clouds were generated for each model in Agisoft PhotoScan Professional (version 1.4.3 build 6529, 64 bit). Figure 43 contains the 3D point cloud created for the baseline flight in the Lower SAM drift.



Figure 43. Looking obliquely east in CloudCompare at the 3D point cloud generate from video captured during the first flight up the Lower SAM drift on 17 July 2018.

The individual point clouds were imported into CloudCompare, co-registered with each other, and then compared to each other using the *cloud-to-cloud distance tool*. The results, displayed in Figure 44, show that the objects placed before the second flight were detected as changes in the geometry of the point cloud.

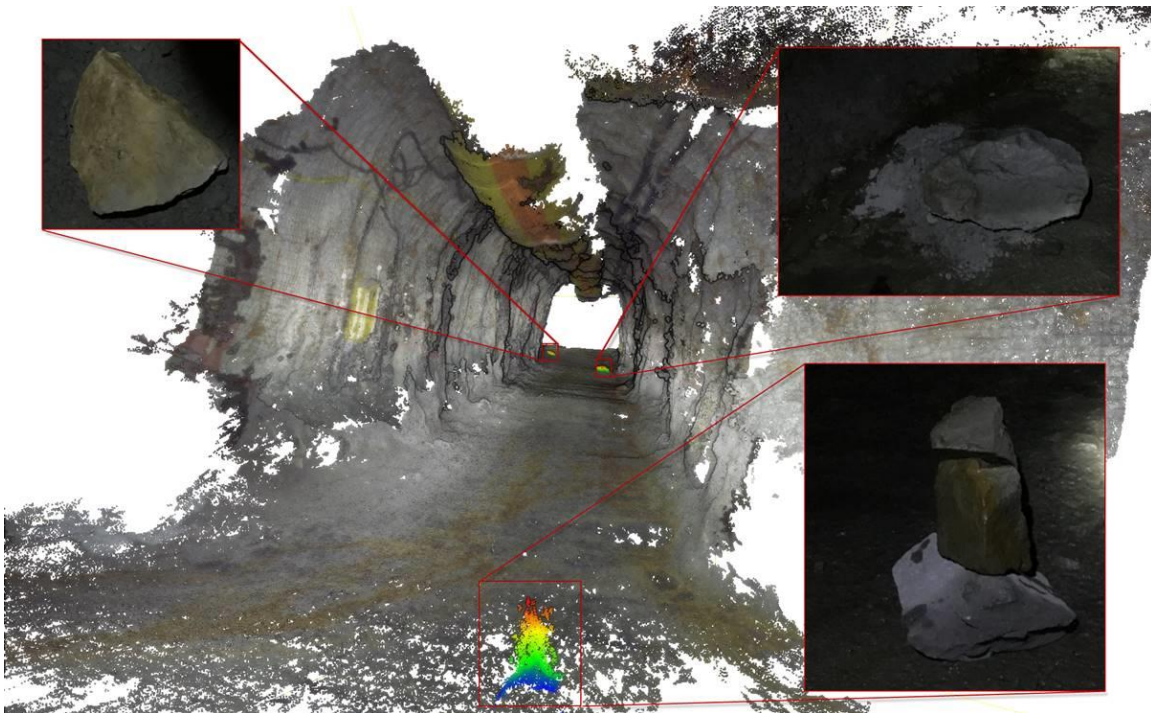


Figure 44. Looking down (north) the Lower SAM drift in CloudCompare at the results of the “cloud-to-cloud distance tool” computation. The 3 objects (rocks) placed in between flights are indicated by the scalar field points.

5.0 PROJECT COMPONENT #2B: Thermal & Multispectral Imagery Acquisition & Modeling

The use of thermal and multispectral cameras to detect loose ground and discontinuities within stopes was investigated as part of this research. Cameras were flown into stopes on board UAVs, and the imagery captured was used to generate 3D point clouds and meshes. The 3D point clouds and meshes were reviewed and compared to RGB point clouds and meshes to identify and map any geological structures and potentially loose ground.

Loose ground is an omnipresent hazard in many underground mines, and it can be subtle to the point of being undetectable to the human eye. National Institute of Occupational Safety and Health (NIOSH) researchers Iverson and Signer (2014) found that temperature differences as low as 0.2° C (0.36° F) captured with a thermal imager could be used to determine the location of loose ground. Their study evaluated the ability of thermal cameras to detect loose ground in six underground mines, and they found that warm, loose rock could be detected if the ventilation was cool. Underground ventilation can create a thermal contrast when cooler air decreases (or warmer air increases) the temperature of the loose rock relative to the in-situ rock temperature.

Multispectral cameras capable of being mounted to drones are primarily used for agriculture, and there is little to no research on their use in geology or geological engineering. However, there is a considerable body of research regarding the use of multispectral and hyperspectral imagery for identifying geological features. The intent of this research is to determine if infill materials along discontinuities can be distinguished from intact, unfractured rock masses. If the infill materials can be distinguished and modeled, then they can be captured in 3D and used for geotechnical analyses and designs. Multispectral imagery is generated by capturing specific bands of the visible and non-visible light spectrum either using multiple image sensors or by subdividing different spectral bands within a single image. The multispectral imagery is typically processed so that individual bands of the spectrum can be distinguished visually (MicaSense, 2019).

Rock masses at the Barrick Golden Sunlight Mine are either structurally massive breccia bodies, or thickly-bedded quartzites and sandstones. Deformation occurs along structural planes, and failure of the rock mass is rare. Water, gypsum, pyrite, chlorite, talc, and clay (montmorillonite) are found along structures bounding the rock masses, and it was expected that these features would have cooler temperatures than intact rock and could be distinguished by analyzing different spectral bands.

5.1 PC-2B Proof-of-Concept (Prototype) Technology Components

Thermal imagery was collected from a DJI Zenmuse XT radiometric camera (list price \$10,000) with a 9.0 mm fixed focal length lens at a resolution of 640 x 512 pixels. The much less expensive FLIR C3 handheld unit (academic price \$419.16) was also evaluated as a low cost alternative. Multispectral images were collected using a MicaSense RedEdge-M camera (borrowed from the University of Montana), which collects imagery at the 5 narrow wavelengths with 5.4 mm fixed lenses. Appendix F contains a table comparing the parameters for these imaging devices and a figure listing the details of the multispectral device. Lighting for the multispectral imagery was produced by a StratusLED ARM LED module that was mounted to the UAV, which generates 13,000 lumens of light. Flights were completed with Montana Tech's DJI Matrice 100 UAV, and Unmanned Aerial Services Emesent Hovermap *Standard* system. Thermal imagery was reviewed and set to a linear temperature scale in the FLIR ResearchIR software. Multispectral and thermal imagery was processed and built into 3D models using Agisoft PhotoScan (version 1.4.3).

5.2 PC-2B Proof-of-Concept (Prototype) Evaluation

This section contains separate subsections describing the investigation of the ability to build 3D models from the thermal imagery, and from the multispectral imagery. Step-by-step procedures to produce models from thermal and multispectral imagery are presented in Appendices G and H.

5.2.1 Thermal imagery acquisition and modeling

To capture the thermal imagery, several radiometric FLIR devices were evaluated. The radiometric devices provide thermal data for each pixel in the image, as opposed to the much lower cost non-radiometric devices that provide quantitative thermal data only for the center pixel in the image. A FLIR C3 thermal camera was initially tested underground due to its low cost (less than \$500 educational price) that was attractive for use in a high-risk environment in which the instrument can easily be lost. Although it is a useful camera for learning about thermal imagery and can detect thermal contrasts in rock masses when they exceed 0.1°C , the low resolution (80 x 60 pixels) and the relatively shallow depth of field of the images made the generation of photogrammetric models difficult. After multiple tests in the field and during processing, only a single 3D point cloud was generated in Agisoft PhotoScan using this camera (Figure 45). Also, there are no readily available gimbals (devices that attach the instrument to the UAV) for the C3, and the lack of video recording makes using this camera difficult on a UAV (FLIR, 2017).

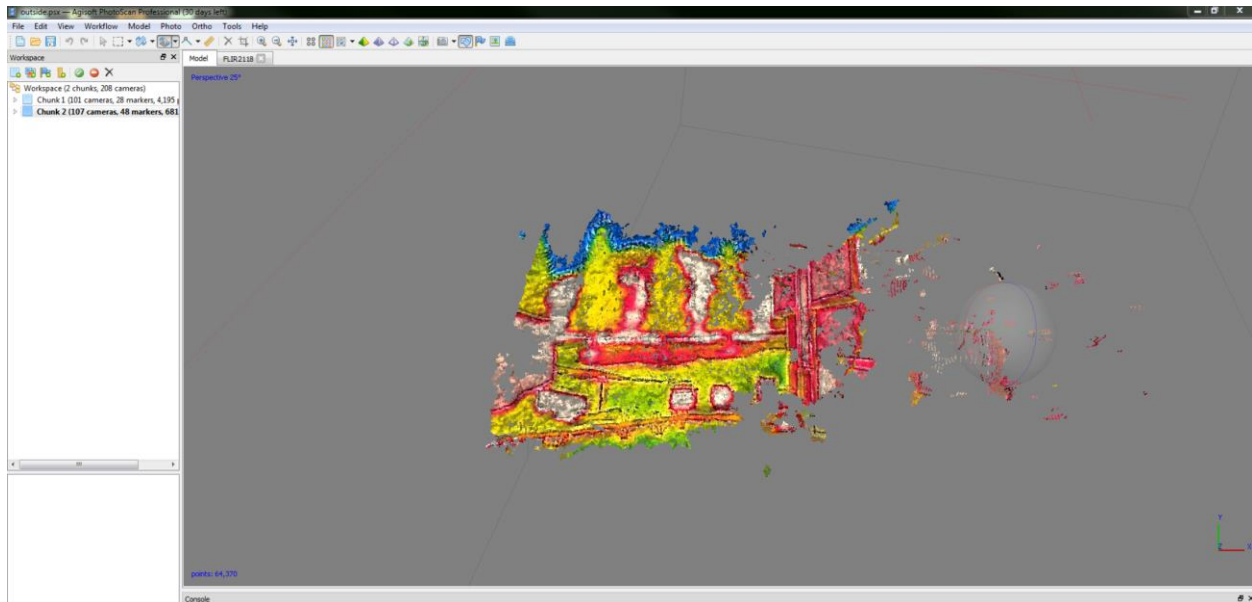


Figure 45. The only 3D point cloud generated from imagery using the FLIR C3 camera. The images were manually matched using individual, user-designated points, rather than pairs and radiometric data matching.

Research-quality thermal imagery was captured in drifts and stopes underground using the DJI Zenmuse XT thermal camera flown on the M100. This camera is integrated with a 3-axis gimbal and can be used on a variety of DJI UAVs (DJI, May 2016). Due to the relatively short distances anticipated between the camera and the walls of the stopes, a 9 mm lens was selected because it provided the widest field of view and higher magnification than provided by other lens choices. Although the cost was more than twice as high, the high-resolution version of the camera (640 pixels x 512 pixels) was selected over the low-resolution version (336 pixels x 256 pixels) because it would provide the highest quality data. Thermal imagery was analyzed and exported

using FLIR ResearchIR, software that allows users to query the radiometric data embedded in the imagery. It was found that thermal images with narrow temperature ranges using gray scale defined the detail of images better than color scales, which typically had blurry textures. Also, it was found that only TIFF imagery with radiometric metadata could successfully be used for generating 3D models in Agisoft PhotoScan. The DJI Zenmuse XT is also capable of capturing radiometric JPEGs, but these can only be utilized in the software FLIR ResearchIR. Still images extracted from .MOV videos captured by the DJI Zenmuse XT do not contain radiometric metadata because they are exported as .png files, and they typically yield zero-resolution point clouds in Agisoft PhotoScan which cannot be used to generate 3D point clouds.

After the M100 was successfully flown with the Zenmuse X3 (RGB) camera in March 2018, the Zenmuse XT (thermal) camera was tested at Barrick Golden Sunlight in the 375 drift, which has an exposure of the West Shear fault and loose rock contained by welded wire mesh. Ventilation was active in the drift, and using a *Pyle PMA90* anemometer, the dry bulb air temperature was found to be 19.8-20.3° C (67.6-68.5° F). Using a *Craftsman 50455* infrared thermometer, the temperatures of the rock mass and loose rock were found to be 15.7-15.8° C (60.3-60.4° F) and 15.6-15.7° C (60.1-60.3° F) respectively. Magnetic strobe lights fixed to friction bolts were used as georeferencing points because they are observable in the RGB imagery and as hot spots in the thermal imagery. Figure 46 shows an example of loose ground (dark is warm) found above a muck pile and a magnetic strobe light.

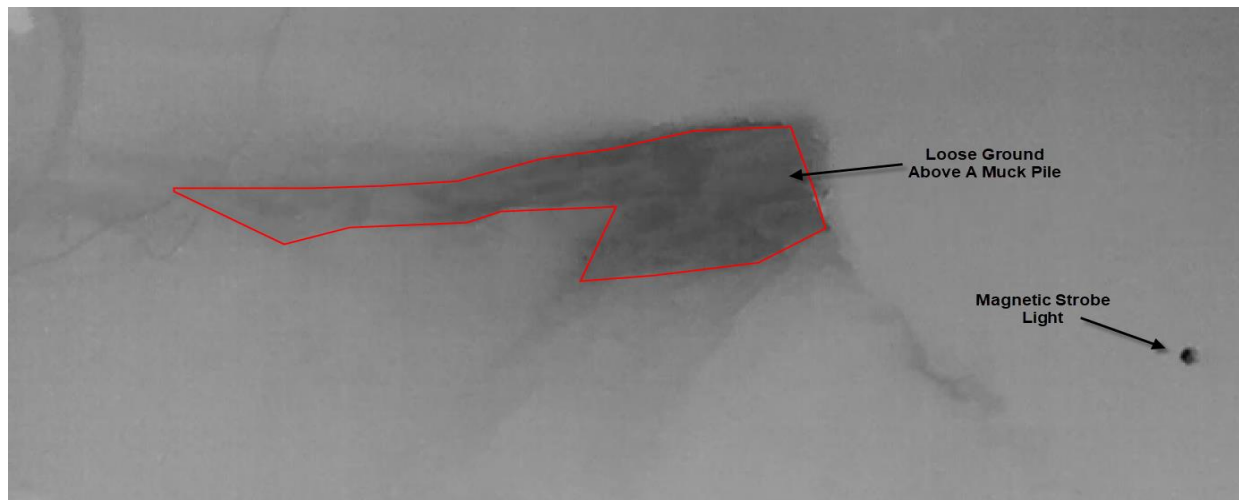


Figure 46. A thermal still from a video recorded with the Zenmuse XT on the M100 while flying in the 375 drift. Warm material is indicated by darker colors, and loose ground (outlined in red) can be observed above the muck pile. The loose rock had temperatures up to 18.6° C (65.4° F), while the intact rock around it had temperatures up to 17.2° C (63° F). A magnetic strobe light was used as a reference point.

Video imagery from the Zenmuse XT and Zenmuse X3 was used to generate 3D point clouds of the 375 drift in Agisoft PhotoScan. Three-dimensional point clouds generated using just the thermal imagery (.png files) were difficult to interpret because points were typically monotone in color, and the software had difficulty in matching points when no reference points were established. Instead, the RGB imagery was used to generate the 3D point cloud, and thermal images were used in 2D form to verify if loose ground and dilated structures were present (Figures 47 and 48). The West Shear fault was detected by the Zenmuse XT in flight, because its damp clay infill was found to have a cooler temperature (14.7° C/ 57.7° F) than the surrounding rock, and it shows up as a dark lineation on the thermal imagery (Figure 48, bottom image).

In September 2018, Unmanned Aerial Surveys of Sudbury, Ontario, was contracted to fly in underground stopes at the Golden Sunlight Mine while carrying individual payloads of RGB, thermal, and multispectral cameras. Unmanned Aerial Surveys was selected for the contract because their pilots were found to be the most experienced during the underground drone trials, and because they had a Emesent Hovermap system that could navigate safely within stopes while carrying a large payload. Multiple flights were completed successfully in the 102 and 735 stopes, and for each stope RGB, thermal, multispectral, and LiDAR data were collected. Thermal video imagery was collected in flight using a DJI Zenmuse XT camera at a frame rate of 30 frames per second, and .png still images were extracted from the video every 10 frames using Agisoft PhotoScan. The .png still images did not have embedded, radiometric metadata, which made aligning the images in Agisoft PhotoScan difficult, and the generated point clouds were of very low quality. The authors learned that the format of the thermal imagery is very important, and that .tif files are more easily aligned and used for 3D model generation in Agisoft PhotoScan. At the time of this writing, the authors are working to align the photos and “drape” them over a 3D mesh of the 102 stope.

In January 2019 after a large wedge came out of the crown pillar of the 945-480 stope at the Golden Sunlight Mine, the M100 was flown to investigate the stability of the stope using the Zenmuse X3 (RGB) and Zenmuse XT (thermal) cameras. Ventilation was active in the drift, and using a *Pyle PMA90* anemometer, the dry bulb air temperature was found to be 6.1° C (43° F). Using a *Craftsman 50455* infrared thermometer, the temperatures of the rock mass was found to be 1.1-1.7° C (34-35° F). Magnetic strobe lights fixed to friction bolts were used as georeferencing points because they are observable in the RGB imagery and as hot spots in the thermal imagery. Two flights were completed successfully using the Zenmuse X3 in the stope, and two flights were completed successfully using the Zenmuse XT. Thermal imagery from these flights was successfully used to generate 3D models of the stope and the drift that accesses the top of the stope. From 3D meshes generated from the imagery, discontinuities that bound loose blocks within the crown pillar of the stope were identified due to the relatively warmer air flowing through dilated structures within the rock mass (Figure 49).

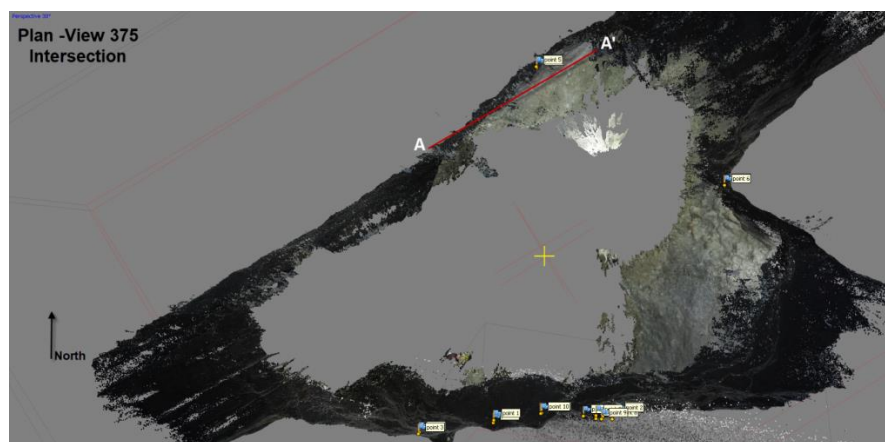


Figure 47. Plan-view of a 3D point cloud generated from RGB imagery for the 375 intersection. The red section line indicates the location and orientation of the images in Figure 48.

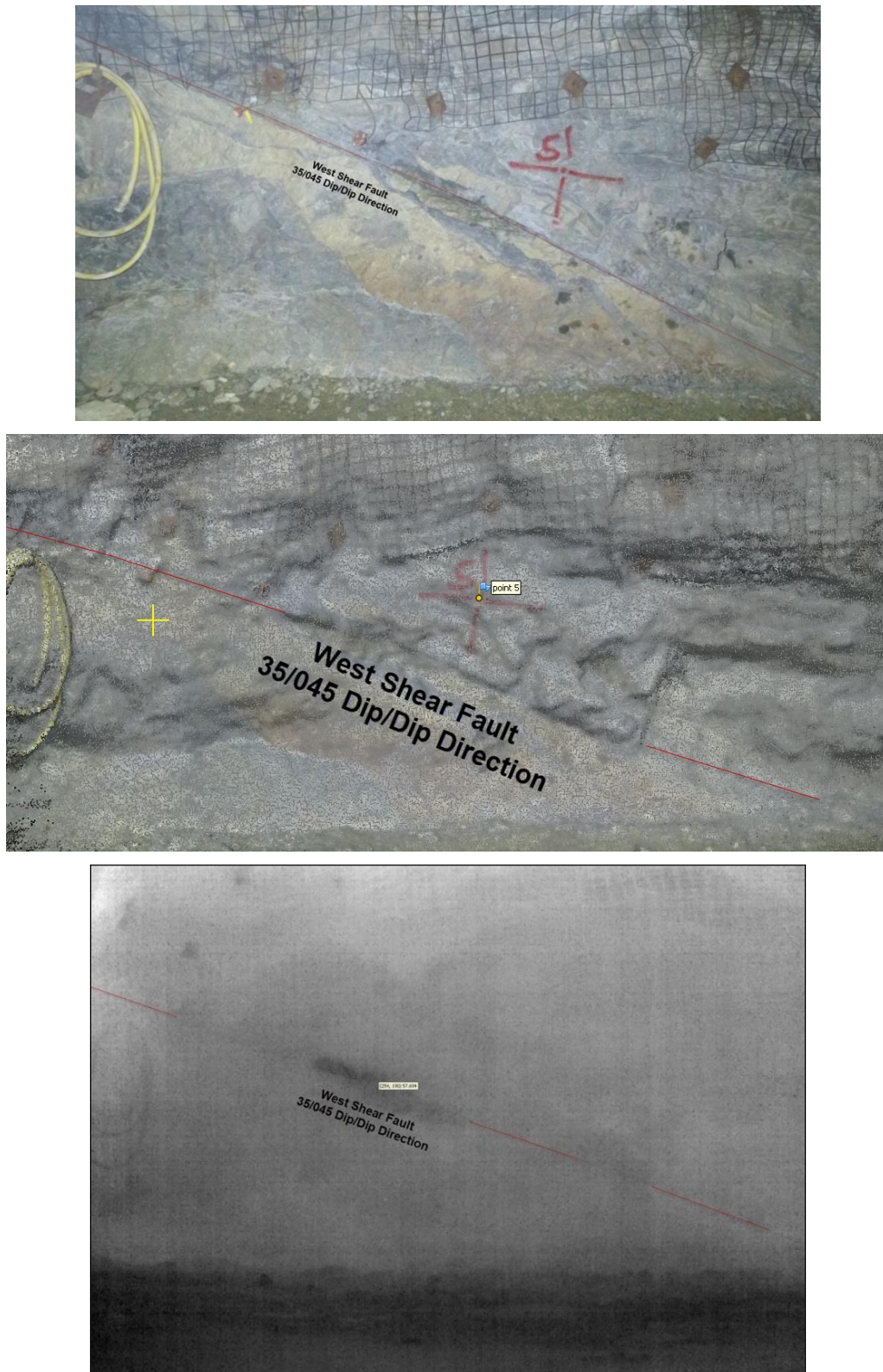
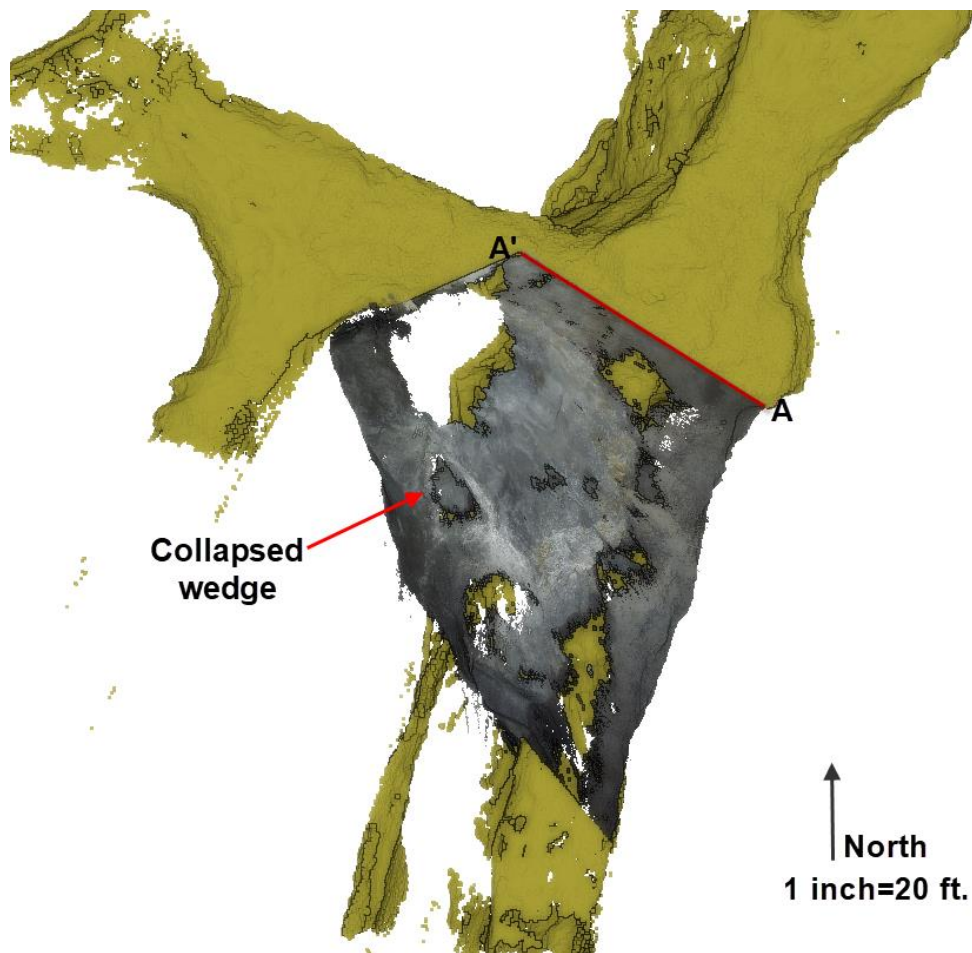


Figure 48. Three images looking north at an exposure of the West Shear fault with RGB (top), 3D point cloud (middle), and thermal (bottom) imagery from two separate flights by the M100. The fault is a basal release plane for a global instability at the mine, and typically has damp to wet montmorillonite as infill. In the thermal imagery, the clay is cooler (14.7° C/ 57.7° F) than the surrounding rock and is indicated by a dark lineation.



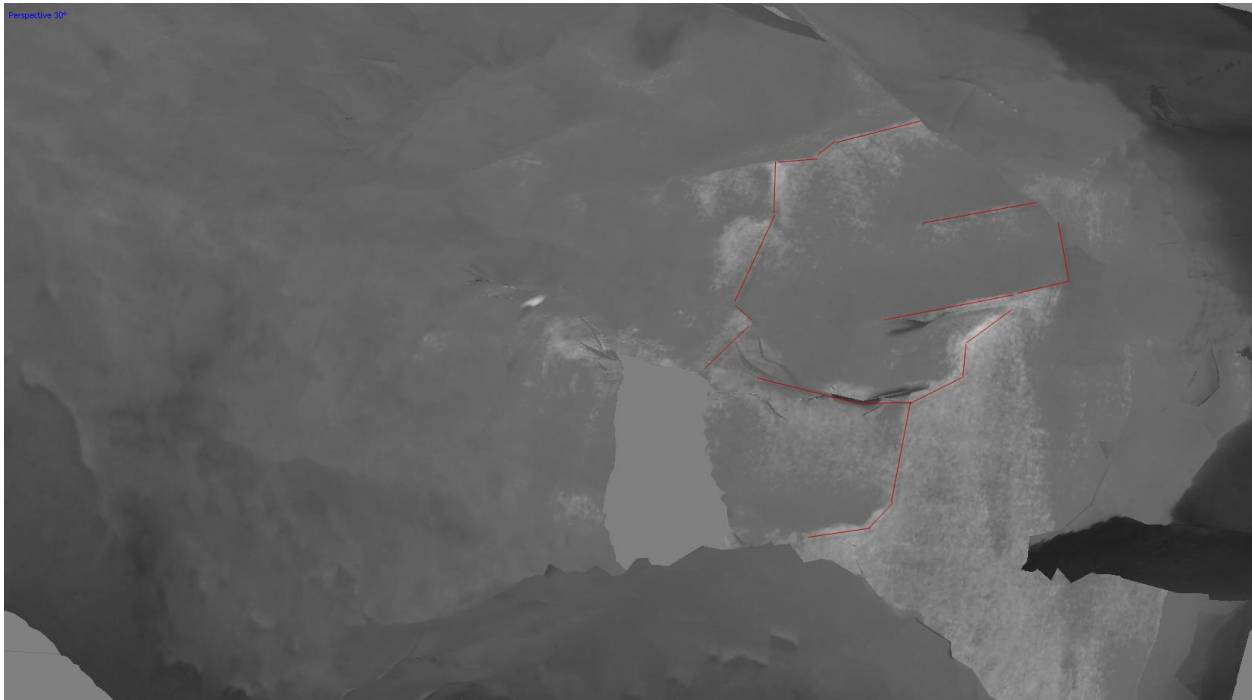


Figure 49. The top image shows a plan-view of a 3D point cloud generated from RGB imagery for the top of the 945-480 stopes where the LiDAR data is shown in tan. The red section line indicates the location and orientation of the lower images. The lower three images are looking west into the top of the stope at the failed block and the loose blocks in the crown with an RGB still (second from top), a thermal still (second from bottom), and a thermal 3D mesh (bottom) from two separate flights by the M100. The lighter colors in the 3D thermal mesh indicate where warmer ventilation is circulating through dilated discontinuities, indicating that the crown pillar will release more wedges.

5.2.2 Multispectral imagery acquisition and modeling

In September 2018, Unmanned Aerial Services of Sudbury, Ontario, was contracted to fly in underground stopes at the Golden Sunlight Mine with the MicaSense RedEdge-M multispectral camera. Multispectral imagery was collected at a capture interval of 1 second during each flight using the MicaSense RedEdge-M, and each band was captured individually as a .tif file. Prior to each flight, a calibrated reflectance panel was positioned in front of the camera so that the lighting conditions could be calibrated against during processing. Each flight was illuminated using a StratusLED 100W ARM LED light module that was mounted facing forward on the Emesent Hovermap system. Flights in the 102 stope were flown as vertical strips, where each still image captures at least 50% of the field of view observed in the previous frame. Flights in the 102 stope captured the lower half of the stope from the 735 draw point (Figure 19).

Using Agisoft PhotoScan, each multispectral band was processed individually to generate point clouds and tiled models using a procedure recommended by the USGS that is available online (USGS, 2017). If working to identify individual minerals using a multispectral camera, a digital archive of the reflectance for a variety of materials is available online from the USGS Spectroscopy Lab (USGS, 2018). The models built for the 102 stope using individual multispectral bands are shown in Figures 50 through 54.

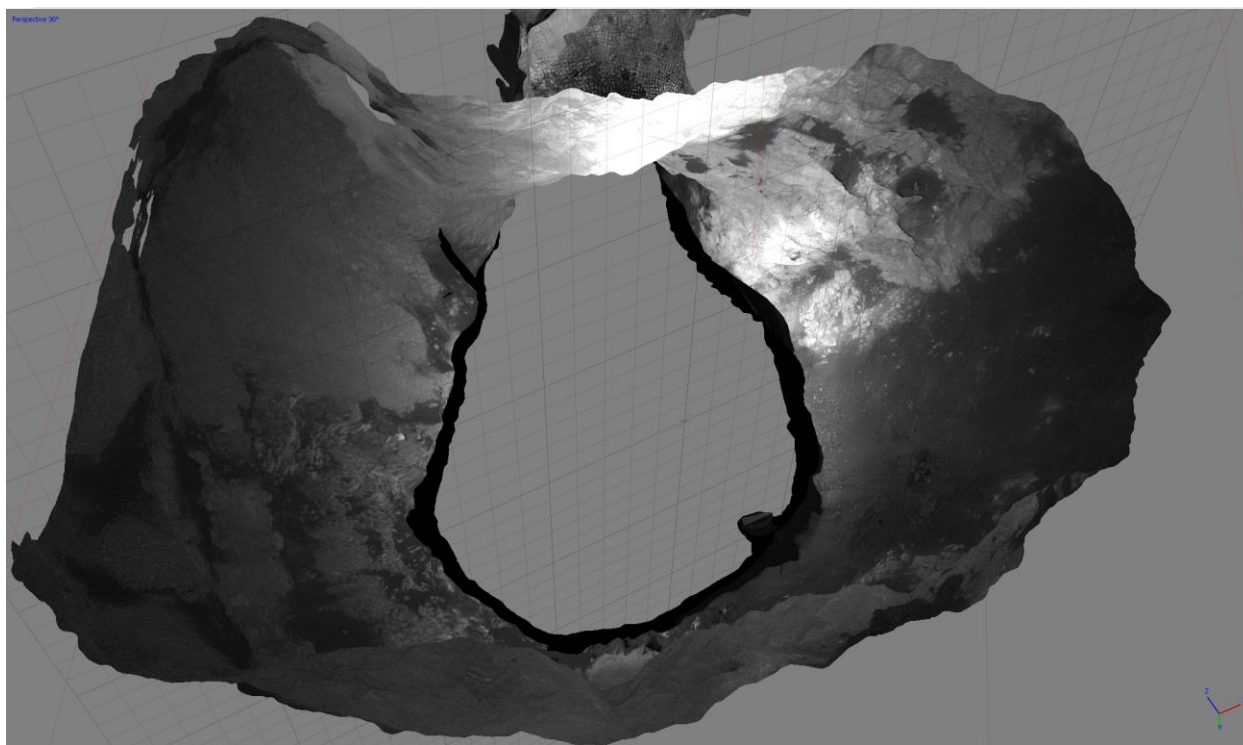


Figure 50 Plan view of the 102 stope of a model built using the “green” multispectral band in Agisoft PhotoScan.

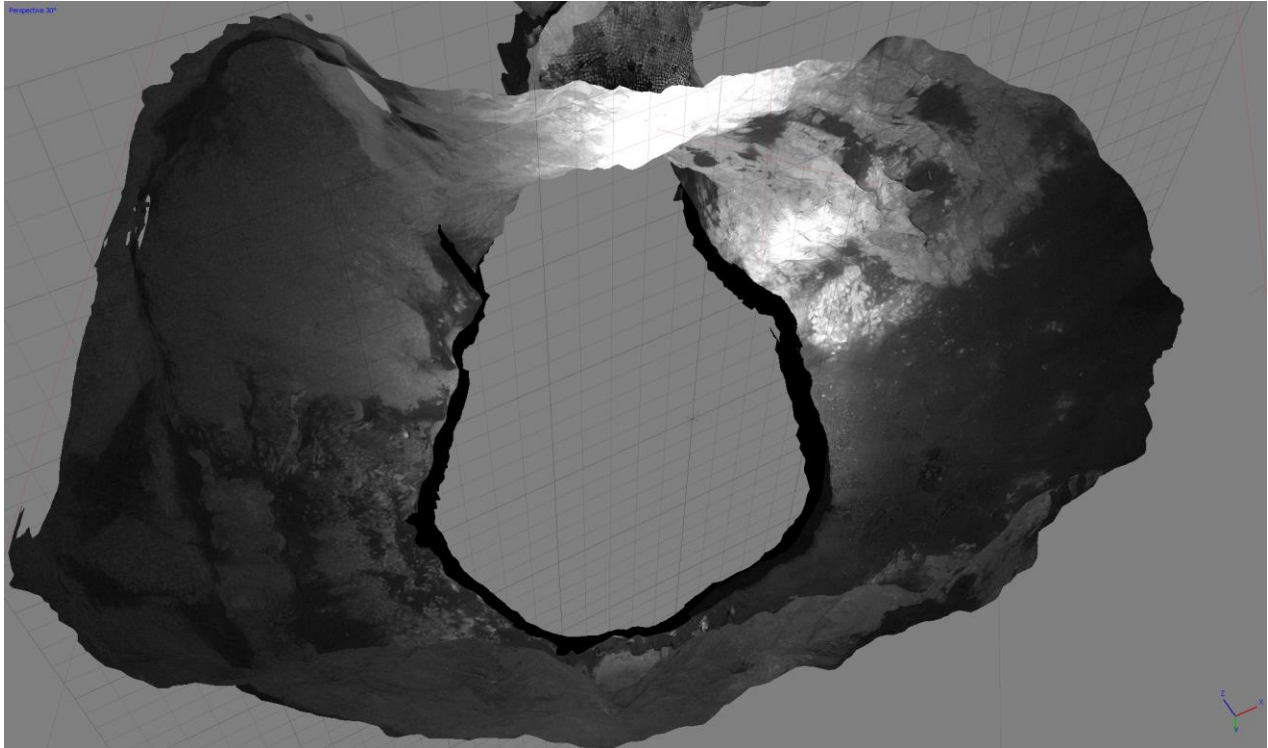


Figure 51. Plan view of the 102 stope of a model built using the “blue” multispectral band in Agisoft PhotoScan.

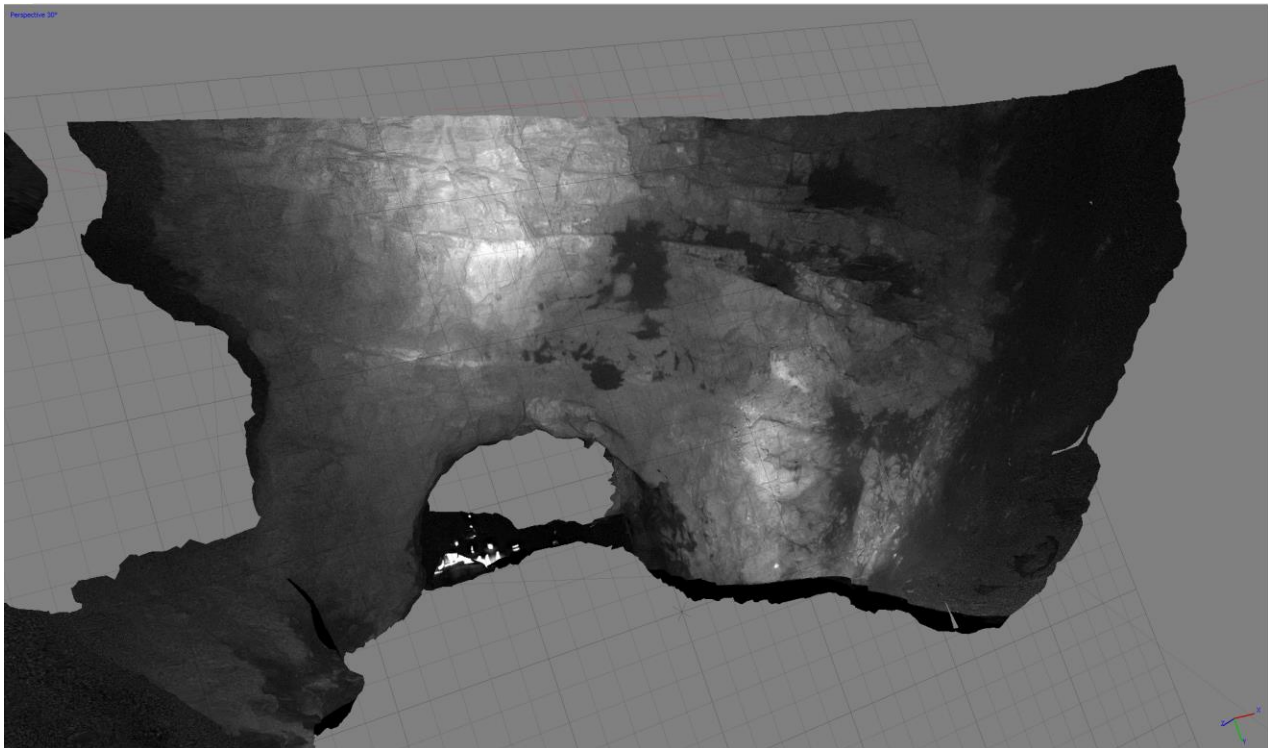


Figure 52. Looking W obliquely at the 102 stope in a model built using the “red” multispectral band in Agisoft PhotoScan.

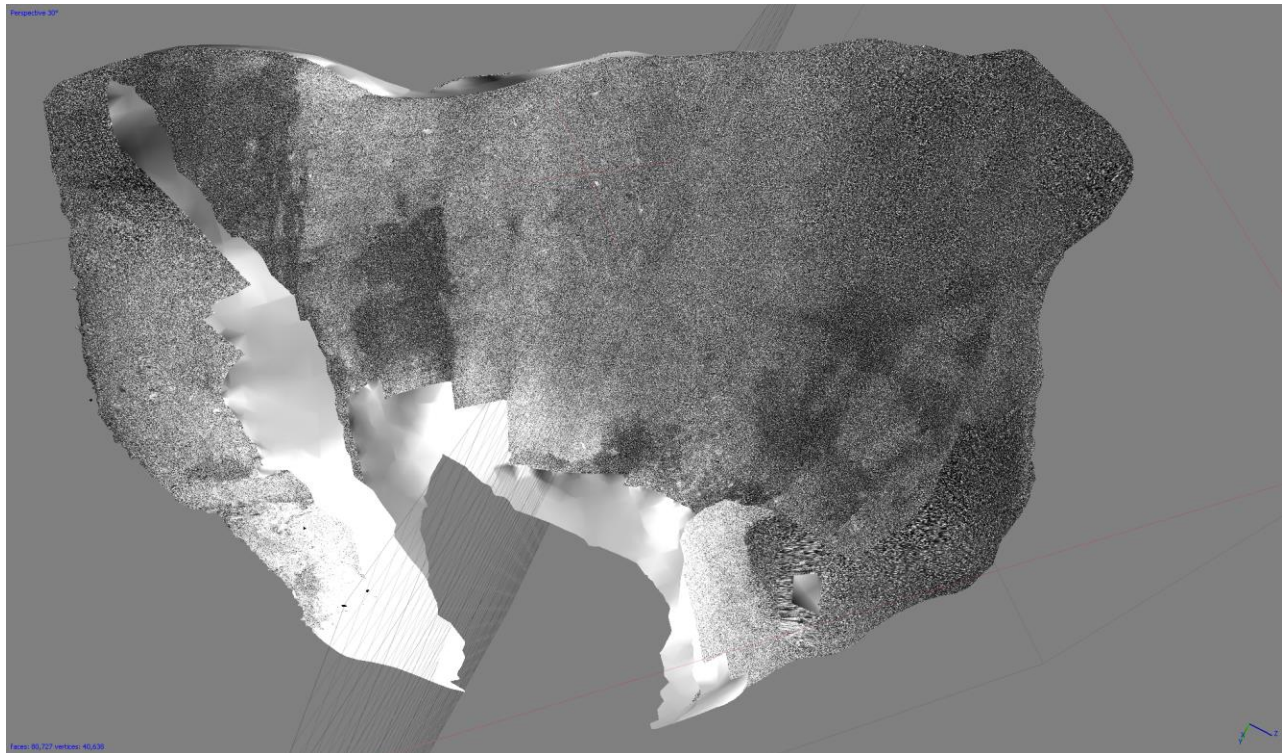


Figure 53. Looking NE obliquely at the 102 stope in a model built using the “red edge” multispectral band in Agisoft PhotoScan.



Figure 54. Plan view of the 102 stope of a model built using the “near infrared” multispectral band in Agisoft PhotoScan. The imagery for this model had little variation or detail. However, the darker bands reflect zones where water and pyrite mineralization are observed in the stope, and it is thought that because they absorb near infrared energy they are can be distinguished.

6.0 TECHNOLOGY READINESS ASSESSMENTS

Since this project was focused on developing systems from off-the-shelf components and evaluating pre-existing software and systems, the technology used was beyond proof-of-concept and into the prototype and commercially developed stages. The four project components were evaluated in terms of the nine technology readiness levels (TRLs) from the National Aeronautics and Space Administration (NASA). Technology readiness levels were developed by NASA researcher Stan Sadin in 1974 as a methodology for determining where a component or technology landed on a 7-level scale (now 9 levels) that ranged from basic scientific research to full implementation in space (Banke, 2017). Using the 9-level scale shown in Table 6 (Bolat, 2014), each system was evaluated to determine if it was fully capable of operating in an underground mine without issues (TRL 9), or if it was still in development (TRL 4-8). A more detailed table of the TRL may be found in Appendix I. For systems involving both hardware and software, although the overall success is dependent upon both hardware and software working optimally, these were evaluated separately.

Table 6. Summary of NASA's technology readiness levels from Bolat (2014).

- TRL 0: Idea.** Unproven concept, no testing has been performed.
- TRL 1: Basic research.** Principles postulated and observed but no experimental proof available.
- TRL 2: Technology formulation.** Concept and application have been formulated.
- TRL 3: Applied research.** First laboratory tests completed; proof of concept.
- TRL 4: Small scale prototype** built in a laboratory environment ("ugly" prototype).
- TRL 5: Large scale prototype** tested in intended environment.
- TRL 6: Prototype system** tested in intended environment close to expected performance.
- TRL 7: Demonstration system** operating in operational environment at pre-commercial scale.
- TRL 8: First of a kind commercial system.** Manufacturing issues solved.
- TRL 9: Full commercial application,** technology available for consumers.

In addition to the hardware and software TRL, the durability, or how well the system would survive underground, of each system was evaluated to determine an ingress protection (IP) level. The IP level is a 2-part number rating that estimates how well a piece of hardware will prevent ingress from dust (1st number, 0-6) and water (2nd number, 0-8), where a rating of IP68 indicates absolute protection from dust and water in most conditions (DSM&T, 2018). Appendix I contains a more detailed table of the IP value definitions.

6.1 Project Component 1: Basic UAV Systems and Imagery Acquisition

Based on direct experience with assembling and operating the DJI Matrice 100 and its components, including the Guidance system, both its hardware and software were rated at TRL 5 (Table 7).

Table 7. Definitions associated with Technology Readiness Level 5 (NASA, 2013).

5	Component and/or breadboard validation in relevant environment.	A medium fidelity system/component breadboard is built and operated to demonstrate overall performance in a simulated operational environment with realistic support elements that demonstrate overall performance in critical areas. Performance predictions are made for subsequent development phases.	End-to-end software elements implemented and interfaced with existing systems/simulations conforming to target environment. End-to-end software system tested in relevant environment, meeting predicted performance. Operational environment performance predicted. Prototype implementations developed.	Documented test performance demonstrating agreement with analytical predictions. Documented definition of scaling requirements.
---	---	---	---	---

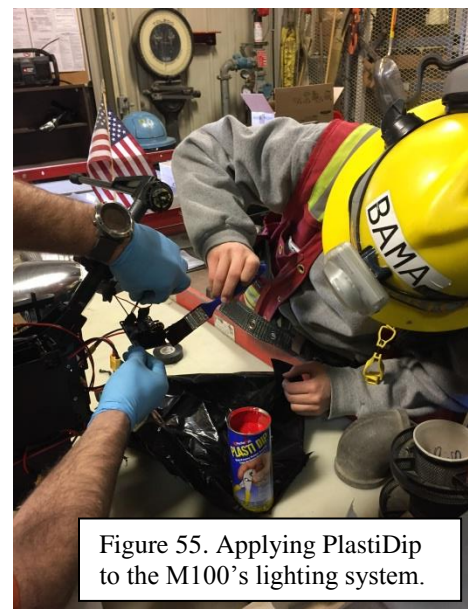
Although the hardware is commercially available for use above ground, for use underground, which is not its intended purpose, it is considered to be at prototype level.

- Lift capacity of motors overstated by DJI, even with use of propellers appropriate for use above 5000 ft.
- The UAV had difficulties with payload and would enter yaw spins when the battery voltage dropped to 55%.
- It was found to be necessary to mount Guidance below main deck of UAV due to interference from propellers, rather than above or below as stated in the Guidance documentation.

In terms of the software:

- The optical flow (stereo vision) lux requirements for the Guidance are understated in the documentation. It is necessary to use very bright (13,000 lumens) LED for successful flights underground or in dark conditions.
- Ultrasonics are not effective when Guidance is mounted above the propellers.
- The UAV capable of limited BVLOS flights, but the RC and live video transmission frequencies are not ideal for environments with complex geometries.

The M100 was assigned an IP rating of 52. The electronics are housed in enclosures that prevent most dust and droplets of water from causing damage, but some wires and ports are exposed (Figure 6). In Figure 55, a PlastiDip coating is being applied to protect exposed wiring and circuitry. The M100 was flown in dusty conditions underground and through drops of water that fell vertically without issues. After most flights, the enclosures were cleared of dust using canned air to prevent electronic shorts.



6.1.1 Underground UAV Collision Avoidance Research at Montana Tech

A portion of this research involved development of a custom UAV collision avoidance system that would have a low cost and the ability to be applied to a variety of remote controlled devices without the need to modify the device. This portion of the research was conducted in collaboration with Prof. Bryce Hill and graduate student Tyler Holliday of Montana Tech's Department of Electrical Engineering.

Their proposed design of the custom system would be the use of a microcontroller to act as an intermediary device (monkey-in-the-middle or MITM) between the receiver and flight controller. This controller would read in the signal from the receiver and based on sensor data modify the signal to avoid possible obstacles. The modified signal would then be passed on to the flight controller.

The signals that are sent by the receiver use the S.Bus protocol. This proprietary protocol uses a modified universal asynchronous receiver-transmitter (UART) communication that combines all of the commands for the individual motors on a drone into a single digital signal comprised of 16 channels. Therefore, S.Bus protocol needs only a single connection to the flight controller. This connection to flight controller is where the MITM is placed so it can modify the S.Bus signal according to sensor data. Most of the research done over the last five months has been to create an algorithm that decodes the S.Bus protocol down to the 16 individual channels. With each individual channel separated the MITM can then modify each channel to account for obstacle avoidance. For example if there is a wall detected in the forward direction, the MITM would modify the channel(s) responsible for the forward control of the drone. Once the MITM has finished modifying the individual channels, it will rebuild the S.Bus signal with the modified channels and transmit it to the flight controller.

The proposed design involves using two different types of sensors. The first sensor makes use of ultrasonic waves. When triggered the sensor will send a pulse out and wait for an echo to be received. The amount of time between triggering and receiving is measured by a dedicated microcontroller that then takes that time value and converts it to a distance value. The second sensor is an infrared range finder that operates in the same manner as the ultrasonic but with infrared light waves. In comparison of the two sensors the infrared is significantly faster but is adversely affected by surfaces that have a sheen, such as water. The ultrasonic has a longer trigger-echo cycle but is less susceptible to the changing texture of obstacles. Either sensor mostly covers for the deficiencies of the other thus the reason that both are being used in the design.

As research progresses the sensors will be integrated into a standalone package with a dedicated microcontroller. The package will be able to move to any direction on a remote controlled vehicle. In the case of a drone that would mean six packages, one for each direction on the three axes of motion (forward-backward, right-left, and up-down). The dedicated controller in the package would operate both sensors and convert the time measurements into distances. The distances will then be compared and the microcontroller would report the shortest distance to the MITM.

To date, the proof-of-concept has been established and a prototype has been tested on a terrestrial device (rover), with the next step to test on a UAV. This component of the project is judged to be at TRL 3-4.

6.1.2 Recommendations for future research and development

It was observed in this study that the ability to capture imagery of locations that are not accessible is extremely valuable in itself, regardless of the quality of the models that are produced. Continued research to develop low-cost UAVs assembled using off-the-shelf components and evaluate the performance will undoubtedly be valuable to the underground mining community. In addition to geotechnical applications, UAVs have potential uses in mines ranging from mine rescue to gas monitoring to surveying to vehicle collision prevention.

While it is the mechanical and electrical engineers that develop the technology, geotechnical engineers are best able to steer and evaluate the performance of the systems in the underground mining environment, in terms of the ability to contribute to stability analysis. The interdisciplinary collaboration is one very attractive aspect of this project.

Examples of specific technologies that are currently available and can be evaluated include time-of-flight (pulse LiDAR) sensors. The Inkonova platforms and a forthcoming platform from Flyability use this technology for enhanced navigation, at a cost of less than \$50,000. TerraBee (www.terabee.com), a French company, offers pulse LiDAR sensor systems at a reasonable cost (around \$1000). Figure 56 shows an “indoor drone” with the yellow and black TerraBee sensors mounted on top for obstacle avoidance.



Figure 56. Indoor drone with TerraBee sensors for obstacle avoidance (<https://www.terabee.com/drone-obstacle-avoidance-indoor-flight/>).

In addition, technology advances are bringing miniaturized and lower mass sensors to market that can be utilized in UAV-based systems. The size and weight of the Velodyne LiDAR puck has dictated that the systems using LiDAR and SLAM for enhanced navigation have significant payload capacity and consequently rather large size. This limits their use in tight spaces, which are generally the most in need of exploration. Inkonova’s Ranger uses the Hokuyo miniature LiDAR, developed in Japan, and other smaller LiDAR based sensors are likely to be commercially available within a short period of time.

The benefits of continuing this project include the experience and expertise established by the research team, the excellent underground test facility available due to the partnership with Barrick, and the human and technological resources available at Montana Tech. The opportunity to contribute to this new and exciting field of research is greatly appreciated.

6.2 Project Component 1B: Systems for Enhanced Navigation

During the drone trials, each UAV system tested was evaluated in terms of if the technology was ready for immediate use in the underground environment and how well the system would survive underground. The systems that underwent the trials were either commercially available systems or prototypes still undergoing development, and it was initially difficult to quantify how well each system would perform underground, but the NASA TRL system worked well. The estimation of the TRL and IP rating of each system is summarized below. It should be noted that these ratings were made when the systems were tested in the underground trials during the summer months of 2018. At the time of this report, the systems have likely improved in terms of technology readiness levels and ingress protection. An assessment of each system's status in terms of safety and risk is also presented.

Emesent demonstrated two UAV Hovermap payloads at the trials, the *Standard* payload and the *Mining* payload, and both performed exceptionally well. The hardware for both payloads was rated at TRL 9 (Table 8). The UAVs successfully completed all missions during the trial and the hardware performed well in underground with no issues.

The software for the *Standard* payload was rated at TRL 9 (Table 8). The Obstacle detection and avoidance work well underground in a variety of conditions and the UAV was successfully operated out of line-of-sight multiple times. The software for the *Mining* payload was rated at TRL 8 (Table 8). The obstacle detection, point cloud generation, and navigation beyond line-of-sight worked without issues on multiple missions. However, a fail safe error and switch to DJI flight controller caused the drone to crash in a stope after multiple missions. This was thought to be caused by DJI SDK rather than Emesent software, but is still an issue that needs to be addressed.

Table 8. Definitions associated with Technology Readiness Levels 8 to 9 (NASA, 2013).

8	Actual system completed and "flight qualified" through test and demonstration.	The final product in its final configuration is successfully demonstrated through test and analysis for its intended operational environment and platform (ground, airborne, or space).	All software has been thoroughly debugged and fully integrated with all operational hardware and software systems. All user documentation, training documentation, and maintenance documentation completed. All functionality successfully demonstrated in simulated operational scenarios. Verification and validation completed.	Documented test performance verifying analytical predictions.
9	Actual system flight proven through successful mission operations.	The final product is successfully operated in an actual mission.	All software has been thoroughly debugged and fully integrated with all operational hardware and software systems. All documentation has been completed. Sustaining software support is in place. System has been successfully operated in the operational environment.	Documented mission operational results.

Both of Emesent's Hovermap payloads were assigned an IP rating of 64. The electronics are encapsulated in resin for protection. The *Standard* payload was flown through water streaming from the back (roof) of the underground workings and in very dusty conditions where visibility was obscured (Figure 57, left) without any issues. The *Mining* payload crashed in the 102 stope and was partially submerged in 2 ft. of standing water for several hours; upon recovery, no water or dust was found within the drone or the Hovermap payload (Figure 57, right).



Figure 57.
Left: The Emesent Hovermap Standard in flight in very dusty conditions underground.
Right: The Emesent Hovermap Mine in flight in the 102 stope.

Flyability's Elios platform also performed exceptionally well at the trials. Both the hardware and software were rated at TRL 9 (Table 8). The UAVs successfully completed all missions during the trial and the hardware performed well in underground with no issues. The rolling cage prevented any physical damage to the UAV throughout the trials. The radio control, video transmission, and flight controller all worked well and the Elios was successfully operated BVLOS multiple times. The ingress protection was also rated highly at IP64. It was flown through streaming water and in very dusty conditions (Figure 58) in stopes and raises without issue. Currently, the primary drawback of using the Elios for photogrammetry is that the cage must be removed from the imagery; this is possible but not trivial. Flyability is developing a platform that will provide better imagery for photogrammetry and expects to release this platform in 2019.

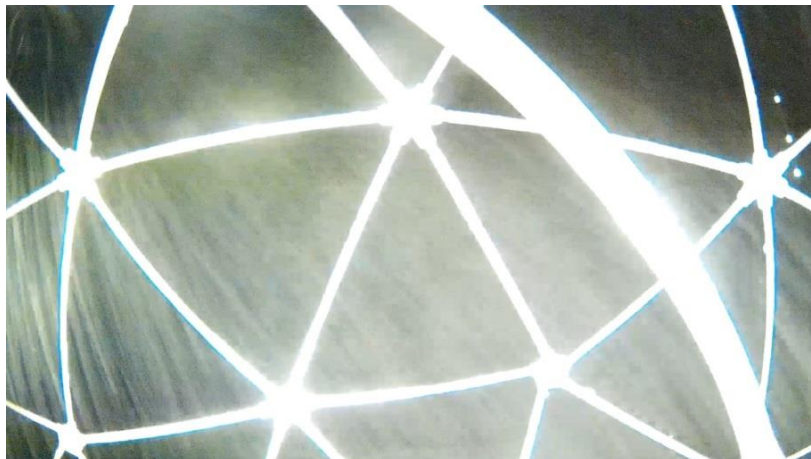


Figure 58. Live-view screenshot from the Elios while being flown in very dusty conditions underground.

Inkonova demonstrated two UAV platforms at the trials, the Ranger and the Batonomous unit. The Ranger performed exceptionally well, rated at TRL 9 (Table 8) for both hardware and software. The Ranger successfully completed all missions during the trial the obstacle detection and avoidance worked well and the unit was successfully operated BVLOS multiple times. The Ranger's IP rating was 64, based on the fact that it was observed flying through water and there was no damage or degradation of flight capability after landing in mud. It did receive minor cosmetic damage when it clipped a rib underground (Flight 3a, 895 drift, 26 August 2018) as shown in Figure 59, but subsequent flights were not impacted.



Figure 59.
Images of the
Ranger after it
clipped a rib
underground.

The Batonomous unit brought to the trials was a prototype build, rated at TRL 6 for hardware and TRL 7 for software (Table 9). The obstacle detection, point cloud generation, and navigation worked well, but a loss of communication was observed that caused the UAV to land in a puddle rather than hover and maintain position. The Batonomous prototype was rated at IP50. Its wiring, boards, and on-board processor were exposed. After landing in muddy puddle, the UAV had to be thoroughly cleaned before subsequent flights (Figure 60).

Table 9. Definitions associated with TRLs 6 to 7 (NASA, 2013).

6	System/sub-system model or prototype demonstration in a relevant environment.	A high fidelity system/component prototype that adequately addresses all critical scaling issues is built and operated in a relevant environment to demonstrate operations under critical environmental conditions.	Prototype implementations of the software demonstrated on full-scale, realistic problems. Partially integrated with existing hardware/software systems. Limited documentation available. Engineering feasibility fully demonstrated.	Documented test performance demonstrating agreement with analytical predictions.
7	System prototype demonstration in an operational environment.	A high fidelity engineering unit that adequately addresses all critical scaling issues is built and operated in a relevant environment to demonstrate performance in the actual operational environment and platform (ground, airborne, or space).	Prototype software exists having all key functionality available for demonstration and test. Well integrated with operational hardware/software systems demonstrating operational feasibility. Most software bugs removed. Limited documentation available.	Documented test performance demonstrating agreement with analytical predictions.

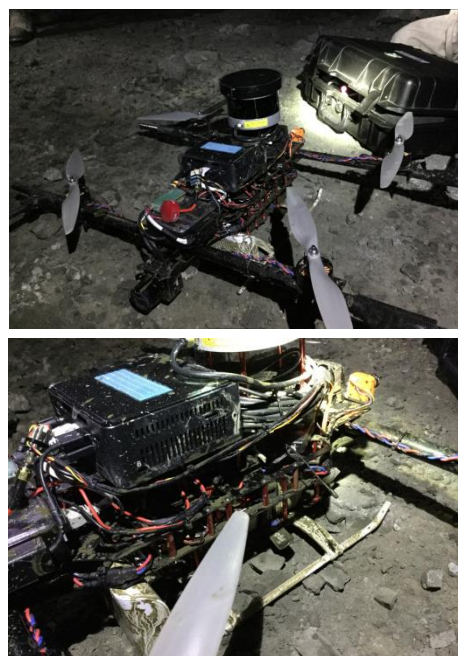


Figure 60: Images of the Batonomous
after it landed in a puddle underground.

Near Earth Autonomy demonstrated its prototype M2 system, and the hardware and software were both rated at TRL 5 (Table 7). The UAV had difficulties carrying its imagery payload and frequently entered yaw spins. Its obstacle detection is designed to work in a 2-dimensional plane and it was not successfully operated BVLOS without crashing. An IP rating of 50 was assigned, based on its exposed wiring, boards, and on-board processor, and the fact that the UAV was rendered inoperable after water dripping on the unit caused the payload to short out.

6.2.1 Safety and Risk Assessment

All new technology that is introduced into a mining environment is held to a high standard of safety. Due to the inherent hazards of working with UAVs, such as the quickly rotating propellers and potential autonomy of the system, all actions should be taken to minimize the likelihood that a collision could inflict harm to a person or cause a lost-time incident. The UAVs that were involved in the underground trials were all evaluated for the likelihood and potential impact of an incident based on observations made during the trials. The safety and risk assessment table used by Barrick, which combines likelihood and impact (cost) into a rating of low/medium/high risk, is presented in Table I.3 in Appendix I.

The obstacle detection and avoidance capabilities of Emesent's Hovermap *Standard* Payload and *Mining* Payload were both tested in a situation simulating a mine personnel approaching the UAV. In a flight that took place above ground, an obstacle (shovel) was introduced into the path of the UAV on a pre-programmed flight mission. The UAV immediately identified the obstacle and stopped moving forward. It momentarily held its position and attempted to fly around the obstacle. The obstacle was repeatedly moved in front of the path of the UAV, but it continued to maintain its distance from the obstacle. When the obstacle was removed from the flight path, the UAV resumed its mission. The obstacle sensing was also demonstrated by numerous underground flights in which the UAV avoided hanging bolts, blast lines, rope, welded wire mesh, utilities, and ventilation fans. When using *Assisted Flight with Collision Avoidance* mode, both Hovermap systems provide feedback to the pilot about the position of obstacles and actively prevents collisions by maintaining a minimum distance away from any detected obstacles. Based on the success of all attempted trials, the Hovermap platform is given a *low* risk rating. While the likelihood of an incident is extremely unlikely, with less than 5% probability of occurrence, it could cause up to a moderate amount of damage including a reportable injury or \$250-500K cash flow impact.

A demonstration of the M2 obstacle detection and avoidance system was not completed during the trials; observations were instead made during other flight trials. Due to the M2 being flown near its maximum payload, the UAV would lose control easily and enter an uncontrolled yaw spin. The M2 would have to be landed quickly when this occurred. Despite SLAM-assisted obstacle detection and avoidance, there were multiple collisions with the ribs during the trials. The M2 did use propeller guards which act as a physical barrier around the propellers during a low-velocity collision, however the propeller guards would likely break during a high-velocity collision. The M2 platform is given a *medium* risk rating based on the performance of the UAV throughout the trials. The combination of SLAM-assisted obstacle avoidance and the propeller guards make it unlikely that an incident will occur, with a 5-30% probability. However, the occurrence of an incident could cause a moderate amount of damage including a reportable injury or \$250-500K cash flow impact.

The obstacle detection and avoidance of the TiltRanger was tested underground by moving an obstacle (folding table) in front of the UAV during flight. The TiltRanger responded quickly

when the obstacle was introduced by moving away from the obstacle as it approached. As the obstacle got closer, the TiltRanger continued to move away from the obstacle, maintaining a defined distance. This method was used to test the obstacle detection in all directions. The upward obstacle detection was also tested by flying the TiltRanger upward toward the back. The TiltRanger would not fly closer than the defined distance even when the pilot was commanding it to. The obstacle detection capabilities of the Batonomous were not tested based on a malfunction early in the trial. However, the Batonomous relies on the same technology used in the TiltRanger and has the added benefit of carrying a LiDAR that is used for SLAM. Based on the demonstration of the TiltRanger, both the TiltRanger and Batonomous are given a *low* risk rating. It is extremely unlikely that an incident will occur, however an incident could have a moderate impact including a reportable injury or \$250-500K cash flow impact.

Rather than relying on a LiDAR scanner to detect obstacles, the Elios has a physical barrier between the moving parts of the UAV and the user. Throughout the trials, the carbon-fiber cage was demonstrated to be effective for minimizing any interaction between the propellers and humans, utilities, or other equipment. The Elios could be launched from a person's hands and caught in mid-flight, as long as the user kept their fingers on the outside of the cage. The Elios was even nudged against people during the trials and the cage successfully kept the propellers from doing any harm. The Flyability Elios is given a *low* risk rating based on the ease with which the UAV could be flown around people with little concern for interaction with the propellers. Although there is no automated obstacle avoidance system in place, the UAV is unlikely to do any damage if it were to collide with mine personnel or equipment. It is extremely unlikely that the Elios would be involved in an incident, and could have only an insignificant impact such as minor first aid and less than \$100K cash flow impact.

6.2.2 Summary and recommendations for future research and development

The most important lesson learned from this component of the research is the importance of having an experienced pilot: technology is not a substitute for piloting skills. Table 10 contains a summary of the important features of the different systems. The systems using LiDAR-enhanced navigation are much more powerful than the others (Ranger and Elios) but are also much more expensive. The inherent risk associated with the underground mining environment suggests that low cost systems may be attractive in some situations. The following bullets include a brief summary and recommendations based on observations during the trials:

- Emesent's Hovermap payloads performed very well. Suggestions for future improvements include decreasing the size of the platform for easier maneuverability in confined spaces, including a multi-gas detector (e.g. Industrial Scientific MX6) with readings displayed for the pilot to enhance its use for mine safety and gas monitoring, add a feature that will allow the ability of the unit to determine its starting position using resection.
- Inkonova's prototype Batonomous unit performed quite well in terms of its obstacle detection, point cloud generation, and navigation. Loss of communication when flown BVLOS caused the UAV to crash and land in a puddle, rendering the system inoperable. The communication issue needs to be addressed and the units components need better protection. Specific suggestions would be to relocate the LiDAR so that it can scan above and below the UAV, and to adjust the system to allow longer flight times.
- Near Earth Autonomy's M2 unit likely performs quite well for the conditions it was designed for, but the layout and environment at GSM proved challenging. Suggestions

include using a different UAV platform with a larger payload capacity, repositioning the LiDAR to allow scans above and below the UAV, incorporate the ability to generate a 3D map for multi-level exploration, integrate a pilot-guided exploration mode, implement faster and more sensitive reaction to obstacles as well as a higher refresh rate so that obstacles can be cleared from the map once they are out of the way of the flight mission.

Table 10. Comparison of important features of the systems evaluated.

Team	System	Flight Time (5000 ft elev.)	On-Board Lighting	Obstacle Detection System	IP Rating	BVLOS Test Success?	Risk Rating	Technology Readiness Level
Emesent	Hovermap: <i>Standard</i>	15 min	StratusLED ~13,000 lumens (sufficient)	LiDAR (VLP-16) - enabled SLAM	IP65	Yes	Low	Hardware:9 Software: 9
	Hovermap: <i>Mining</i>	15 min	StratusLED ~13,000 lumens (sufficient)	LiDAR (VLP-16) - enabled SLAM	IP65	Yes	Low	Hardware:9 Software: 8
Near Earth Autonomy	M2	3 min	N/A (insufficient)	LiDAR (VLP-16) - enabled SLAM	IP50	No	Medium	Hardware:5 Software: 5
Inkonova	Tilt Ranger	9 min	Small LEDs (sufficient)	Time-of-flight sensors	IP64	Yes	Low	Hardware:9 Software: 9
	Batomous	6 min	Small LEDs (sufficient)	LiDAR (VLP-16 & Hokuyo) - enabled SLAM	IP50	No	Low	Hardware:6 Software: 7
Flyability	Elios	6-7 min	Small LEDs (sufficient)	None; carbon fiber cage	IP64	Yes	Low	Hardware:9 Software: 9

Continuation of this component of the research would provide:

- The ability to assess, evaluate, fine-tune, and expand the system evaluation process that was based on the experiments performed during the trials.
- The opportunity to evaluate new systems and re-evaluate improvements to existing systems.

Technology is constantly improving and with it, the range of applications for the technology. UAV-based systems are the perfect example. Their use is exploding and they really have the potential to transform current methods of accomplishing tasks ranging from engineering to communications to safety and security. One barrier to the development of UAV systems for use in underground mining is that the electrical and mechanical engineers who are developing the systems are completely unfamiliar with the variety of conditions encountered at underground mines. While the DARPA Underground Challenge is providing incentive for research and development of UAVs for underground applications, the scenarios are not specifically equivalent to those in an active underground mine. This project has helped the developers make connections within the mining industry that will facilitate future development for mining applications. Another barrier is the lack of a good location in which to test the equipment. It is not easy for mining operations, particularly underground mines, to adjust their activities to allow access for research and development pursuits. Barrick was an exceptionally cooperative partner and went to great lengths to provide the best possible environment for the trials. This was very much appreciated and created a win-win-win scenario in which the Golden Sunlight Mine, the Montana Tech researchers, and the UAV system developers all were able to benefit.

6.3 Project Component 2: Photogrammetric Modeling

All of the photogrammetric software packages evaluated are high quality, commercially available products. The quality of the models constructed using the default settings does vary and is in general proportional to the cost, the quality can be adjusted by changing parameters within the software. Higher quality models can be constructed assuming that good imagery and adequate computing power are available. The tradeoff is that higher quality models are associated with much larger files that take more storage space and are more difficult to manipulate.

The georeferencing techniques used in this research (paintball marks for RGB imagery and reflective balls for LiDAR imagery) work well. Figure 61 contains a point cloud in which the reflective balls are readily observable. The public domain program CloudCompare is an excellent tool for manipulating and performing analyses on point clouds.



Figure 61. 3D point cloud in CloudCompare of the 995 intersection with the reflective survey spheres indicated.

Recommendations for future research and development

Extending this component of the research would provide the opportunity to perform more quantitative, detailed, and comprehensive comparisons. Additional software packages could be evaluated, as well, including those that provide features for geologic mapping and geotechnical characterization.

6.4 Project Component 2B: Thermal and Multispectral Image Acquisition and Modeling

Both thermal and multispectral imagery were used to generate 3D models in the underground, and they are of a quality that would allow individual structures to be mapped. Thermal imagery can be utilized for detecting loose ground and identifying adverse geological structures if there is a thermal contrast between the infill material and the host rock mass or ambient air. Multispectral imagery allows different material types to be distinguished if the materials reflect radiation that falls within specific spectral ranges visible to the imager(s), and this will be dependent upon the mine's mineralogy and lithology. At the current state of technology, multispectral imagers capture higher quality imagery than thermal imagers due to higher resolutions, making the data easier to work with for mapping and 3D model generation. Useful implementation of thermal and multispectral imagers for geotechnical and geological investigations underground is currently possible, but the body of knowledge is relatively small and could benefit from further research and case studies.

Using the NASA technology readiness levels, the DJI Zenmuse XT and MicaSense RedEdge-M were evaluated to determine if they are ready for immediate use in the underground mining environment. Both systems are considered to be at a technology readiness level "9" (Table 8), because they were successfully used in the underground mining environment to capture data that was utilized for generating 3D photogrammetric models. During this research, both imaging devices were used repeatedly without software or hardware issues in an environment for which they were not designed. Based upon observations of the thermal and multispectral imagers in the field, the ingress protection (IP) rating (detailed in Table I.2 in Appendix I) of the DJI Zenmuse XT is estimated to be IP54, while the MicaSense RedEdge-M is estimated to be IP52. The point of dust and water ingress for the Zenmuse XT is where the gimbal attaches to the M100, while for the MicaSense RedEdge-M, ingress is possible through the ports and around the seams of the camera housing. There could be further improvements in terms of compatibility with multiple UAV makes and models, a higher resolution sensor for the Zenmuse XT, and a higher ingress protection (IP) rating for the MicaSense RedEdge-M (now replaced by the RedEdge-MX which does have a higher IP rating).

A major drawback to using these devices underground in inaccessible locations is the risk of losing the device. Montana Tech's Zenmuse XT (list price \$10,000) was lost when the M100 crashed in a stope at GSM in January, 2019, and to date all attempts to recover the device have failed.

Recommendations for future research and development

Future research with thermal and multispectral imagers should include the following:

1. Case studies and further investigations, image acquisitions, modeling, and mapping in surface and underground mines/openings to develop techniques, procedures, and a body of knowledge that can be successfully used in industry. Individual sites should create a "library" of imagery utilizing existing core samples or rock exposures that can be used to identify unknown materials or conditions.
2. Routine geological and geotechnical mapping in underground headings. Capturing and combining LiDAR, RGB, thermal, and multispectral data would allow mine personnel to make more informed decisions about ore control routing, structural/lithological mapping, and hazard identification. The DJI Zenmuse XT has both an integrated RGB camera and thermal camera. LiDAR devices that embed RGB imagery with point clouds as metadata make data

management potentially easier, and further work could be completed to incorporate thermal and multispectral imagery.

3. Investigate if thermal cameras can be used as a tool to detect and identify noxious gases underground. Handheld thermal cameras could potentially be used as a tool to supplement multi-gas detectors in the field.
4. Investigate use of hyperspectral cameras in underground workings. Multispectral imagers are limited to small number of spectral ranges that can be captured and are catered more to use in agriculture. Hyperspectral imagers capture many small “slices” of the electromagnetic spectrum and can be used to further define geological materials and possibly identify subtle structures. A relatively large body of knowledge exists for using hyperspectral imagery for geological investigations, but the technology is currently limited by the physical size and cost of imagers that can be used in the field.
5. Investigation of the use of thermal imagers for obstacle detection on heavy equipment. Machinery, heavy equipment, and mine personnel typically vary in temperature compared to rock masses and shotcrete. Mobile heavy equipment could potentially utilize thermal imagers to identify obstacles, in particular mine personnel who are on foot. Thermal imagers would be deployed on each side of the equipment so that multiple fields of view could be analyzed. Processing would have to occur in real-time on the heavy equipment, and programming would be necessary to flag obstacles that differ from ambient rock/shotcrete temperatures. Extensive research and field trials may be required.

REFERENCES

- ADAM Technology (2010). How Accurate is Photogrammetry? Part 2. Retrieved from <https://www.adamtech.com.au/Blog/?p=167>
- Banke, J. (2017). Technology Readiness Levels Demystified. National Aeronautics and Space Administration, USA. Retrieved 23 October 2018 from https://www.nasa.gov/topics/aeronautics/features/trl_demystified.html
- Becker, R.E., L.J. Galayda, and M.M. MacLaughlin (2018). Digital Photogrammetry Software Comparison for Rock Mass Characterization, Proceedings of the 52nd U.S. Rock Mechanics Symposium, Seattle, WA, Paper 18-1211 (7 pp).
- Bolat, S. (2014). Technology Readiness Level (TRL) math for innovative SMEs. Istanbul, Turkey. Retrieved 23 October 2018 from <https://serkanbolat.com/2014/11/03/technology-readiness-level-trl-math-for-innovative-smes/>
- DJI (2015). Guidance User Manual. Version 1.6, 21-22. Shenzhen, China.
- DJI (2016a). DJI Matrice M100 User Manual. Version 1.6, 59, 72. Shenzhen, China. Retrieved from https://dl.djicdn.com/downloads/m100/M100_User_Manual_EN.pdf
- DJI (2016b). Zenmuse XT User Manual, Version 1.2, 17-18. Shenzhen, China.
- DJI (2017). DJI Inspire 1 User Manual (2017.12). DJI, Shenzhen, China. Retrieved from <https://www.dji.com/inspire-1/info>
- DJI (2019). Matrice M100 - Quadcopter for Developers. DJI, Shenzhen, China. Retrieved from <https://www.dji.com/matrice100>
- DSM&T (2018). IP Rating Chart. DSM&T Company, Fontana, California. Retrieved 23 October 2018 from <http://www.dsm-t.com/resources/ip-rating-chart/>
- FLIR (2017). User's Manual FLIR Cx Series. Formatted 02 May 2017. <http://support.flir.com>
- Flyability SA (2018). Elios - Inspect & Explore Indoor and Confined Spaces. EPFL Innovation Park — Building C, 1015 Lausanne, Switzerland. Retrieved 15 March 2018, from <https://www.flyability.com/elios/>
- Inkonova (2018). TILT Ranger - World's First Drone Solution for Underground Mines. Retrieved 15 March 2018 from <http://inkonova.se/tilt-ranger/>
- Iverson, S. and S. Signer (2014). Assessment and Detection of Loose Rock Hazards in Underground Metal Mines Using Thermal Imaging. 2014 SME Annual Meeting & Exhibit (SME 2014): Leadership in Uncertain Times, Salt Lake City, 23-26 February 2014. Society for Mining, Metallurgy, and Exploration, Inc., July 2014. p. 666-672. Englewood, CO
- MicaSense (2019). MicaSense RedEdge MX Professional Multispectral Sensor Kit. MicaSense, Inc. 1300 N Northlake Way, Suite 100 Seattle, WA 98103. Retrieved 20 December 2018 from <https://www.micasense.com/rededge-mx/>
- MicaSense Inc. (2017). MicaSense RedEdge-M Multispectral Camera User Manual. Rev 01-October 2017; Seattle, WA.
- NASA (2013). Subject: NASA Systems Engineering Processes and Requirements (Updated w/Change 4). Appendix E. Technology Readiness Levels. Retrieved 24 October 2018 from

https://nodis3.gsfc.nasa.gov/displayDir.cfm?Internal_ID=N_PR_7123_001B_&page_name=AppendixE

Russell, E.A. (2018). UAV-based Geotechnical Modeling and Mapping of an Inaccessible Underground Site, Montana Tech master's thesis (95 pp), available via Montana Tech's Digital Commons https://digitalcommons.mtech.edu/grad_rschr/.

Russell, E.A., M.M. MacLaughlin, and R.M. Turner (2018). UAV-based Geotechnical Modeling and Mapping of an Inaccessible Underground Site, Proceedings of the 52nd U.S. Rock Mechanics Symposium, Seattle, WA, Paper 18-516 (9 pp).

Turner, R.M., N.P. Bhagwat, L.J. Galayda, C.S. Knoll, E.A. Russell, and M.M. MacLaughlin (2018). Geotechnical Characterization of Underground Mine Excavations from UAV-Captured Photogrammetric & Thermal Imagery, Proceedings of the 52nd U.S. Rock Mechanics Symposium, Seattle, WA, Paper 18-508 (11 pp).

United States Geological Survey (1993). Geologic map of the Dillon 1 degree x 2 degrees Quadrangle, Idaho and Montana. Map. Miscellaneous Investigations Series Map I-1803-H. Reston, VA: U.S. Department of the Interior.

USGS (2017). Unmanned Aircraft Systems Data Post-Processing: Section 2-MicaSense 5-band Multispectral Imagery. USGS National UAS Project Office-March 2017. Lakewood, CO.

USGS (2018). USGS Spectroscopy Lab. <https://speclab.cr.usgs.gov/>

ACKNOWLEDGEMENTS

Montana Tech graduate students Rachel Becker, Ryan Turner, and Elizabeth Russell contributed significantly to this report. Students Charlie Linney, Micah Gregory-Lederer, Ninad Bhagwat, Jack Fitzgerald, Jay Hillygus, Cooper Knoll, and Liana Galayda, and Sam Kraha assisted with various aspects of this project. Prof. Bryce Hill and student Tyler Holliday of Montana Tech's Electrical Engineering department contributed expertise for development of the autonomous technologies. Dr. M.H. Zaluski generously provided access to facilities for indoor test flights. Dr. Beverly Hartline, Vice Chancellor for Research & Graduate Studies, provided immense support.

Barrick Gold Corporation's Golden Sunlight Mine and underground contractor Redpath Mining helped to make this project possible by providing a safe site for the fieldwork. D. Banghart, C. Mortensen, S. Thiam, B. Dale, and S. Friesz of the Golden Sunlight Mine provided technical support and allowed this research to happen. T. Allen, T. South, B. Bowman, J. Brown, S. Chabot, K. Osborne, E. Ryan, B. Morgan, and C. Finlay of J.S. Redpath helped considerably with facilitating the underground work. Gerald Rosas of Barrick Gold was instrumental in the business communications between the UAV demonstration teams, Barrick, and Montana Tech.

This project relied on the generous cooperation of the demonstration participants and contacts:

Emesent: Stefan Hrabar, Farid Kendou, Glenn Wagner

Near Earth Autonomy: Patrick DeFranco, Tamir Klaff, David Murphy, Ji Zhang

Inkonova: Ahmed AlNomaly, Camil Muresan, José Manuel Castaño Domínguez, José Maria Navarro

Flyability: Nicholas Rey, Patrick Thevoz

Special thanks to Matt McKinnon of Unmanned Aerial Services Incorporated.

The assistance of NIOSH researcher Stephen Iverson was instrumental in establishing a procedure for analysis of the thermal data.

APPENDIX A: UAV SYSTEMS AND COMPONENTS

Table A.1. Mass and cost of M100 and accessories.

Component	Mass (g)	Cost	Notes
Structure			
M100	1755	\$3,299	Mass is whole unit without battery
GPS	-	\$599	
Expansion Bay	45	\$62	
Propulsion System			
Motors (DJI 3510)	212/pair	\$109/pair	
Propellers (DJI 1345s)	91/pair	\$15/pair	
Propeller Guards	200	\$43	Not included with M100
Battery			
Battery Compartment	160	\$139	
Intelligent Flight Battery (TB47D)	600	\$189	
Intelligent Flight Battery (TB48D)	676	\$219	Not included with M100
Guidance System			
Guidance Sensors	337	\$1,249	Not included with M100
Connector Kit	-	\$79	Not included with M100
Zenmuse X3			
Camera and Gimbal	247	\$459	Not included with M100
Gimbal Installation Kit	-	\$62	Not included with M100
Remote Controller			
Remote Controller	-	\$539	

Table A.2. Components and cost of custom built heavy lifting UAV.

Component	Mass (g)	Cost	Notes
Structure			
Vulcan Black Widow X8 950	1500	\$1,864.35	Mass of X8 chassis only
Propulsion System			
Motors (KDE 5215XF 330KV) – 8x total	2880	\$1,559.60	Eight (8) motors required
Propellers (KDE 18.5x6.3x3 Carbon w/ Hubs)	587.2	\$871.40	Four (4) propellers required
Battery			
Lumenier 6s 10000mAh Batteries – 2x total	2490.0	\$359.98	Two (2) batteries required
Electronics			
Electronic Speed Controller (KDE Direct KDEXF-UAS75HVC) – 8x total	624	\$1,191.60	Eight (8) ESCs required
Device Manager (KDE Direct Device Manager KDEXF-DMA)	0	\$17.95	
Wiring, battery connector, and accessories	840	\$299.96	
Flight Controller and Remote Control			
DJI A3 Flight Controller	186.0	\$899.99	
DJI Lightbridge 2	70.0	\$999.00	
Total	9177.2	\$8,023.86	

APPENDIX B: LISTS & DETAILS OF FLIGHTS CONDUCTED (SUMMER 2018)

Videos for these flights will be posted on https://digitalcommons.mtech.edu/geol_engr/

Team: Emesent									
Date	Time	Platform	Flight Location	Length	Imagery		Models Constructed		
					Imaging Device	File Type	Agisoft	Bentley	Pix4D
15 July 2018	n/a	Standard Payload	Surface Lawn	2 min	-	-	-	-	-
	n/a	Standard Payload	Surface Wash Bay	3 min	-	-	-	-	-
	n/a	Standard Payload	Surface Wash Bay	5 min	-	-	-	-	-
16 July 2018	n/a	Standard Payload	Lower SAM	5 min	Zenmuse X3	.MP4	Y	-	-
	n/a	Standard Payload	Lower SAM	3 min	-	-	Y	-	-
17 July 2018	10:00a	Mining Payload	Lower SAM	1.5 min	Zenmuse X3 and GoPro	.MP4	Y	-	-
	10:30a	Mining Payload	Lower SAM	2 min	Zenmuse X3 and GoPro	.MP4	Y	-	-
	11:30	Mining Payload	Lower SAM	5 min	Zenmuse X3 and GoPro	.MP4	Y	-	-
	2:00p	Mining Payload	995-480 Drift	3 min	Zenmuse X3 and GoPro	.MP4	Y	-	-
	2:15p	Mining Payload	995-480 Drift	9 min	Zenmuse X3 and GoPro	.MP4	Y	-	-
	4:00p	Mining Payload	Lower SAM	11.5 min	Zenmuse X3 and GoPro	.MP4	Y	-	-
	4:15p	Mining Payload	Lower SAM	5.5 min	Zenmuse X3 and GoPro	.MP4	Y	-	-
18 July 2018	n/a	Mining Payload	735-102 Stope	5 min	GoPro	.MP4	Y	-	-
	n/a	Mining Payload	735-102 Stope	7.5 min	GoPro	.MP4	Y	-	-
	n/a	Standard Payload	895-102 Stope	3.5 min	-	-	-	-	-
	n/a	Standard Payload	895-102 Stope	7 min	Zenmuse X3	.MP4	Y	-	-
	n/a	Standard Payload	735-102 Stope	8.5 min	Zenmuse X3	.MP4	Y	-	-
19 July 2018	n/a	Standard Payload	895-945 Stope	5 min	-	-	-	-	-
	n/a	Standard Payload	735-102 Stope	2 min	-	-	-	-	-
	n/a	Standard Payload	735-102 Stope	3 min	-	-	-	-	-
	n/a	Standard Payload	735-102 Stope	4 min	-	-	-	-	-

Team: Near Earth Autonomy									
Date	Time	Platform	Flight Location	Length	Imagery		Models Constructed		
					Imaging Device	File Type	Agisoft	Bentley	Pix4D
31 July 2018	10:30a	M2	Lower SAM	0.5 min	Zenmuse X3	-	-	-	-
	10:50a	M2	Lower SAM	4 min	-	-	-	-	-
	11:08a	M2	Lower SAM	1 min	-	-	-	-	-
	11:15a	M2	Lower SAM	6 min	-	-	-	-	-
	11:35a	M2	Lower SAM	0.5 min	Zenmuse X3	-	-	-	-
	11:40a	M2	Lower SAM	1 min	Zenmuse X3	-	-	-	-
	11:50a	M2	Lower SAM	2 min	GoPro	.MP4	Y	Y	Y
	12:13p	M2	Lower SAM	0.5 min	GoPro	-	-	-	-
	12:18p	M2	Lower SAM	3 min	GoPro	.MP4	Y	Y	Y
	12:25p	M2	Lower SAM	3 min	GoPro	.MP4	Y	Y	Y
	2:00p	M2	995 Drift	2 min	GoPro	-	-	-	-
	2:08p	M2	995 Drift	3.5 min	GoPro	-	-	-	-
01 Aug 2018	11:01a	M2	Surface Wash Bay	0.5 min	-	-	-	-	-
	1:30p	M2	995 to 895 Drift	10 min	-	-	-	-	-
	1:54p	M2	895-945 Stope Scan	2 min	-	-	-	-	-

Team: Flyability									
Date	Time	Platform	Flight Location	Length	Imagery		Models Constructed		
					Imaging Device	File Type	Agisoft	Bentley	Pix4D
13 Sept 2018	10:44a	Undisclosed	895 Drift	7 min	1080 HD	.MP4	Y	Y	-
	11:16a	Elios	895-102 Stope	7.5 min	1080 HD	.MP4	-	-	-
	12:04p	Elios	750-735 Stope	5 min	1080 HD	.MP4	-	-	-
	12:31p	Elios	750-735 Stope	6 min	1080 HD	.MP4	Y	Y	Y
	1:03p	Elios	750-735 Stope	5 min	1080 HD	.MP4	-	-	-
	1:24p	Elios	750-735 Stope	6.5 min	1080 HD	.MP4	-	-	-
	1:35p	Elios	735 Drift	6.5 min	1080 HD	.MP4	-	-	-
	1:53p	Undisclosed	735 Drift	6 min	1080 HD	.MP4	Y	-	-
	2:10p	Undisclosed	735 Drift	8 min	1080 HD	.MP4	Y	Y	Y
	2:20p	Elios	735 Drift	5 min	1080 HD	.MP4	-	-	-
	2:55p	Undisclosed	995-945 Stope	1 min	1080 HD	.MP4	Y	-	-
14 Sept 2018	10:45a	Undisclosed	895-102 Stope	2 min	1080 HD	.MP4	Y	-	-
	10:55a	Undisclosed	895-102 Stope	3 min	1080 HD	.MP4	Y	-	-
	12:00p	Elios	895 Ventilation Raise	5 min	1080 HD	.MP4	-	-	-
	12:15p	Undisclosed	895 Ventilation Raise	5 min	1080 HD	.MP4	Y	Y	Y
	1:20p	Undisclosed	735-102 Stope	5 min	1080 HD	.MP4	Y	Y	Y
	1:37p	Undisclosed	735-102 Stope	6 min	1080 HD	.MP4	Y	-	-
	1:50p	Elios	735 Drift	5 min	1080 HD	.MP4	-	-	-

Team: Inkonova									
Date	Time	Platform	Flight Location	Length	Imagery		Models Constructed		
					Imaging Device	File Type	Agisoft	Bentley	Pix4D
26 Aug 2018	12:45p	Batonomous	895 Drift	3 min	-	-	-	-	-
	1:05p	Batonomous	895 Drift	2 min	-	-	-	-	-
	2:05p	Ranger	895 Drift	2 min	GoPro Hero 3+	.MP4	-	-	-
	2:15p	Ranger	895 Drift	1.5 min	GoPro Hero 3+	.MP4	-	-	-
	2:18p	Ranger	895 Drift	1.5 min	GoPro Hero 3+	.MP4	-	-	-
	2:35p	Ranger	895 Drift	1.5 min	GoPro Hero 3+	.MP4	Y	Y	Y
	2:40p	Ranger	895 Drift	1.5 min	GoPro Hero 3+	.MP4	-	-	-
	2:50p	Ranger	895 Drift	1 min	GoPro Hero 3+	.MP4	Y	Y	-
	2:55p	Ranger	895 Drift	0.5 min	GoPro Hero 3+	.MP4	Y	Y	-
27 Aug 2018	9:00a	Batonomous	Wash Bay	1.5 min	-	-	-	-	-
	12:40p	Batonomous	895 Drift	3 min	-	-	-	-	-
	1:12p	Batonomous	895 Drift	0.5 min	-	-	-	-	-
	2:20p	Ranger	750-735 Stope	5 min	GoPro Hero 3+	.MP4	-	-	-
	2:52p	Ranger	750-735 Stope	1 min	GoPro Hero 3+	.MP4	-	-	-
	2:53p	Ranger	750-735 Stope	2.5 min	GoPro Hero 3+	.MP4	Y	-	-
	3:23p	Ranger	750-735 Stope	1.5 min	GoPro Hero 3+	.MP4	Y	Y	Y
	3:26p	Ranger	750 Drift	3 min	GoPro Hero 3+	.MP4	Y	Y	Y

Team: Unmanned Aerial Services (UAS)									
Date	Time	Platform	Flight Location	Length	Imagery		Models Constructed		
					Imaging Device	File Type	Agisoft	Bentley	Pix4D
10 Sep 2018	n/a	Hovermap Std Payload	102 Stope	5 min	Zenmuse X3	.MOV	Y	-	-
11 Sep 2018	n/a	Hovermap Std Payload	102 Stope	9.5 min	Zenmuse X3	.MOV	Y	Y	Y
	n/a	Hovermap Std Payload	735 Stope	7 min	Zenmuse X3	.MOV	Y	Y	Y
	n/a	Hovermap Std Payload	735 Stope	7 min	Zenmuse X3	.MOV	Y	-	Y

Team: Montana Tech									
Date	Time	Platform	Flight Location	Length	Imagery		Models Constructed		
					Imaging Device	File Type	Agisoft	Bentley	Pix4D
01 Mar 2018	n/a	M100	815 Drift	-	Zenmuse X3	.MP4	Y	Y	
18 Mar 2018	n/a	M100	375 Intersection	-	Zenmuse XT	.MP4	Y	-	-
14 June 2018	n/a	M100	375 Intersection	-	Zenmuse XT	.MP4	Y	-	-
13 July 2018	n/a	M100	375 Drift	-	Zenmuse X3	.MP4	Y	-	-
09 Aug 2018	n/a	M100	945 Stope	-	Zenmuse X3	.MP4	Y	-	-
31 Aug 2018	n/a	M100	735 Stope	3.5 min	Zenmuse X3	.MP4	Y	-	-

APPENDIX C: COMPUTING RESOURCES

Installation of each of the software packages requires a modern PC with a 64-bit operating system (Windows 8, 10, Server 2008, or Server 2012) or a Mac computer running Boot Camp. The system requirements for photogrammetry processing vary depending on the computational demands of the project and the performance demands of the user, and processing time can vary considerably between different computer systems. While the stated minimum and recommended system requirements differed between the software manufacturers, the following hardware specifications may be regarded as the minimum system capabilities required to effectively process photogrammetry models across the three software packages:

- CPU: Quad-core CPU minimum, Hexa-Core or Octa-Core CPU or better preferred (ie. Intel Core i7, i9, Xeon, etc.);
- RAM: 8 GB minimum, 16 GB or better preferred;
- Hard Disk: Fast Hard Disk Drive (HDD) with ~60GB free space minimum; Solid State Drive (SSD) preferred;
- GPU: Nvidia GeForce GTX 980 or better (GTX 1080, Titan X, etc.).

The following computer systems and hardware configurations were used during the project for the indicated photogrammetry model processing and computing tasks:

Lenovo ThinkStation (Barrick Gold Corp.) Quantity: 1

- OS: Windows 10 Enterprise
- CPU: Intel Xeon CPU E5-2620 v4 @ 2.1GHz (Octa-Core)
- RAM: 64 GB
- Hard Disk: 256 GB SSD
- GPU: Nvidia Quadro M4000

Uses: Photogrammetry modeling – RGB, thermal and multispectral imagery (Agisoft PhotoScan Professional 1.4.5); FLIR Tools.

Dell Precision T5500 (Montana Tech) Quantity: 2

- OS: Windows 7 Enterprise
- CPU: Intel Xeon CPU E5620 @ 2.40 GHz (Quad-Core)
- RAM: 12 GB
- Hard Disk: 500 GB HDD
- GPU: Nvidia Quadro 6000

Uses: Photogrammetry modeling - RGB (Pix4Dmapper 4.3.31, Agisoft PhotoScan Professional 1.4.5, Bentley ContextCapture 4.4.8.561)



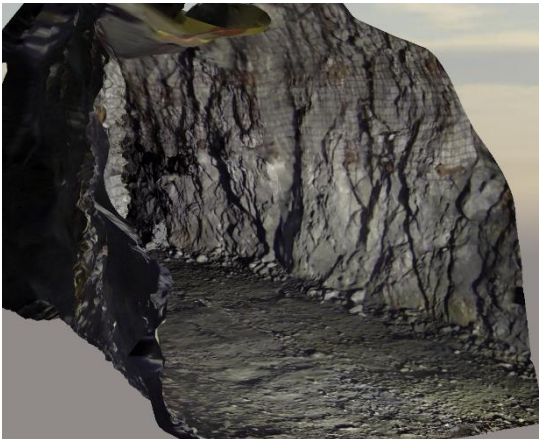
Dell Precision 5810 (Montana Tech) Quantity: 1

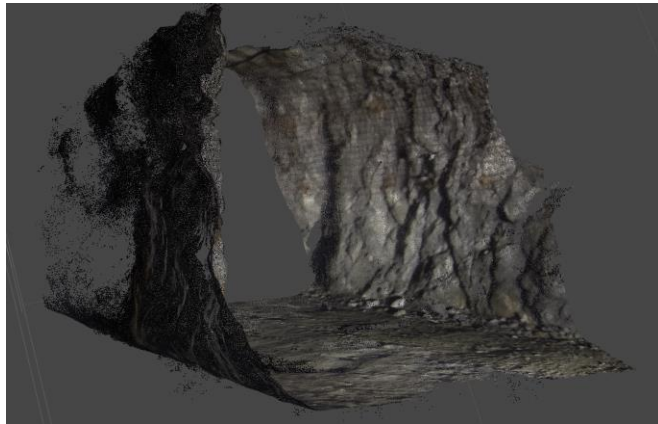
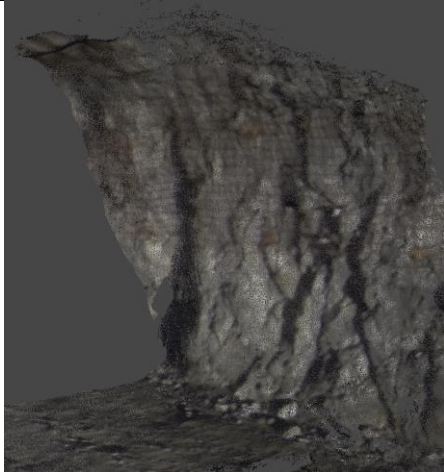
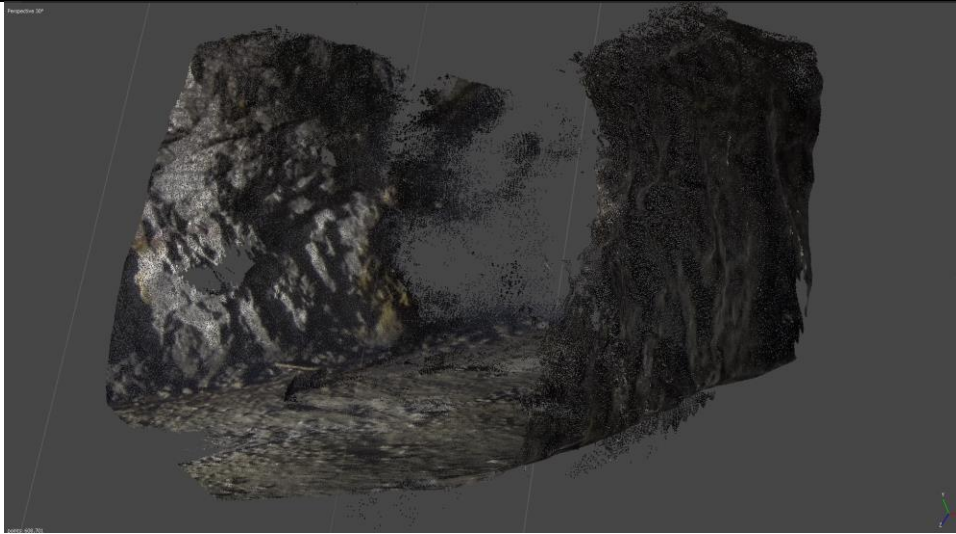
- OS: Windows 10 Enterprise
- CPU: Intel Xeon CPU ES-1620 v3 @ 3.5 GHz (Quad-Core)
- RAM: 16 GB
- Hard Disk: 500 GB HDD
- GPU: Nvidia Quadro M2000

Uses: Photogrammetry modeling - RGB (Pix4Dmapper 4.3.31, Bentley ContextCapture 4.4.8.561)

APPENDIX D: SUMMARIES OF PHOTOGRAMMETRIC MODELS (SUMMER 2018)

This appendix contains summaries of 36 3D photogrammetric models created for this study, using imagery collected using a number of different UAV platforms, and created with three different software packages (Agisoft PhotoScan, Bentley ContextCapture, and Pix4Dmapper).

NEAR EARTH AUTONOMY: FLIGHT 6, LOWER SAM DRIFT – JULY 31, 2018	
BENTLEY CONTEXTCAPTURE	
	
	
CAMERA: 1280 x 720 (RGB)	KEYPOINTS PER IMAGE (MEDIAN): 5,583
IMAGES (TOTAL): 233	TIE POINTS PER IMAGE (MEDIAN): 1,443
IMAGES (CALIBRATED): 218	TIME FOR INITIAL PROCESSING (HR:MIN:SEC): 00:15:54

NEAR EARTH AUTONOMY: FLIGHT 6, LOWER SAM – JULY 31, 2018**AGISOFT PHOTOSCAN VERSION 1.4.3 (64 BIT)****IMAGE RESOLUTION: 1280 X 720 (RGB)
(GoPro HERO 3-VIDEO CAPTURE)****AVG. DENSITY (PER CUBIC METER): N/A****IMAGES (TOTAL): 258****KEYPOINTS PER IMAGE (LIMIT): 40,000****IMAGES (CALIBRATED): 258****MATCHES PER CALIBRATED IMAGE (LIMIT): 4,000****RMS REPROJECTION ERROR (PIXELS):
0.977676****MAX REPROJECTION ERROR (PIXELS): 38.3162****NO. OF 3D DENSIFIED POINTS: 608,701
(MEDIUM QUALITY DENSE CLOUD)****TIME FOR INITIAL PROCESSING (HR:MIN:SEC): 0 HOURS: 20
MINUTES: 11 SECONDS (CPU: INTEL® XEON® CPU-E5-2620 v4
@ 2.1GHZ, 63.9 GB RAM, OPENGL RENDERER: NVIDIA
QUADRO M4000/PCIe/SSE2**

NEAR EARTH AUTONOMY: FLIGHT 6, LOWER SAM - JULY 31, 2018

PIX4DMAPPER



CAMERA: 1920 x 1080 (RGB)

AVG. POINT DENSITY (PER CUBIC METER): 295.65

IMAGES (TOTAL): 448

KEYPOINTS PER IMAGE (MEDIAN): 113,713

IMAGES (CALIBRATED): 448

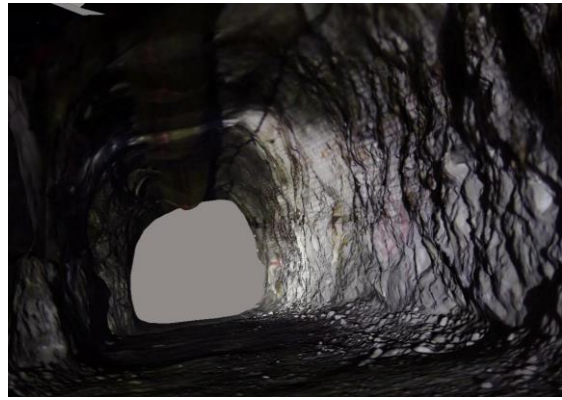
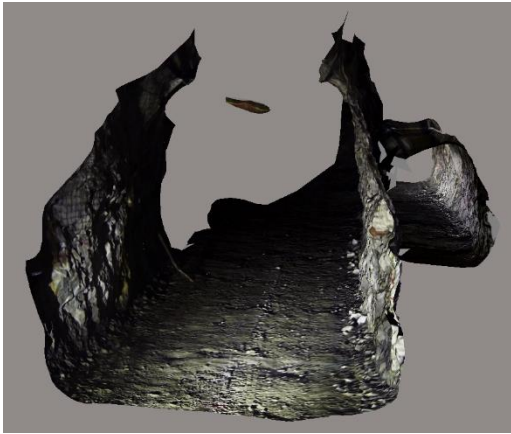
MATCHES PER CALIBRATED IMAGE (MEDIAN): 4,423

NO. OF 3D DENSIFIED POINTS: 1,819,472

TIME FOR INITIAL PROCESSING (HR:MIN:SEC): 1:59:45

NEAR EARTH AUTONOMY: FLIGHT 7B, LOWER SAM DRIFT – JULY 31, 2018

BENTLEY CONTEXTCAPTURE



CAMERA: 1280 x 720 (RGB)

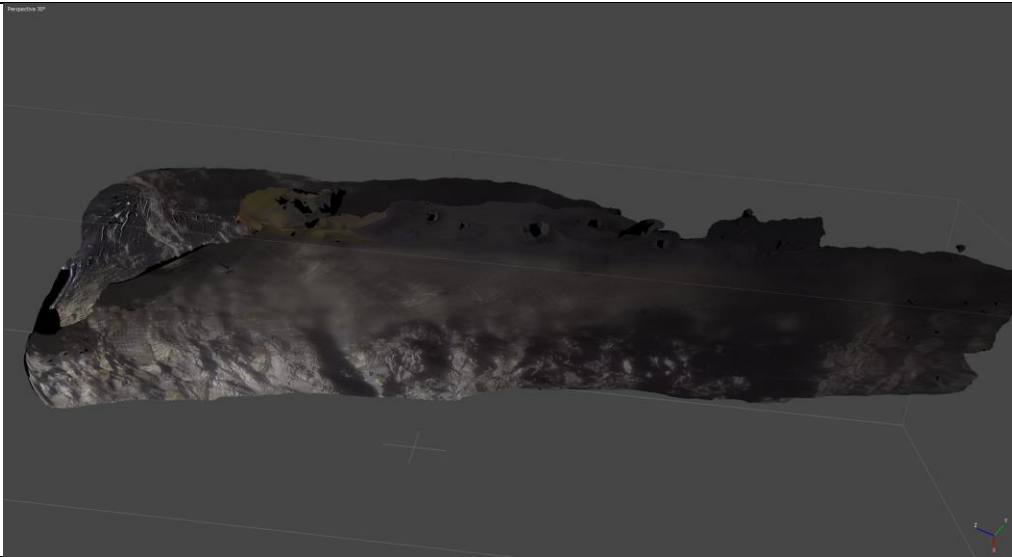
KEYPOINTS PER IMAGE (MEDIAN): 4,919

IMAGES (TOTAL): 171

TIE POINTS PER IMAGE (MEDIAN): 754

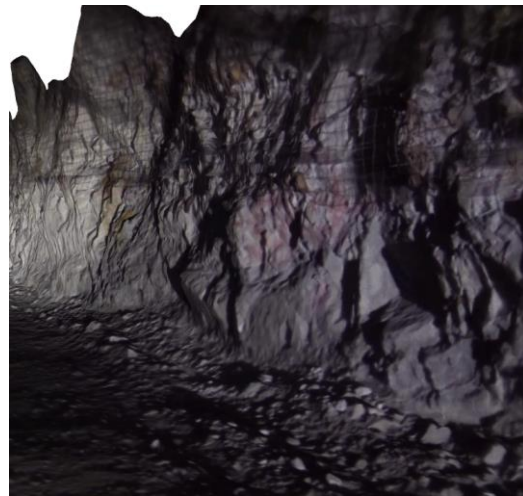
IMAGES (CALIBRATED): 105

TIME FOR INITIAL PROCESSING (HR:MIN:SEC): 00:06:08

NEAR EARTH AUTONOMY: FLIGHT 7B, LOWER SAM – JULY 31, 2018**AGISOFT PHOTOSCAN VERSION 1.4.3 (64 BIT)****IMAGE RESOLUTION: 1280 X 720 (RGB)
(GoPro HERO 3-VIDEO CAPTURE)****AVG. DENSITY (PER CUBIC METER): N/A****IMAGES (TOTAL): 101****KEYPOINTS PER IMAGE (LIMIT): 40,000****IMAGES (CALIBRATED): 101****MATCHES PER CALIBRATED IMAGE (LIMIT): 4,000****RMS REPROJECTION ERROR (PIXELS):
0.649225****MAX REPROJECTION ERROR (PIXELS): 17.2284****NO. OF 3D DENSIFIED POINTS: 1,716,010
(HIGH QUALITY DENSE CLOUD)****TIME FOR INITIAL PROCESSING (HR:MIN:SEC): 0 HOURS: 8
MINUTES: 12 SECONDS (CPU: INTEL® XEON® CPU-E5-2620
v4 @ 2.1GHZ, 63.9 GB RAM, OPENGL RENDERER: NVIDIA
QUADRO M4000/PCIe/SSE2)**

NEAR EARTH AUTONOMY: FLIGHT 7B, LOWER SAM - JULY 31, 2018

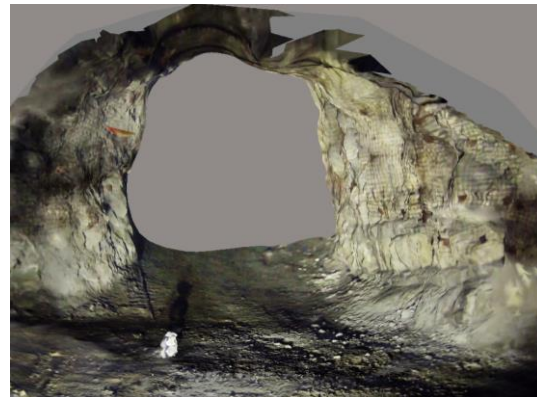
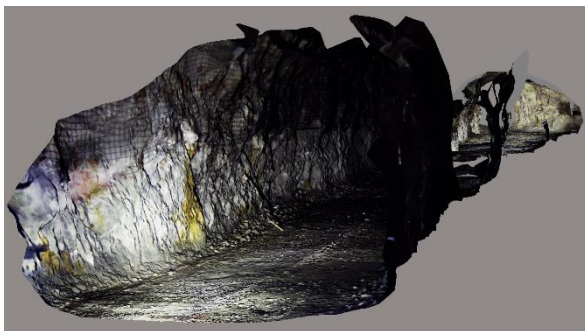
PIX4DMAPPER



CAMERA: 1280 x 720 (RGB)	AVG. POINT DENSITY (PER CUBIC METER): 19.48
IMAGES (TOTAL): 319	KEYPOINTS PER IMAGE (MEDIAN): 18,242
IMAGES (CALIBRATED): 203	MATCHES PER CALIBRATED IMAGE (MEDIAN): 5,071
NO. OF 3D DENSIFIED POINTS: 527,644	TIME FOR INITIAL PROCESSING (HR:MIN:SEC): 1:06:35

NEAR EARTH AUTONOMY: FLIGHT 7C, LOWER SAM DRIFT – JULY 31, 2018

BENTLEY CONTEXTCAPTURE



CAMERA: 1280 x 720 (RGB)

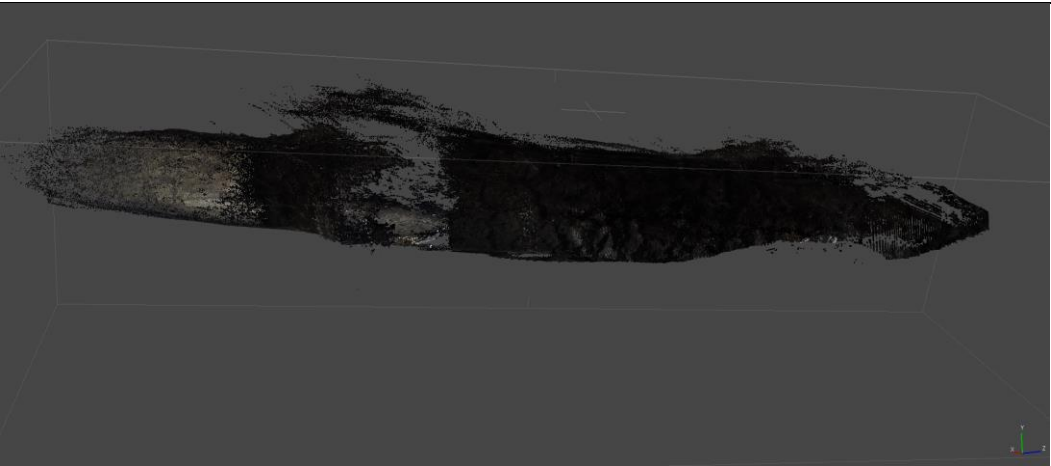

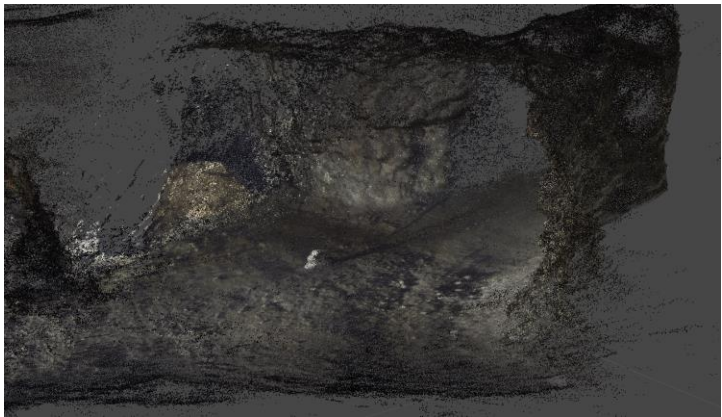
KEYPOINTS PER IMAGE (MEDIAN): 5,712

IMAGES (TOTAL): 347

TIE POINTS PER IMAGE (MEDIAN): 1,468

IMAGES (CALIBRATED): 293

TIME FOR INITIAL PROCESSING (HR:MIN:SEC): 00:31:42

NEAR EARTH AUTONOMY: FLIGHT 7c, LOWER SAM – JULY 31, 2018	
AGISOFT PHOTOSCAN VERSION 1.4.3 (64 BIT)	
	
	
IMAGE RESOLUTION: 1280 X 720 (RGB) (GoPro HERO 3-VIDEO CAPTURE)	AVG. DENSITY (PER CUBIC METER): N/A
IMAGES (TOTAL): 681	KEYPOINTS PER IMAGE (LIMIT): 40,000
IMAGES (CALIBRATED): 681	MATCHES PER CALIBRATED IMAGE (LIMIT): 4,000
RMS REPROJECTION ERROR (PIXELS): 1.0805	MAX REPROJECTION ERROR (PIXELS): 34.6118
NO. OF 3D DENSIFIED POINTS: 3,038,161 (MEDIUM QUALITY DENSE CLOUD)	TIME FOR INITIAL PROCESSING (HR:MIN:SEC): 2 HOURS: 35 MINUTES: 3 SECONDS (CPU: INTEL® XEON® CPU-E5-2620 v4 @ 2.1GHz, 63.9 GB RAM, OpenGL RENDERER: NVIDIA QUADRO M4000/PCIe/SSE2)

NEAR EARTH AUTONOMY: FLIGHT 7C, LOWER SAM - JULY 31, 2018

PIX4DMAPPER



CAMERA: 1920 x 1080 (RGB)

AVG. POINT DENSITY (PER CUBIC METER): 612.76

IMAGES (TOTAL): 575

KEYPOINTS PER IMAGE (MEDIAN): 13,957

IMAGES (CALIBRATED): 570

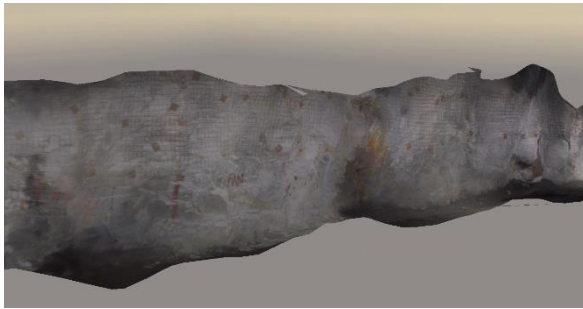
MATCHES PER CALIBRATED IMAGE (MEDIAN): 5,704

NO. OF 3D DENSIFIED POINTS: 2,611,884


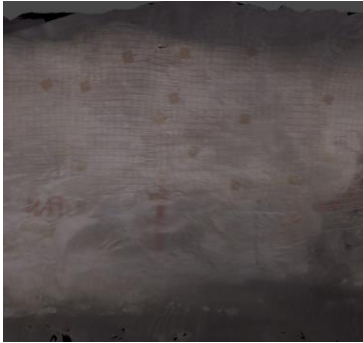
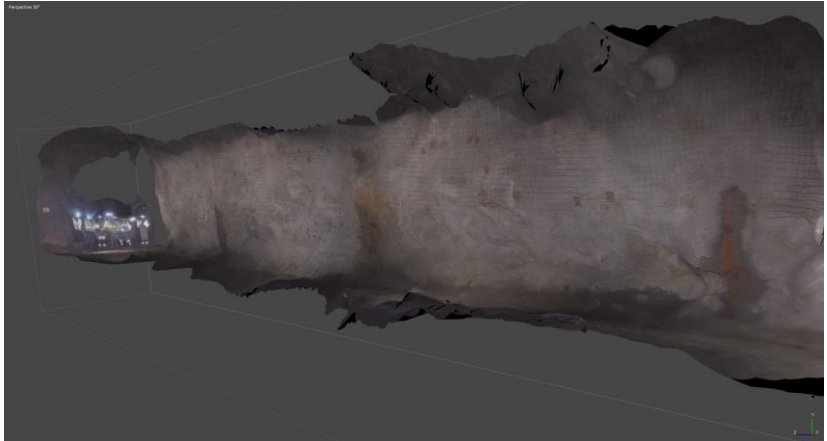
TIME FOR INITIAL PROCESSING (HR:MIN:SEC): 2:23:13




INKONOVA: FLIGHT 5, 895 DRIFT – AUGUST 26, 2018

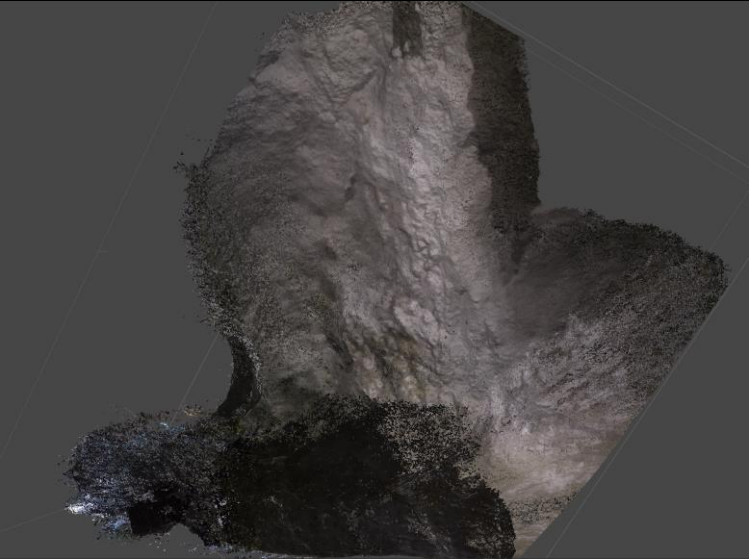


BENTLEY CONTEXTCAPTURE



CAMERA: 1280 x 720 (RGB)	KEYPOINTS PER IMAGE (MEDIAN): 5,009
IMAGES (TOTAL): 322	TIE POINTS PER IMAGE (MEDIAN): 485
IMAGES (CALIBRATED): 138	TIME FOR INITIAL PROCESSING (HR:MIN:SEC): 00:12:26

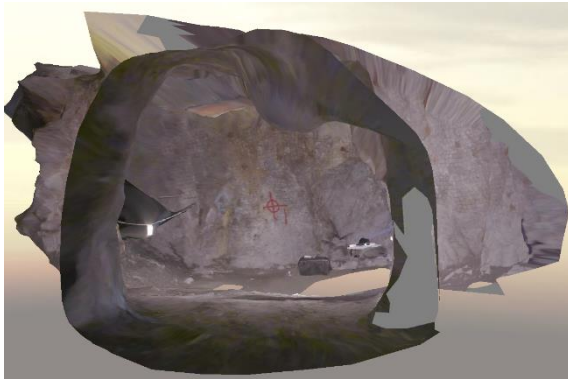
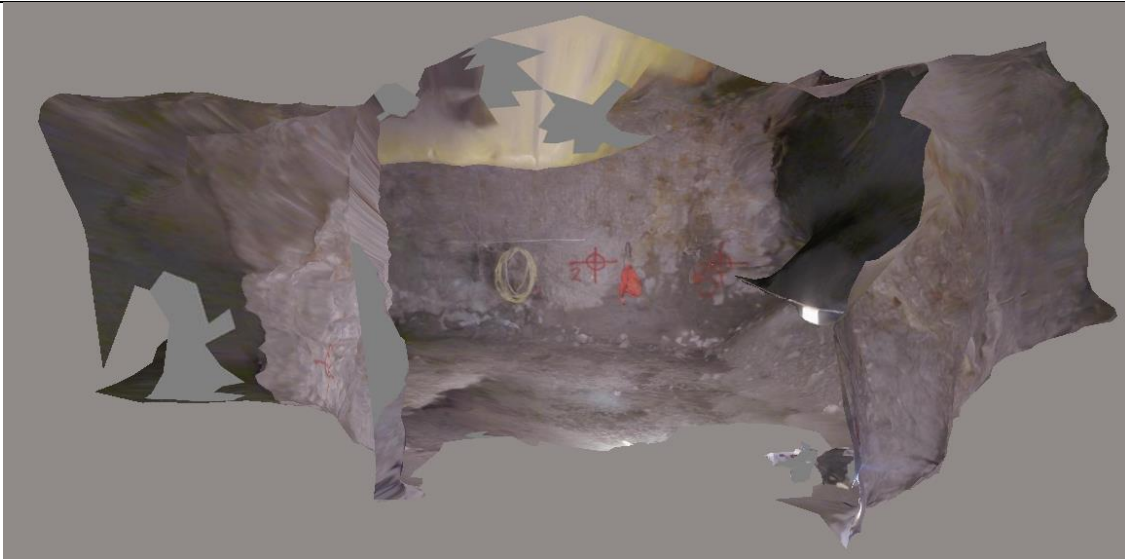
INKONOVA: FLIGHT 5, 895 DRIFT – AUGUST 26, 2018	
AGISOFT PHOTOSCAN VERSION 1.4.3 (64 BIT)	
	
	
IMAGE RESOLUTION: 1920 X 1080 (RGB) (GoPro HERO 3-VIDEO CAPTURE)	AVG. DENSITY (PER CUBIC METER): N/A
IMAGES (TOTAL): 181	KEYPOINTS PER IMAGE (LIMIT): 40,000
IMAGES (CALIBRATED): 181	MATCHES PER CALIBRATED IMAGE (LIMIT): 4,000
RMS REPROJECTION ERROR (PIXELS): 2.11597	MAX REPROJECTION ERROR (PIXELS): 423.605
NO. OF 3D DENSIFIED POINTS: 3,356,572 (HIGH QUALITY DENSE CLOUD)	TIME FOR INITIAL PROCESSING (HR:MIN:SEC): 0 HOURS: 4 MINUTES: 42 SECONDS (CPU: INTEL ® XEON ® CPU-E5-2620 V4 @ 2.1GHz, 63.9 GB RAM, OPENGL RENDERER: NVIDIA QUADRO M4000/PCIe/SSE2)

INKONOVA: FLIGHT 5, 895 DRIFT – AUGUST 26, 2018	
PIX4DMAPPER	
	
	
CAMERA: 1280 x 720 (RGB)	AVG. POINT DENSITY (PER CUBIC METER): 11,059
IMAGES (TOTAL): 136	KEYPOINTS PER IMAGE (MEDIAN): 18,078
IMAGES (CALIBRATED): 30	MATCHES PER CALIBRATED IMAGE (MEDIAN): 3,154
NO. OF 3D DENSIFIED POINTS: 115,982	TIME FOR INITIAL PROCESSING (HR:MIN:SEC): 0:38:22

INKONOVA: FLIGHT 7, 735 STOPE – AUGUST 27, 2018	
AGISOFT PHOTOSCAN VERSION 1.4.3 (64 BIT)	
	
	
IMAGE RESOLUTION: 1920 X 1080 (RGB) (GoPro HERO 3-VIDEO CAPTURE)	AVG. DENSITY (PER CUBIC METER): N/A
IMAGES (TOTAL): 1042	KEYPOINTS PER IMAGE (LIMIT): 40,000
IMAGES (CALIBRATED): 1042	MATCHES PER CALIBRATED IMAGE (LIMIT): 4,000
RMS REPROJECTION ERROR (PIXELS): 1.52968	MAX REPROJECTION ERROR (PIXELS): 45.5009
NO. OF 3D DENSIFIED POINTS: 2,739,436 (MEDIUM QUALITY DENSE CLOUD)	TIME FOR INITIAL PROCESSING (HR:MIN:SEC): 3 HOURS: 54 MINUTES: 47 SECONDS (CPU: INTEL® XEON® CPU-E5-2620 V4 @ 2.1GHZ, 63.9 GB RAM, OPENGL RENDERER: NVIDIA QUADRO M4000/PCIe/SSE2)

INKONOVA: FLIGHT 8, – AUGUST 27, 2018

BENTLEY CONTEXTCAPTURE



CAMERA: 1280 x 720 (RGB)

KEYPOINTS PER IMAGE (MEDIAN): 5,156

IMAGES (TOTAL): 202

TIE POINTS PER IMAGE (MEDIAN): 439

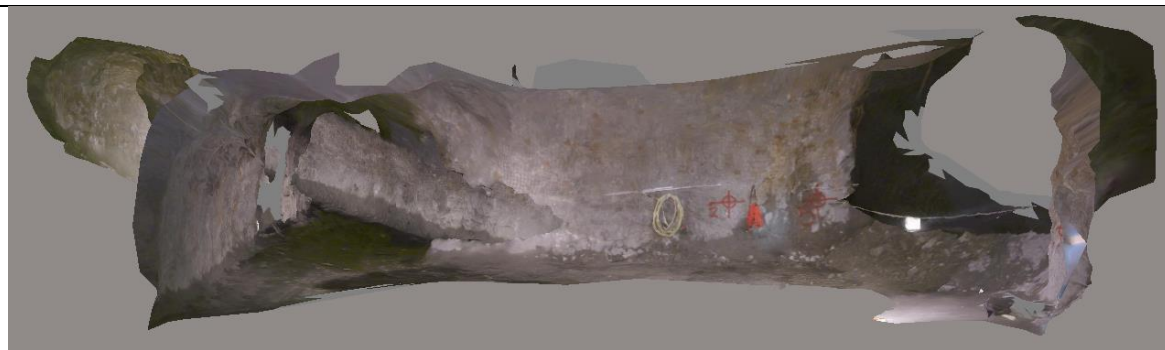
IMAGES (CALIBRATED): 202

TIME FOR INITIAL PROCESSING (HR:MIN:SEC): 00:16:27

INKONOVA – FLIGHT 8 (DENSIFIED POINT CLOUD + TRIANGLE MESH) – AUGUST 27, 2018**PIX4DMAPPER****CAMERA: 1280 x 720 (RGB)****AVG. POINT DENSITY (PER CUBIC METER): 0.08****IMAGES (TOTAL): 158****KEYPOINTS PER IMAGE (MEDIAN): 18,739****IMAGES (CALIBRATED): 158****MATCHES PER CALIBRATED IMAGE (MEDIAN): 3,950****NO. OF 3D DENSIFIED POINTS: 318,607****TIME FOR INITIAL PROCESSING (HR:MIN:SEC):
0:51:03**

INKONOVA: FLIGHT 9, – AUGUST 27, 2018

BENTLEY CONTEXTCAPTURE



CAMERA: 1280 x 720 (RGB)

KEYPOINTS PER IMAGE (MEDIAN): 5,172

IMAGES (TOTAL): 345

TIE POINTS PER IMAGE (MEDIAN): 809

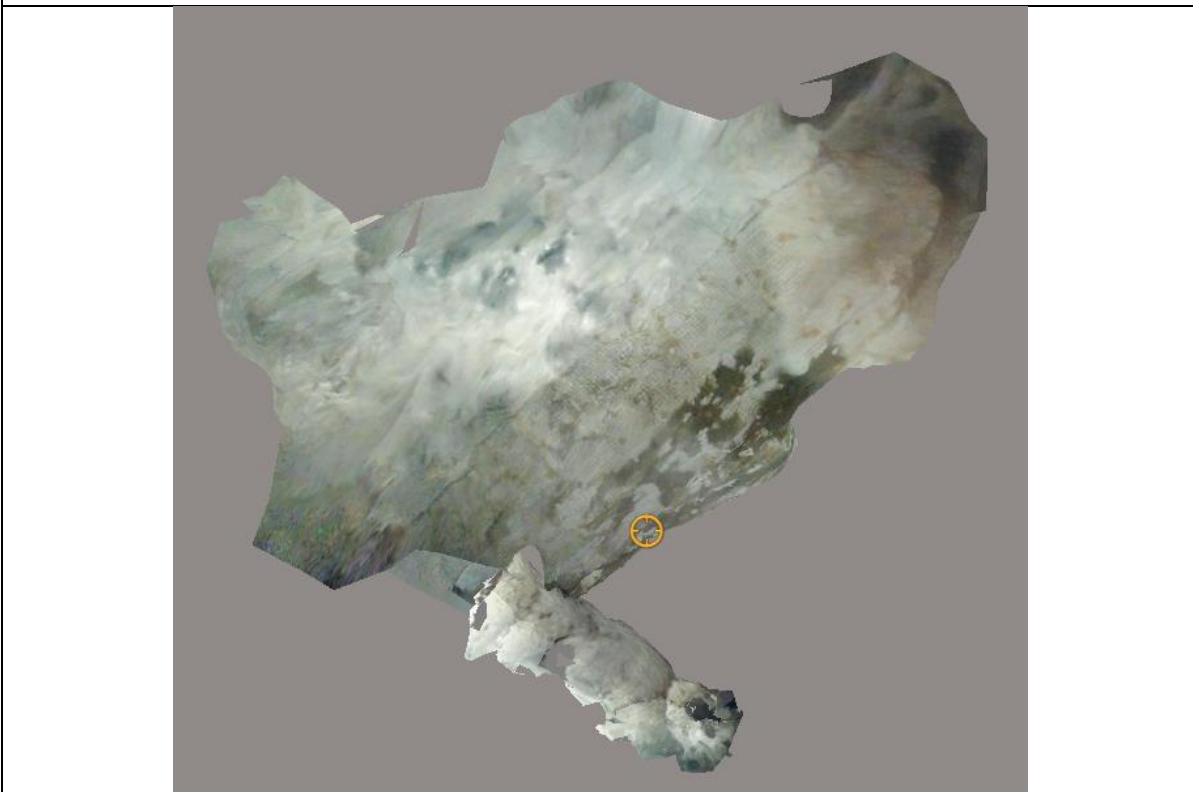
IMAGES (CALIBRATED): 345

TIME FOR INITIAL PROCESSING (HR:MIN:SEC): 00:24:31

INKONOVA – FLIGHT 9 (TRIANGLE MESH) – AUGUST 27, 2018	
PIX4DMAPPER	
	
	
CAMERA: 1280 x 720 (RGB)	AVG. POINT DENSITY (PER CUBIC METER): 10.04
IMAGES (TOTAL): 272	KEYPOINTS PER IMAGE (MEDIAN): 18,855
IMAGES (CALIBRATED): 272	MATCHES PER CALIBRATED IMAGE (MEDIAN): 4,187
NO. OF 3D DENSIFIED POINTS: 852,218	TIME FOR INITIAL PROCESSING (HR:MIN:SEC): 1:08:28

FLYABILITY: FLIGHT 4, 735 STOPE – SEPTEMBER 13, 2018

BENTLEY CONTEXTCAPTURE



CAMERA: 1920 x 1080 (RGB)

KEYPOINTS PER IMAGE (MEDIAN): 5,013

IMAGES (TOTAL): 340

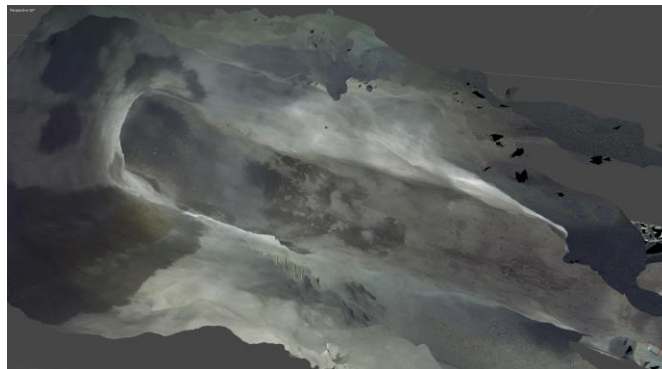
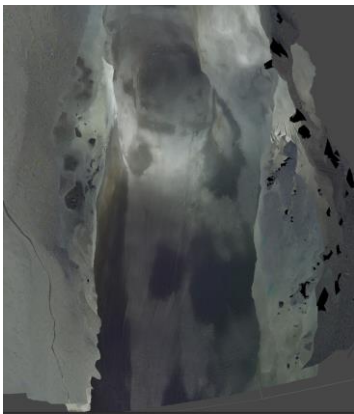
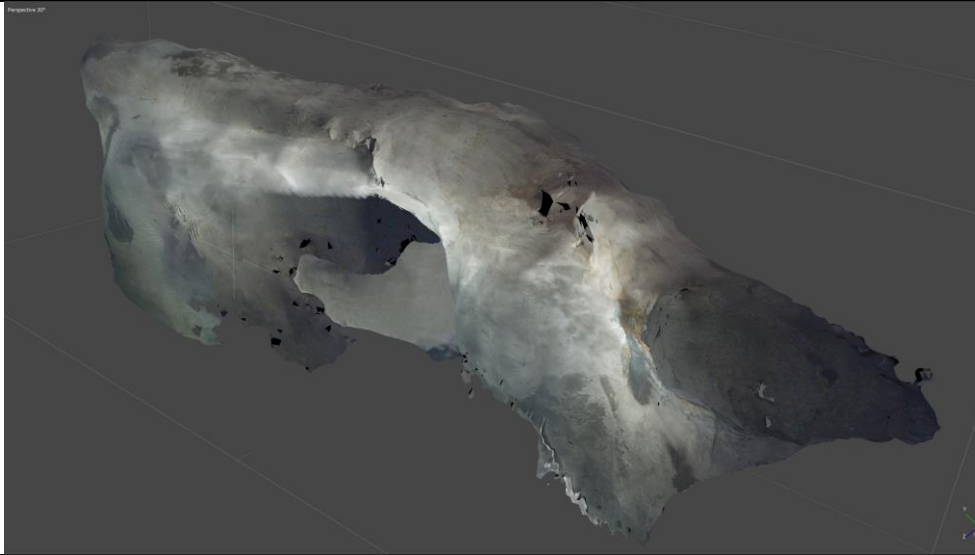
TIE POINTS PER IMAGE (MEDIAN): 160

IMAGES (CALIBRATED): 146

TIME FOR INITIAL PROCESSING (HR:MIN:SEC): 00:08:07

FLYABILITY: FLIGHT 4, 735 STOPE – SEPTEMBER 13, 2018

AGISOFT PHOTOSCAN VERSION 1.4.3 (64 BIT)



**IMAGE RESOLUTION: 1920 x 1080
(RGB) (ELIOS VIDEO CAPTURE)**

AVG. DENSITY (PER CUBIC METER): N/A

IMAGES (TOTAL): 644

KEYPOINTS PER IMAGE (LIMIT): 40,000

IMAGES (CALIBRATED): 644

MATCHES PER CALIBRATED IMAGE (LIMIT): 4,000

**RMS REPROJECTION ERROR (PIXELS):
2.26576**

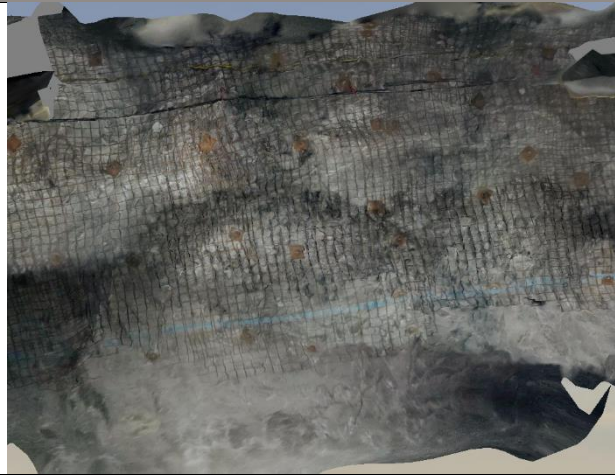
MAX REPROJECTION ERROR (PIXELS): 38.926

**NO. OF 3D DENSIFIED POINTS:
2,698,339 (HIGH QUALITY DENSE
CLOUD)**

**TIME FOR INITIAL PROCESSING (HR:MIN:SEC): 0 HOURS: 37
MINUTES: 13 SECONDS (CPU: INTEL ® XEON ® CPU-E5-2620 v4
@ 2.1GHz, 63.9 GB RAM, OPENGL RENDERER: NVIDIA
QUADRO M4000/PCIe/SSE2**

FLYABILITY: FLIGHT 9, 735 DRIFT – SEPTEMBER 13, 2018

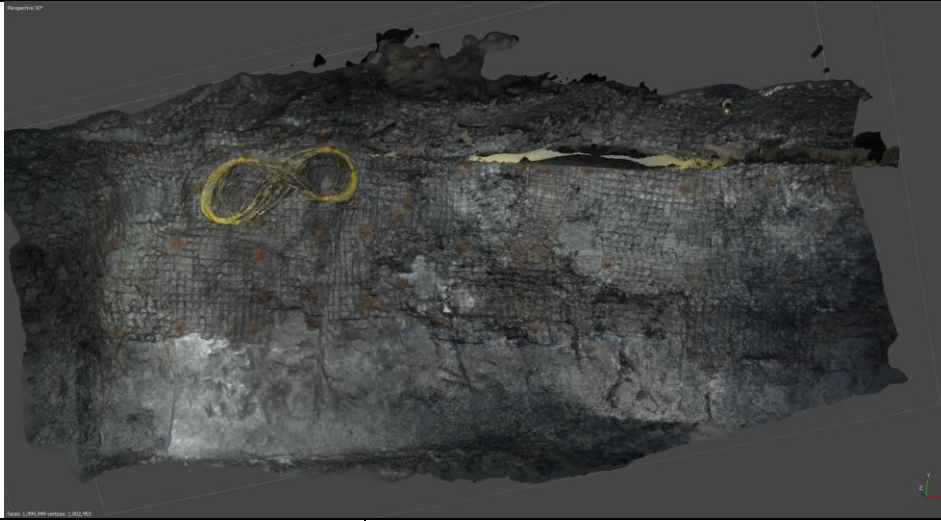
BENTLEY CONTEXTCAPTURE



CAMERA: 1920 x 1080 (RGB)	KEYPOINTS PER IMAGE (MEDIAN): 5,547
IMAGES (TOTAL): 652	TIE POINTS PER IMAGE (MEDIAN): 310
IMAGES (CALIBRATED): 607	TIME FOR INITIAL PROCESSING (HR:MIN:SEC): 00:33:48

FLYABILITY: FLIGHT 9, 735 DRIFT – SEPTEMBER 13, 2018

AGISOFT PHOTOscan VERSION 1.4.3 (64 BIT)



**IMAGE RESOLUTION: 1920 x 1080 (RGB)
(ELIOS VIDEO CAPTURE)**

AVG. DENSITY (PER CUBIC METER): N/A

IMAGES (TOTAL): 182

KEYPOINTS PER IMAGE (LIMIT): 40,000

IMAGES (CALIBRATED): 182

MATCHES PER CALIBRATED IMAGE (LIMIT): 4,000

**RMS REPROJECTION ERROR (PIXELS):
1.35356**

MAX REPROJECTION ERROR (PIXELS): 23.6399

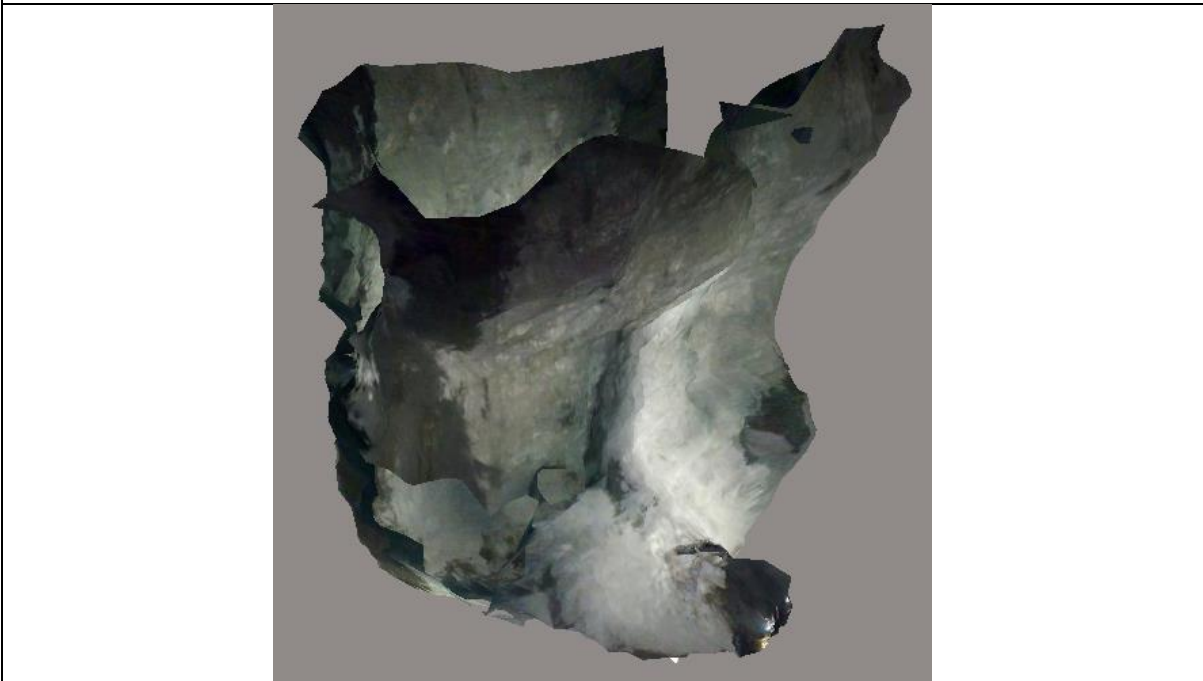
**NO. OF 3D DENSIFIED POINTS: 4,714,033
(HIGH QUALITY DENSE CLOUD)**

**TIME FOR INITIAL PROCESSING (HR:MIN:SEC): 0 HOURS: 19
MINUTES: 4 SECONDS (CPU: INTEL ® XEON ® CPU-E5-2620 v4
@ 2.1GHz, 63.9 GB RAM, OPENGL RENDERER: NVIDIA
QUADRO M4000/PCIe/SSE2**

FLYABILITY: FLIGHT 9, 735 DRIFT – SEPTEMBER 13, 2018	
PIX4DMAPPER	
	
	
CAMERA: 1920 x 1080 (RGB)	AVG. DENSITY (PER CUBIC METER): 106.31
IMAGES (TOTAL): 862	KEYPOINTS PER IMAGE (MEDIAN): 8,425
IMAGES (CALIBRATED): 599	MATCHES PER CALIBRATED IMAGE (MEDIAN): 2,491
NO. OF 3D DENSIFIED POINTS: 2,765,674	TIME FOR INITIAL PROCESSING (HR:MIN:SEC): N/A

FLYABILITY: FLIGHT 5, 102 STOPE – SEPTEMBER 14, 2018

BENTLEY CONTEXTCAPTURE



CAMERA: 1920 x 1080 (RGB)

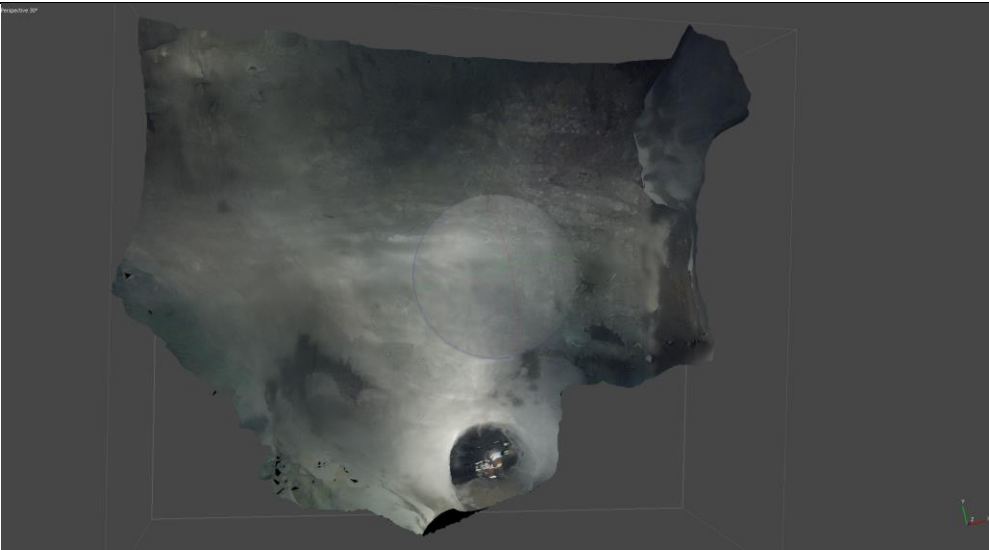
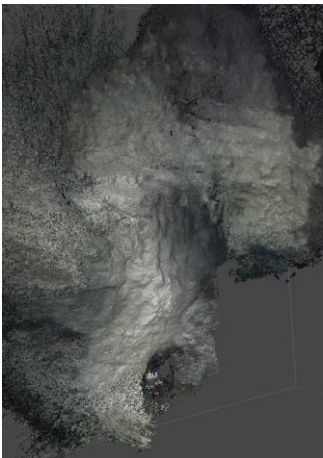
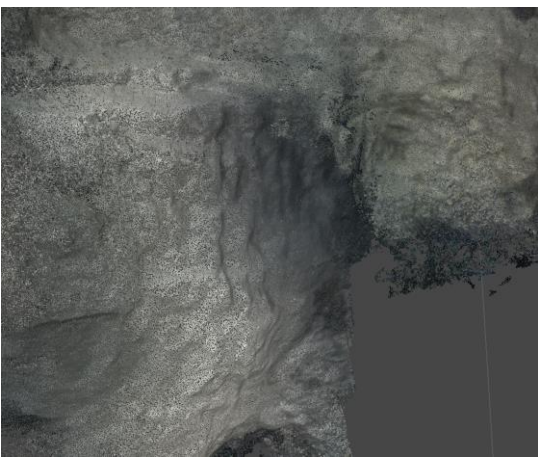
KEYPOINTS PER IMAGE (MEDIAN): 5,038

IMAGES (TOTAL): 430

TIE POINTS PER IMAGE (MEDIAN): 106

IMAGES (CALIBRATED): 347

TIME FOR INITIAL PROCESSING (HR:MIN:SEC): 00:13:02

FLYABILITY: FLIGHT 5, 102 STOPE – SEPTEMBER 14, 2018	
AGISOFT PHOTOSCAN VERSION 1.4.3 (64 BIT)	
	
	
IMAGE RESOLUTION: 3840 X 2160 (RGB) (DJI X3 CAMERA-VIDEO CAPTURE)	AVG. DENSITY (PER CUBIC METER): N/A
IMAGES (TOTAL): 460	KEYPOINTS PER IMAGE (LIMIT): 40,000
IMAGES (CALIBRATED): 460	MATCHES PER CALIBRATED IMAGE (LIMIT): 4,000
RMS REPROJECTION ERROR (PIXELS): 2.4665	MAX REPROJECTION ERROR (PIXELS): 41.5681
NO. OF 3D DENSIFIED POINTS: 1,137,300 (HIGH QUALITY DENSE CLOUD)	TIME FOR INITIAL PROCESSING (HR:MIN:SEC): 0 HOURS: 19 MINUTES: 20 SECONDS (CPU: INTEL ® XEON ® CPU-E5-2620 V4 @ 2.1GHz, 63.9 GB RAM, OPENGL RENDERER: NVIDIA QUADRO M4000/PCIe/SSE2

FLYABILITY: FLIGHT 5, 102 STOPE – SEPTEMBER 14, 2018



CAMERA: 1920 x 1080 (RGB)

AVG. POINT DENSITY (PER CUBIC METER): 1.38

IMAGES (TOTAL): 846

KEYPOINTS PER IMAGE (MEDIAN): 5,259

IMAGES (CALIBRATED): 638

MATCHES PER CALIBRATED IMAGE (MEDIAN): 669

NO. OF 3D DENSIFIED POINTS: 1,853,172

TIME FOR INITIAL PROCESSING (HR:MIN:SEC): 3:36:08

FLYABILITY: FLIGHT 4, 895 RAISE INSPECTION – SEPTEMBER 14, 2018

BENTLEY CONTEXTCAPTURE



CAMERA: 1920 x 1080 (RGB)

KEYPOINTS PER IMAGE (MEDIAN): 5,138

IMAGES (TOTAL): 398

TIE POINTS PER IMAGE (MEDIAN): 284

IMAGES (CALIBRATED): 347

TIME FOR INITIAL PROCESSING (HR:MIN:SEC): 00:33:50

FLYABILITY: FLIGHT 4, 895 RAISE INSPECTION – SEPTEMBER 14, 2018

AGISOFT PHOTOSCAN VERSION 1.4.3 (64 BIT)



IMAGE RESOLUTION: 1920 X 1080 (RGB) (ELIOS VIDEO CAPTURE)

AVG. DENSITY (PER CUBIC METER): N/A

IMAGES (TOTAL): 567

KEYPOINTS PER IMAGE (LIMIT): 40,000

IMAGES (CALIBRATED): 567

MATCHES PER CALIBRATED IMAGE (LIMIT): 4,000

RMS REPROJECTION ERROR (PIXELS): 1.77253

MAX REPROJECTION ERROR (PIXELS): 37.1735

NO. OF 3D DENSIFIED POINTS: 6,047,563 (HIGH QUALITY DENSE CLOUD)

TIME FOR INITIAL PROCESSING (HR:MIN:SEC): 1 HOURS: 6 MINUTES: 11 SECONDS (CPU: INTEL® XEON® CPU-E5-2620 v4 @ 2.1GHz, 63.9 GB RAM, OPENGL RENDERER: NVIDIA QUADRO M4000/PCIe/SSE2)

EMESENT: FLIGHT 6, 102 STOPE – SEPTEMBER 10, 2018

AGISOFT PHOTOScan VERSION 1.4.3 (64 BIT)

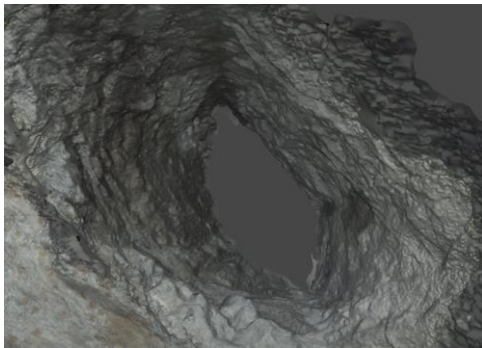
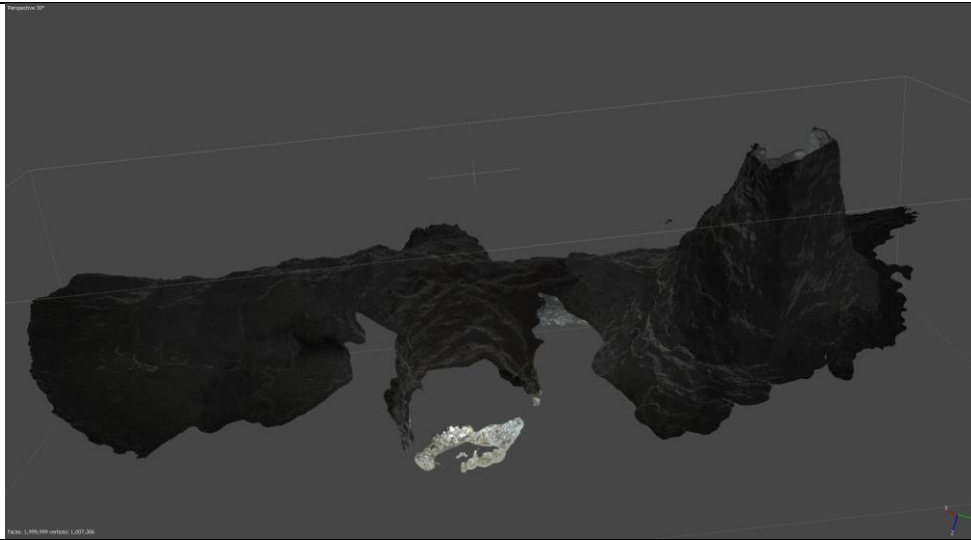


IMAGE RESOLUTION: 3840 X 2160 (RGB) (DJI Z3 CAMERA-VIDEO CAPTURE)

IMAGES (TOTAL): 241

IMAGES (CALIBRATED): 241

RMS REPROJECTION ERROR (PIXELS): 1.99056

**NO. OF 3D DENSIFIED POINTS: 20,741,817
(HIGH QUALITY DENSE CLOUD)**

AVG. DENSITY (PER CUBIC METER): N/A

KEYPOINTS PER IMAGE (LIMIT): 40,000

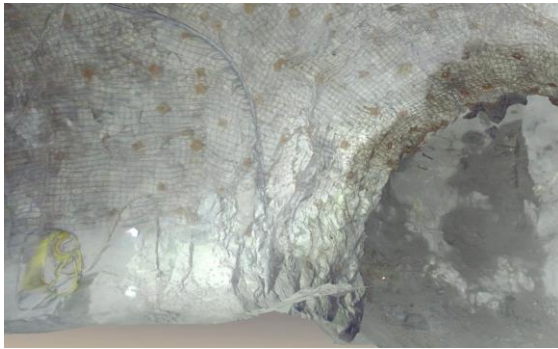
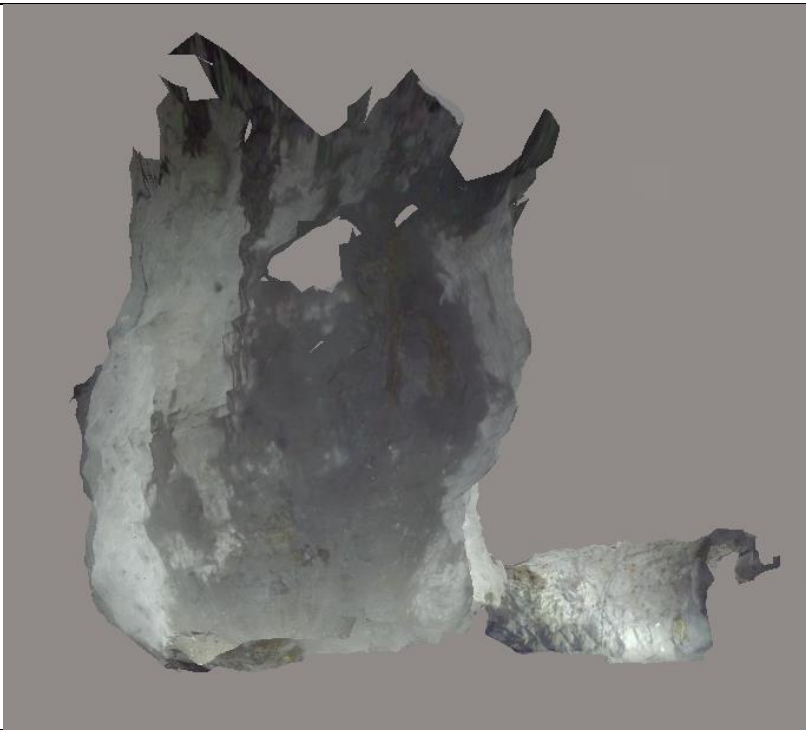
MATCHES PER CALIBRATED IMAGE (LIMIT): 4,000

MAX REPROJECTION ERROR (PIXELS): 61.5286

**TIME FOR INITIAL PROCESSING (HR:MIN:SEC): 1 HOURS: 40
MINUTES: 2 SECONDS (CPU: INTEL® XEON® CPU-E5-2620 v4 @
2.1GHZ, 63.9 GB RAM, OPENGL RENDERER: NVIDIA QUADRO
M4000/PCIe/SSE2)**

EMESENT: FLIGHT 2, 102 STOPE – SEPTEMBER 11, 2018

BENTLEY CONTEXTCAPTURE



CAMERA: 3840 x 2160 (RGB)

KEYPOINTS PER IMAGE (MEDIAN): 7,479

IMAGES (TOTAL): 548

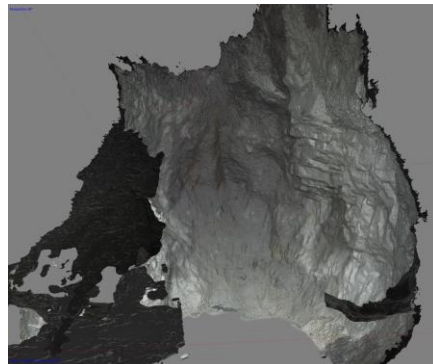
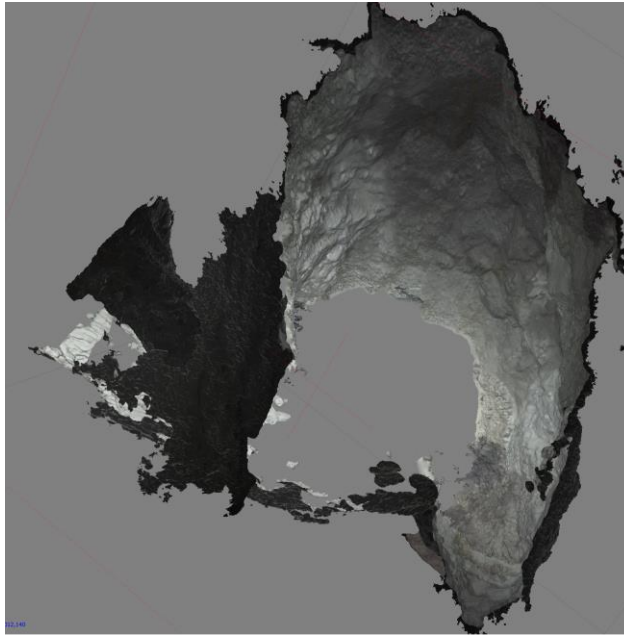
TIE POINTS PER IMAGE (MEDIAN): 207

IMAGES (CALIBRATED): 520

TIME FOR INITIAL PROCESSING (HR:MIN:SEC): 00:36:17

EMESENT: FLIGHT 2, 102 STOPE – SEPTEMBER 11, 2018

AGISOFT PHOTOSCAN VERSION 1.4.3 (64 BIT)



**IMAGE RESOLUTION: 3840 X 2160 (RGB) (DJI X3
CAMERA-VIDEO CAPTURE)**

AVG. DENSITY (PER CUBIC METER): N/A

IMAGES (TOTAL): 547

KEYPOINTS PER IMAGE (LIMIT): 40,000

IMAGES (CALIBRATED): 547

MATCHES PER CALIBRATED IMAGE (LIMIT): 4,000

RMS REPROJECTION ERROR (PIXELS): 2.2622

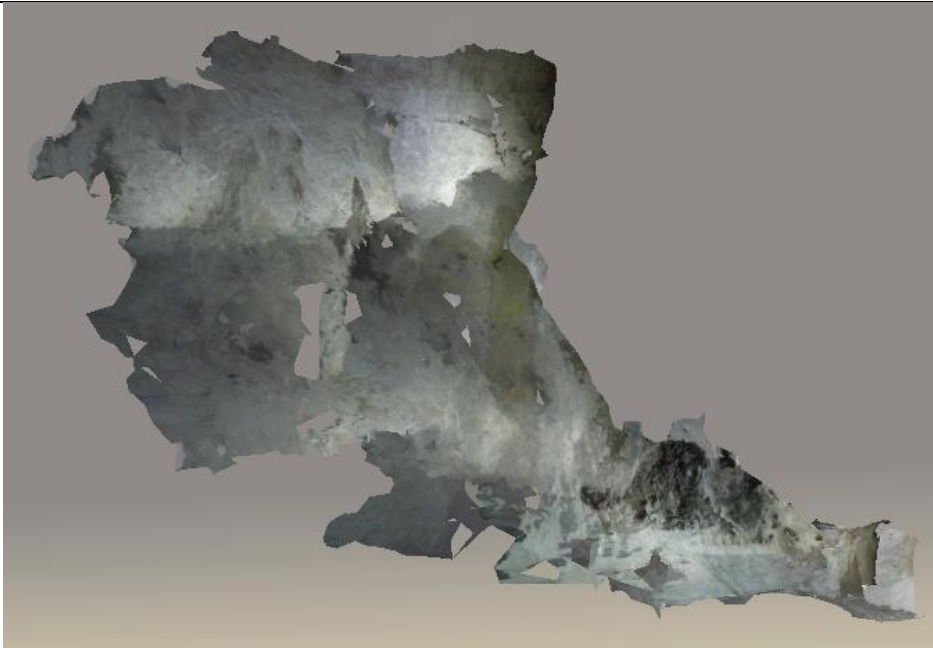
MAX REPROJECTION ERROR (PIXELS): 92.4329

**NO. OF 3D DENSIFIED POINTS: 29,568,654 (HIGH QUALITY
DENSE CLOUD)**

**TIME FOR INITIAL PROCESSING (HR:MIN:SEC): 7 HOURS:
4 MINUTES: 0 SECONDS (CPU: INTEL® XEON® CPU-
E5-2620 V4 @ 2.1GHz, 63.9 GB RAM, OPENGL
RENDERER: NVIDIA QUADRO M4000/PCIe/SSE2**

EMESENT: FLIGHT 5, 735 STOPE – SEPTEMBER 11, 2018

BENTLEY CONTEXTCAPTURE



CAMERA: 3840 x 2160 (RGB)




KEYPOINTS PER IMAGE (MEDIAN): 7,665

IMAGES (TOTAL): 531

TIE POINTS PER IMAGE (MEDIAN): 280

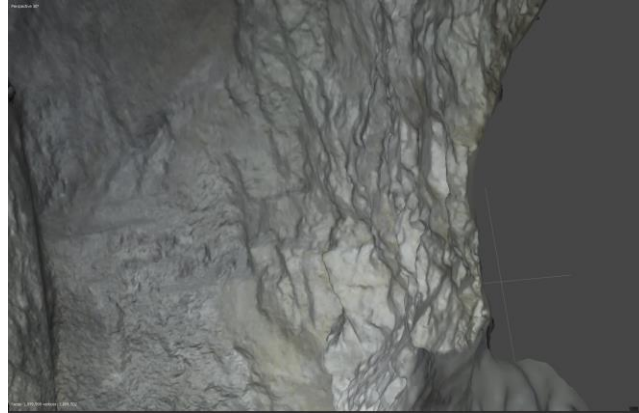
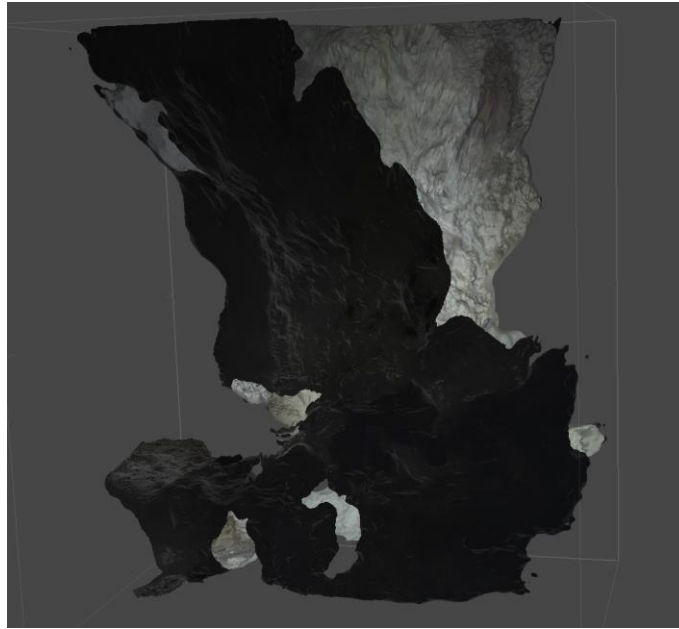
IMAGES (CALIBRATED): 516

TIME FOR INITIAL PROCESSING (HR:MIN:SEC): 00:41:35

EMESENT: FLIGHT 5, 735 STOPE – SEPTEMBER 11, 2018	
AGISOFT PHOTOScan VERSION 1.4.3 (64 BIT)	
	
	
IMAGE RESOLUTION: 3840 X 2160 (RGB) (DJI X3 CAMERA-VIDEO CAPTURE)	AVG. DENSITY (PER CUBIC METER): N/A
IMAGES (TOTAL): 547	KEYPOINTS PER IMAGE (LIMIT): 40,000
IMAGES (CALIBRATED): 547	MATCHES PER CALIBRATED IMAGE (LIMIT): 4,000
RMS REPROJECTION ERROR (PIXELS): 2.2622	MAX REPROJECTION ERROR (PIXELS): 92.4329
NO. OF 3D DENSIFIED POINTS: 29,568,654 (HIGH QUALITY DENSE CLOUD)	TIME FOR INITIAL PROCESSING (HR:MIN:SEC): 7 HOURS: 4 MINUTES: 0 SECONDS (CPU: INTEL ® XEON ® CPU-E5-2620 V4 @ 2.1GHz, 63.9 GB RAM, OPENGGL RENDERER: NVIDIA QUADRO M4000/PCIe/SSE2

EMESENT: FLIGHT 6, 735 STOPE – SEPTEMBER 11, 2018

AGISOFT PHOTOSCAN VERSION 1.4.3 (64 BIT)



**IMAGE RESOLUTION: 3840 X 2160 (RGB)
(DJI X3 CAMERA-VIDEO CAPTURE)**

AVG. DENSITY (PER CUBIC METER): N/A

IMAGES (TOTAL): 894

KEYPOINTS PER IMAGE (LIMIT): 40,000

IMAGES (CALIBRATED): 894

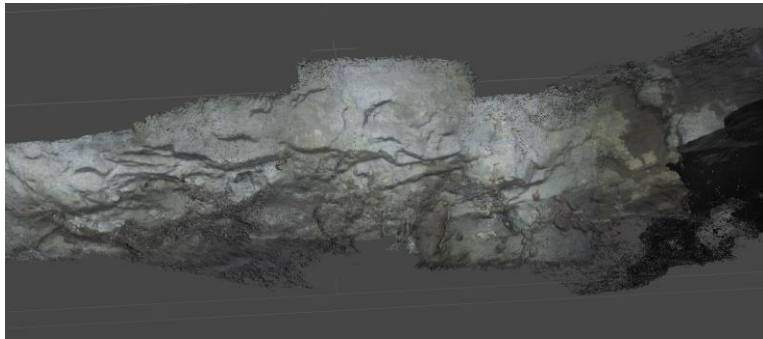
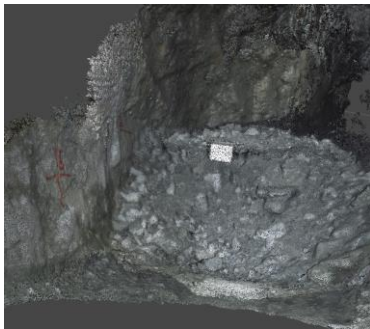
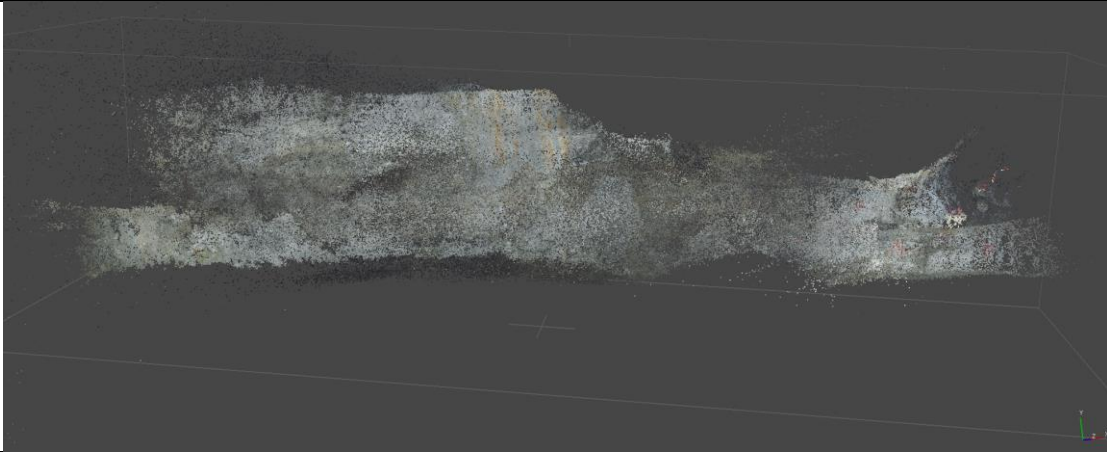
MATCHES PER CALIBRATED IMAGE (LIMIT): 4,000

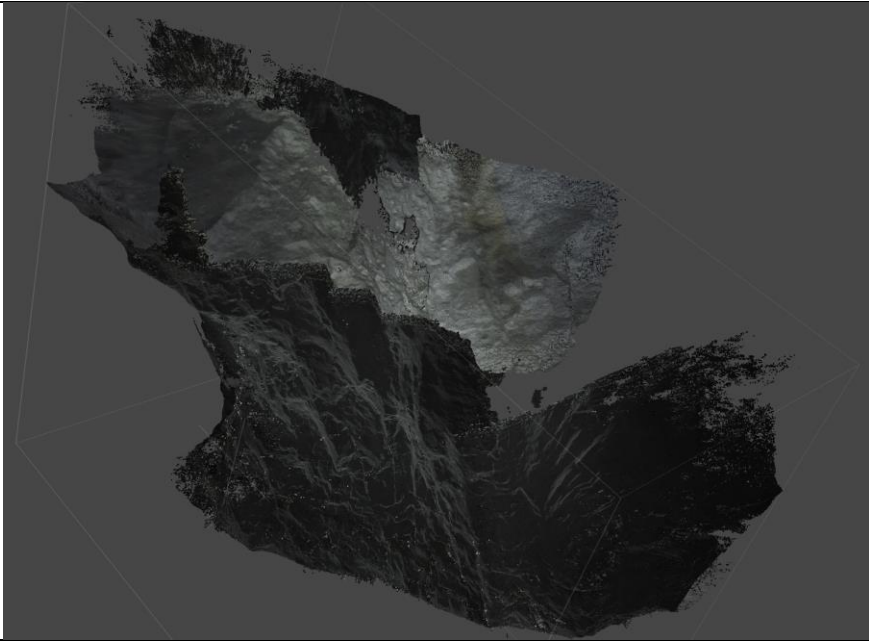

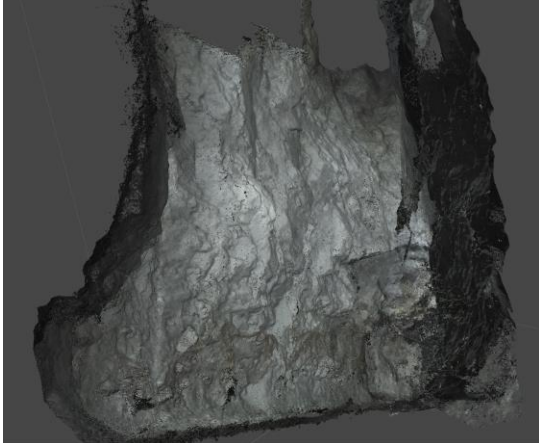
**RMS REPROJECTION ERROR (PIXELS):
2.4508**

MAX REPROJECTION ERROR (PIXELS): 79.005

**NO. OF 3D DENSIFIED POINTS: 7,673,086
(MEDIUM QUALITY DENSE CLOUD)**

**TIME FOR INITIAL PROCESSING (HR:MIN:SEC): 27 HOURS: 21
MINUTES: 0 SECONDS (CPU: INTEL® XEON® CPU-E5-2620 v4
@ 2.1GHz, 63.9 GB RAM, OPENGL RENDERER: NVIDIA
QUADRO M4000/PCIe/SSE2**

MONTANA TECH: FLIGHT 6, 945 STOPE – AUGUST 09, 2018**AGISOFT PHOTOSCAN VERSION 1.4.3 (64 BIT)****IMAGE RESOLUTION: 3840 X 2160 (RGB) (DJI X3 CAMERA-VIDEO CAPTURE)****AVG. DENSITY (PER CUBIC METER): N/A****IMAGES (TOTAL): 1245****KEYPOINTS PER IMAGE (LIMIT): 40,000****IMAGES (CALIBRATED): 1245****MATCHES PER CALIBRATED IMAGE (LIMIT): 4,000****RMS REPROJECTION ERROR (PIXELS): 5.26919****MAX REPROJECTION ERROR (PIXELS): 1914.9****NO. OF 3D DENSIFIED POINTS: 14,883,463 (HIGH QUALITY DENSE CLOUD)****TIME FOR INITIAL PROCESSING (HR:MIN:SEC): 27 HOURS: 56 MINUTES: 0 SECONDS (CPU: INTEL ® XEON ® CPU-E5-2620 v4 @ 2.1GHz, 63.9 GB RAM, OPENGL RENDERER: NVIDIA QUADRO M4000/PCIe/SSE2)**

MONTANA TECH: FLIGHT 1, 735 STOPE – AUGUST 31, 2018	
AGISOFT PHOTOScan VERSION 1.4.3 (64 BIT)	
	
	
IMAGE RESOLUTION: 3840 X 2160 (RGB) (DJI X3 CAMERA-VIDEO CAPTURE)	AVG. DENSITY (PER CUBIC METER): N/A
IMAGES (TOTAL): 1164	KEYPOINTS PER IMAGE (LIMIT): 40,000
IMAGES (CALIBRATED): 1164	MATCHES PER CALIBRATED IMAGE (LIMIT): 4,000
RMS REPROJECTION ERROR (PIXELS): 1.08471	MAX REPROJECTION ERROR (PIXELS): 34.5715
NO. OF 3D DENSIFIED POINTS: 5,138,618 (MEDIUM QUALITY DENSE CLOUD)	TIME FOR INITIAL PROCESSING (HR:MIN:SEC): 0 HOURS: 43 MINUTES: 58 SECONDS (CPU: INTEL ® XEON ® CPU-E5-2620 V4 @ 2.1GHz, 63.9 GB RAM, OPENGL RENDERER: NVIDIA QUADRO M4000/PCIe/SSE2

MONTANA TECH – FLIGHT 1 – AUGUST 31, 2018



CAMERA: 1920 x 1080 (RGB)

AVG. POINT DENSITY (PER CUBIC METER): 3.28

IMAGES (TOTAL): 298

KEYPOINTS PER IMAGE (MEDIAN): 13,406

IMAGES (CALIBRATED): 269

MATCHES PER CALIBRATED IMAGE (MEDIAN): 5,480

NO. OF 3D DENSIFIED POINTS: 1,100,967

**TIME FOR INITIAL PROCESSING (HR:MIN:SEC):
2:46:41**

APPENDIX E: 3D PHOTOGRAMMETRIC 3D POINT CLOUD & MODEL EVALUATION SHEET

PHOTOGRAMMETRIC 3D POINT CLOUD / MODEL EVALUATION SCORE SHEET

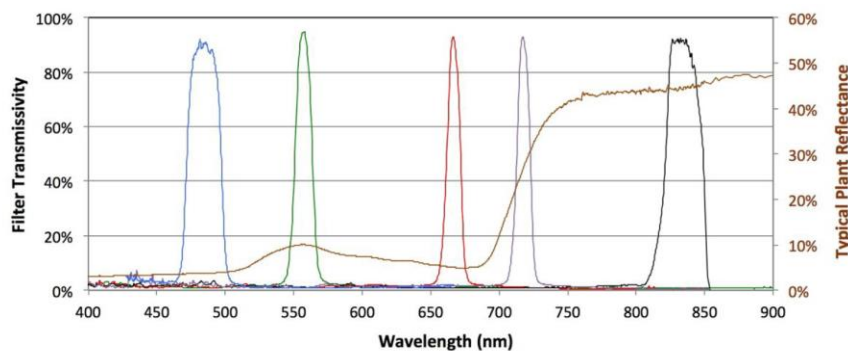
	Completeness					Detail					Comments
	Poor	Mod	Good		Score (1-10)	Poor	Mod	Good		Score (1-10)	
1_1	<input type="checkbox"/>	<input type="checkbox"/>	<input type="checkbox"/>	Continuous surface		<input type="checkbox"/>	<input type="checkbox"/>	<input type="checkbox"/>	Surface texture		
	<input type="checkbox"/>	<input type="checkbox"/>	<input type="checkbox"/>	Realistic geometry		<input type="checkbox"/>	<input type="checkbox"/>	<input type="checkbox"/>	Surface resolution		
	<input type="checkbox"/>	<input type="checkbox"/>	<input type="checkbox"/>	Lack of excessive artifacts		<input type="checkbox"/>	<input type="checkbox"/>	<input type="checkbox"/>	Visible discontinuities		
	<input type="checkbox"/>	<input type="checkbox"/>	<input type="checkbox"/>	Lack of distortion		<input type="checkbox"/>	<input type="checkbox"/>	<input type="checkbox"/>	Recognizable features		
1_2	<input type="checkbox"/>	<input type="checkbox"/>	<input type="checkbox"/>	Continuous surface		<input type="checkbox"/>	<input type="checkbox"/>	<input type="checkbox"/>	Surface texture		
	<input type="checkbox"/>	<input type="checkbox"/>	<input type="checkbox"/>	Realistic geometry		<input type="checkbox"/>	<input type="checkbox"/>	<input type="checkbox"/>	Surface resolution		
	<input type="checkbox"/>	<input type="checkbox"/>	<input type="checkbox"/>	Lack of excessive artifacts		<input type="checkbox"/>	<input type="checkbox"/>	<input type="checkbox"/>	Visible discontinuities		
	<input type="checkbox"/>	<input type="checkbox"/>	<input type="checkbox"/>	Lack of distortion		<input type="checkbox"/>	<input type="checkbox"/>	<input type="checkbox"/>	Recognizable features		
1_3	<input type="checkbox"/>	<input type="checkbox"/>	<input type="checkbox"/>	Continuous surface		<input type="checkbox"/>	<input type="checkbox"/>	<input type="checkbox"/>	Surface texture		
	<input type="checkbox"/>	<input type="checkbox"/>	<input type="checkbox"/>	Realistic geometry		<input type="checkbox"/>	<input type="checkbox"/>	<input type="checkbox"/>	Surface resolution		
	<input type="checkbox"/>	<input type="checkbox"/>	<input type="checkbox"/>	Lack of excessive artifacts		<input type="checkbox"/>	<input type="checkbox"/>	<input type="checkbox"/>	Visible discontinuities		
	<input type="checkbox"/>	<input type="checkbox"/>	<input type="checkbox"/>	Lack of distortion		<input type="checkbox"/>	<input type="checkbox"/>	<input type="checkbox"/>	Recognizable features		
2_1	<input type="checkbox"/>	<input type="checkbox"/>	<input type="checkbox"/>	Continuous surface		<input type="checkbox"/>	<input type="checkbox"/>	<input type="checkbox"/>	Surface texture		
	<input type="checkbox"/>	<input type="checkbox"/>	<input type="checkbox"/>	Realistic geometry		<input type="checkbox"/>	<input type="checkbox"/>	<input type="checkbox"/>	Surface resolution		
	<input type="checkbox"/>	<input type="checkbox"/>	<input type="checkbox"/>	Lack of excessive artifacts		<input type="checkbox"/>	<input type="checkbox"/>	<input type="checkbox"/>	Visible discontinuities		
	<input type="checkbox"/>	<input type="checkbox"/>	<input type="checkbox"/>	Lack of distortion		<input type="checkbox"/>	<input type="checkbox"/>	<input type="checkbox"/>	Recognizable features		
2_2	<input type="checkbox"/>	<input type="checkbox"/>	<input type="checkbox"/>	Continuous surface		<input type="checkbox"/>	<input type="checkbox"/>	<input type="checkbox"/>	Surface texture		
	<input type="checkbox"/>	<input type="checkbox"/>	<input type="checkbox"/>	Realistic geometry		<input type="checkbox"/>	<input type="checkbox"/>	<input type="checkbox"/>	Surface resolution		
	<input type="checkbox"/>	<input type="checkbox"/>	<input type="checkbox"/>	Lack of excessive artifacts		<input type="checkbox"/>	<input type="checkbox"/>	<input type="checkbox"/>	Visible discontinuities		
	<input type="checkbox"/>	<input type="checkbox"/>	<input type="checkbox"/>	Lack of distortion		<input type="checkbox"/>	<input type="checkbox"/>	<input type="checkbox"/>	Recognizable features		
2_3	<input type="checkbox"/>	<input type="checkbox"/>	<input type="checkbox"/>	Continuous surface		<input type="checkbox"/>	<input type="checkbox"/>	<input type="checkbox"/>	Surface texture		
	<input type="checkbox"/>	<input type="checkbox"/>	<input type="checkbox"/>	Realistic geometry		<input type="checkbox"/>	<input type="checkbox"/>	<input type="checkbox"/>	Surface resolution		
	<input type="checkbox"/>	<input type="checkbox"/>	<input type="checkbox"/>	Lack of excessive artifacts		<input type="checkbox"/>	<input type="checkbox"/>	<input type="checkbox"/>	Visible discontinuities		
	<input type="checkbox"/>	<input type="checkbox"/>	<input type="checkbox"/>	Lack of distortion		<input type="checkbox"/>	<input type="checkbox"/>	<input type="checkbox"/>	Recognizable features		
3_1	<input type="checkbox"/>	<input type="checkbox"/>	<input type="checkbox"/>	Continuous surface		<input type="checkbox"/>	<input type="checkbox"/>	<input type="checkbox"/>	Surface texture		
	<input type="checkbox"/>	<input type="checkbox"/>	<input type="checkbox"/>	Realistic geometry		<input type="checkbox"/>	<input type="checkbox"/>	<input type="checkbox"/>	Surface resolution		
	<input type="checkbox"/>	<input type="checkbox"/>	<input type="checkbox"/>	Lack of excessive artifacts		<input type="checkbox"/>	<input type="checkbox"/>	<input type="checkbox"/>	Visible discontinuities		
	<input type="checkbox"/>	<input type="checkbox"/>	<input type="checkbox"/>	Lack of distortion		<input type="checkbox"/>	<input type="checkbox"/>	<input type="checkbox"/>	Recognizable features		
3_2	<input type="checkbox"/>	<input type="checkbox"/>	<input type="checkbox"/>	Continuous surface		<input type="checkbox"/>	<input type="checkbox"/>	<input type="checkbox"/>	Surface texture		
	<input type="checkbox"/>	<input type="checkbox"/>	<input type="checkbox"/>	Realistic geometry		<input type="checkbox"/>	<input type="checkbox"/>	<input type="checkbox"/>	Surface resolution		
	<input type="checkbox"/>	<input type="checkbox"/>	<input type="checkbox"/>	Lack of excessive artifacts		<input type="checkbox"/>	<input type="checkbox"/>	<input type="checkbox"/>	Visible discontinuities		
	<input type="checkbox"/>	<input type="checkbox"/>	<input type="checkbox"/>	Lack of distortion		<input type="checkbox"/>	<input type="checkbox"/>	<input type="checkbox"/>	Recognizable features		
3_3	<input type="checkbox"/>	<input type="checkbox"/>	<input type="checkbox"/>	Continuous surface		<input type="checkbox"/>	<input type="checkbox"/>	<input type="checkbox"/>	Surface texture		
	<input type="checkbox"/>	<input type="checkbox"/>	<input type="checkbox"/>	Realistic geometry		<input type="checkbox"/>	<input type="checkbox"/>	<input type="checkbox"/>	Surface resolution		
	<input type="checkbox"/>	<input type="checkbox"/>	<input type="checkbox"/>	Lack of excessive artifacts		<input type="checkbox"/>	<input type="checkbox"/>	<input type="checkbox"/>	Visible discontinuities		
	<input type="checkbox"/>	<input type="checkbox"/>	<input type="checkbox"/>	Lack of distortion		<input type="checkbox"/>	<input type="checkbox"/>	<input type="checkbox"/>	Recognizable features		
4_1	<input type="checkbox"/>	<input type="checkbox"/>	<input type="checkbox"/>	Continuous surface		<input type="checkbox"/>	<input type="checkbox"/>	<input type="checkbox"/>	Surface texture		
	<input type="checkbox"/>	<input type="checkbox"/>	<input type="checkbox"/>	Realistic geometry		<input type="checkbox"/>	<input type="checkbox"/>	<input type="checkbox"/>	Surface resolution		
	<input type="checkbox"/>	<input type="checkbox"/>	<input type="checkbox"/>	Lack of excessive artifacts		<input type="checkbox"/>	<input type="checkbox"/>	<input type="checkbox"/>	Visible discontinuities		
	<input type="checkbox"/>	<input type="checkbox"/>	<input type="checkbox"/>	Lack of distortion		<input type="checkbox"/>	<input type="checkbox"/>	<input type="checkbox"/>	Recognizable features		
4_2	<input type="checkbox"/>	<input type="checkbox"/>	<input type="checkbox"/>	Continuous surface		<input type="checkbox"/>	<input type="checkbox"/>	<input type="checkbox"/>	Surface texture		
	<input type="checkbox"/>	<input type="checkbox"/>	<input type="checkbox"/>	Realistic geometry		<input type="checkbox"/>	<input type="checkbox"/>	<input type="checkbox"/>	Surface resolution		
	<input type="checkbox"/>	<input type="checkbox"/>	<input type="checkbox"/>	Lack of excessive artifacts		<input type="checkbox"/>	<input type="checkbox"/>	<input type="checkbox"/>	Visible discontinuities		
	<input type="checkbox"/>	<input type="checkbox"/>	<input type="checkbox"/>	Lack of distortion		<input type="checkbox"/>	<input type="checkbox"/>	<input type="checkbox"/>	Recognizable features		
4_3	<input type="checkbox"/>	<input type="checkbox"/>	<input type="checkbox"/>	Continuous surface		<input type="checkbox"/>	<input type="checkbox"/>	<input type="checkbox"/>	Surface texture		
	<input type="checkbox"/>	<input type="checkbox"/>	<input type="checkbox"/>	Realistic geometry		<input type="checkbox"/>	<input type="checkbox"/>	<input type="checkbox"/>	Surface resolution		
	<input type="checkbox"/>	<input type="checkbox"/>	<input type="checkbox"/>	Lack of excessive artifacts		<input type="checkbox"/>	<input type="checkbox"/>	<input type="checkbox"/>	Visible discontinuities		
	<input type="checkbox"/>	<input type="checkbox"/>	<input type="checkbox"/>	Lack of distortion		<input type="checkbox"/>	<input type="checkbox"/>	<input type="checkbox"/>	Recognizable features		

APPENDIX F: THERMAL & MULTISPECTRAL IMAGING DEVICE DETAILS

Table F.1. Specifications of thermal and multispectral imaging devices.

Property	FLIR C3	Zenmuse XT	MicaSense RedEdge-M
Mass	130 g	170 g	170 g
Resolution (pixels)	80 X 60	640 X 512	1280 X 960
Video resolution (pixels)	N/A	640 X 512	N/A
Sensor	Uncooled micro bolometer	Uncooled VOx micro bolometer	Downwelling Light Sensors (5-band)
FOV	41° X 31°	69° X 56°	46° HFOV
Accuracy	± 2° C	± 4° C	N/A
Sensitivity (NEdT)	0.1° C	0.05° C	N/A
Spectral range	7.5-14 µm	7.5-13.5 µm	465-485 nm, 550-570 nm, 663-673 nm, 820-860 nm, 712-722 nm
Radiometric	Yes	Yes	Yes
Image Formats	Radiometric JPEG (14-bit)	Radiometric JPEG (8-bit), TIFF (14-bit), MP4, MOV	DNG (12-bit), TIFF (16-bit)

Figure F.1. Description of wavelengths captured by MicaSense RedEdge-M multispectral camera.



Band Number	Band Name	Center Wavelength (nm)	Bandwidth FWHM (nm)
1	Blue	475	20
2	Green	560	20
3	Red	668	10
4	Near IR	840	40
5	Red Edge	717	10

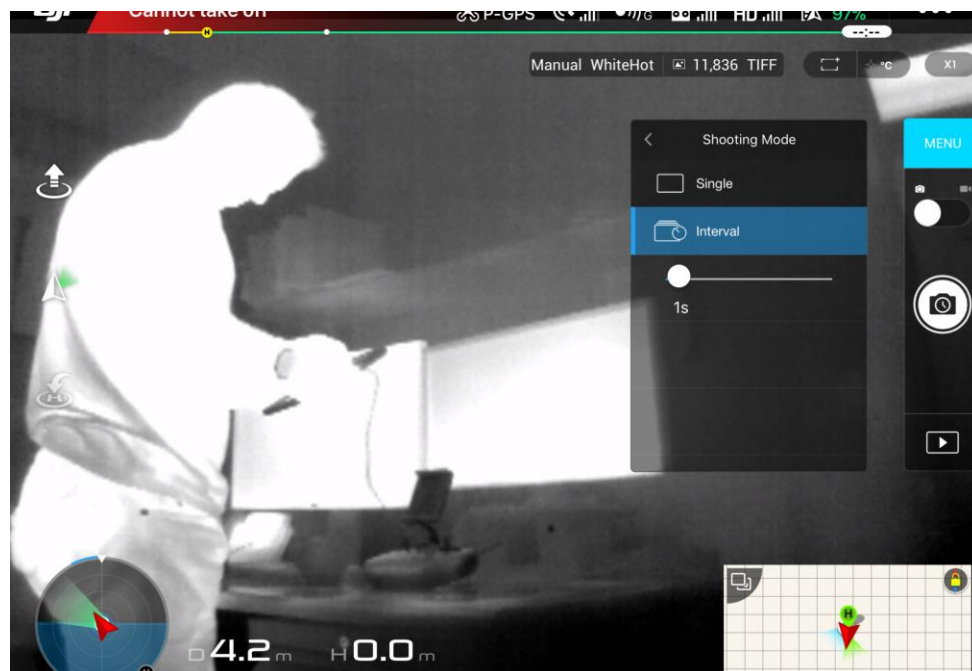
APPENDIX G: WORKFLOW FOR CAPTURING & PROCESSING THERMAL IMAGERY

1. With Zenmuse XT attached to drone, open the DJI GO application and navigate to the settings for the thermal camera and adjust to the following:

- a. Image Format: TIFF



- b. Shooting Mode: every 1 second (do not use video)



c. Settings:



i. Palette: WhiteHot or BlackHot

ii. Scene: Manual
(necessary to adjust Contrast and Brightness in the field before flying)

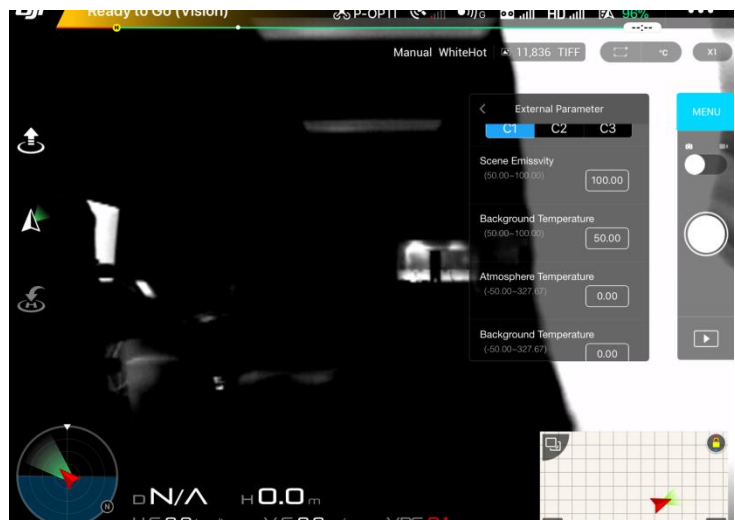
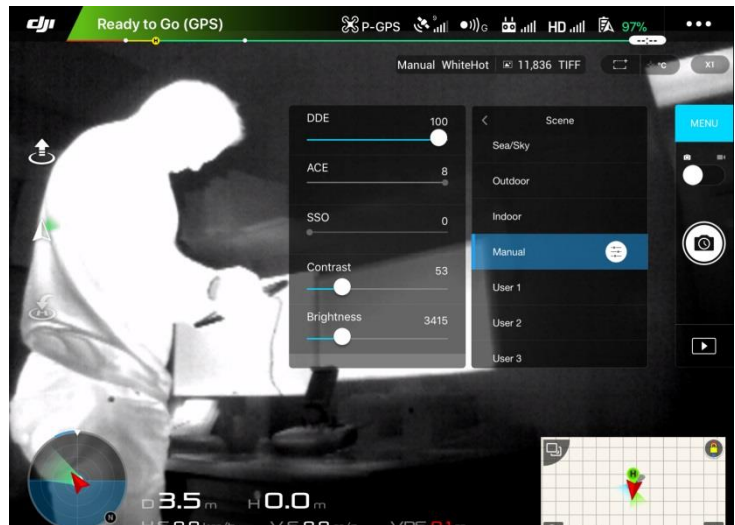
iii. Isotherm: OFF

iv. High Temp. Alert: OFF

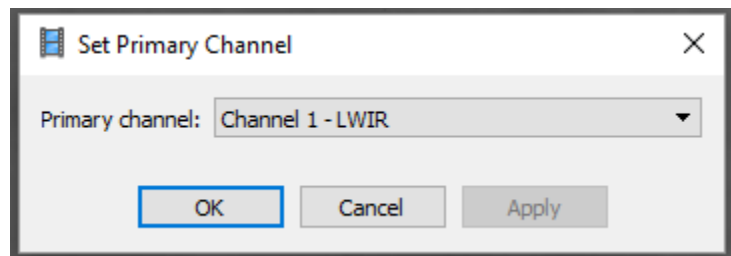
v. Gain Mode: High

vi. External Parameter: C1 (use dry bulb thermometer and infrared thermometer/Zenmuse XT to set background temperature and atmosphere temperature)

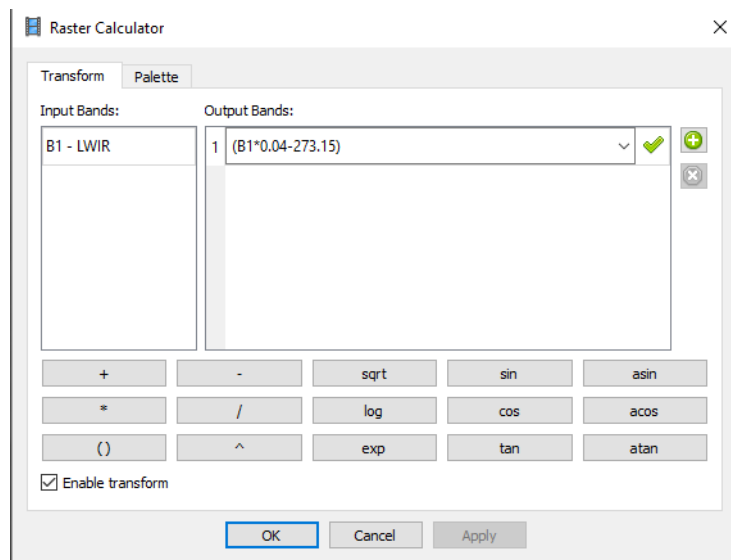
vii. flirFFCMode: Auto



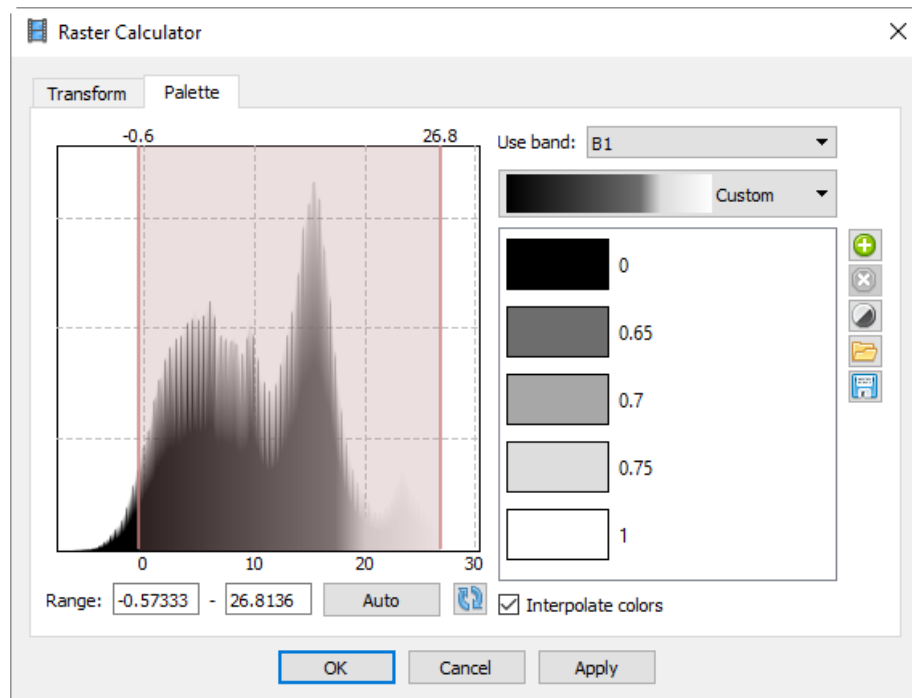
2. Start recording (make sure to be in image capture mode, not video capture) and capture thermal imagery in flight using the aerial strip method with at least 50% overlap between captures. On-board lighting is not necessary while using the Zenmuse XT, but it was used at Golden Sunlight so that the forward-facing Guidance sensor would operate correctly.
3. Download the TIFF files (they will appear as entirely black images in Windows Explorer) and import them into Agisoft PhotoScan.
4. Workflow for Agisoft PhotoScan:
 - a. Create a new chunk, import the thermal photos (TIFF format) into the chunk, and right-click on the chunk to select “Set Primary Channel...”. Set the primary channel to “Channel 1-LWIR”.



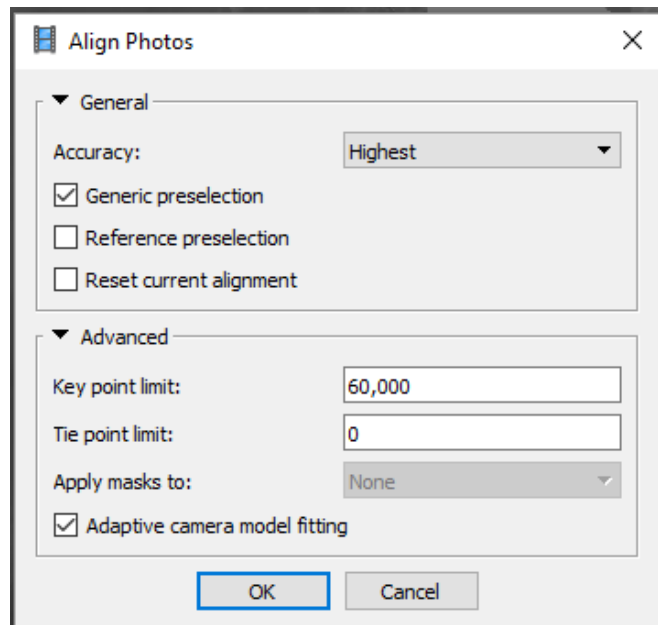
- b. Right-click on the chunk again and select “Set Raster Transform...”. Under the “Transform” tab, enter the equation shown in row 1 below to convert the thermal radiometric data to degrees Celsius.



- c. Under the “Palette” tab adjust the temperature range and temperature palette until the images are clear and there is contrast evident.

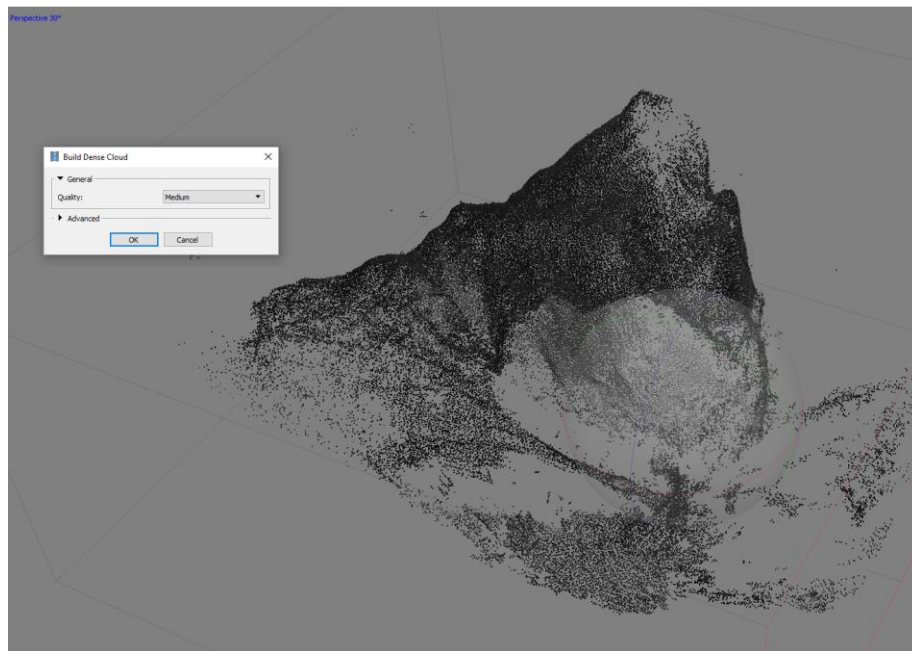
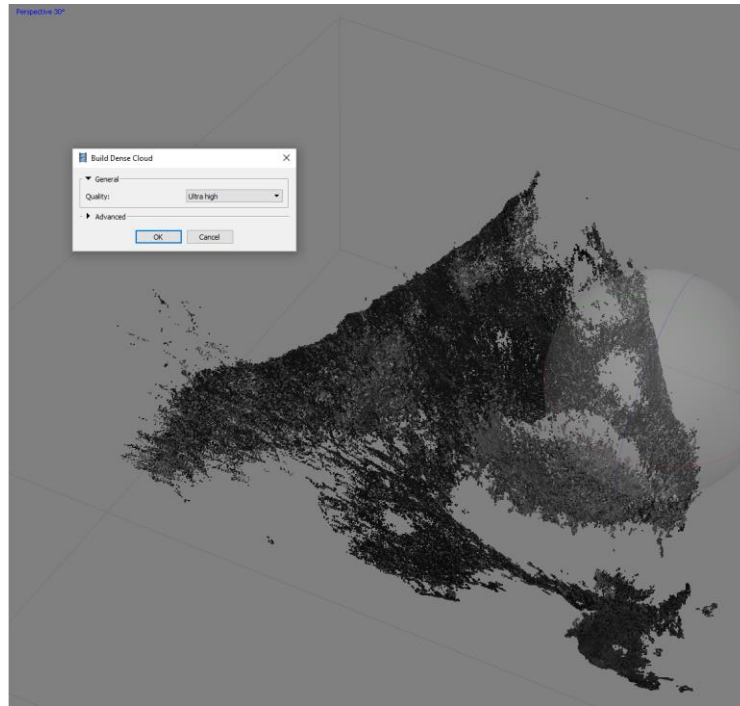


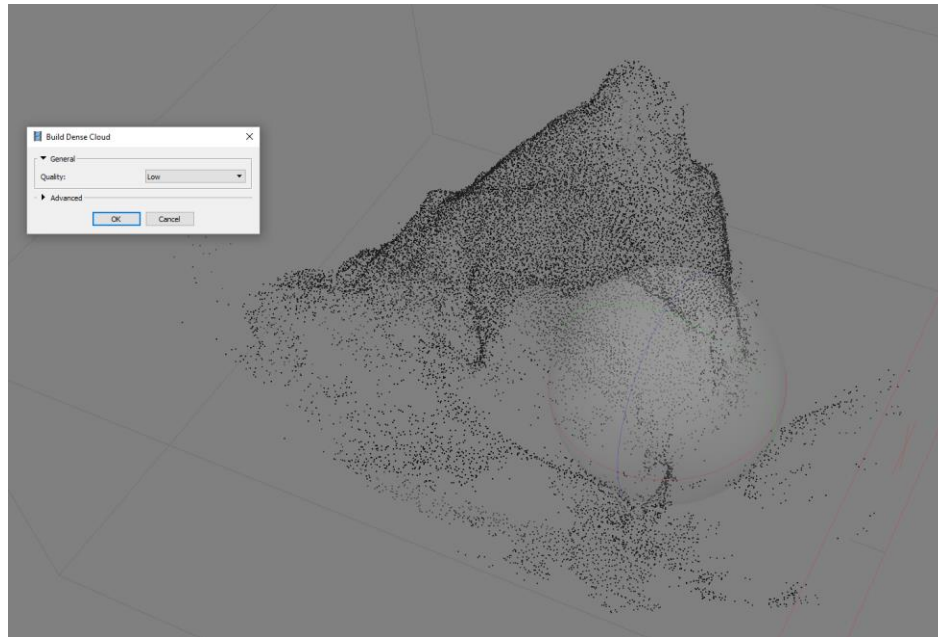
- d. Select the photos to be aligned and under “Workflow” on the top toolbar, select “Align Photos” and use the settings below for thermal imagery:



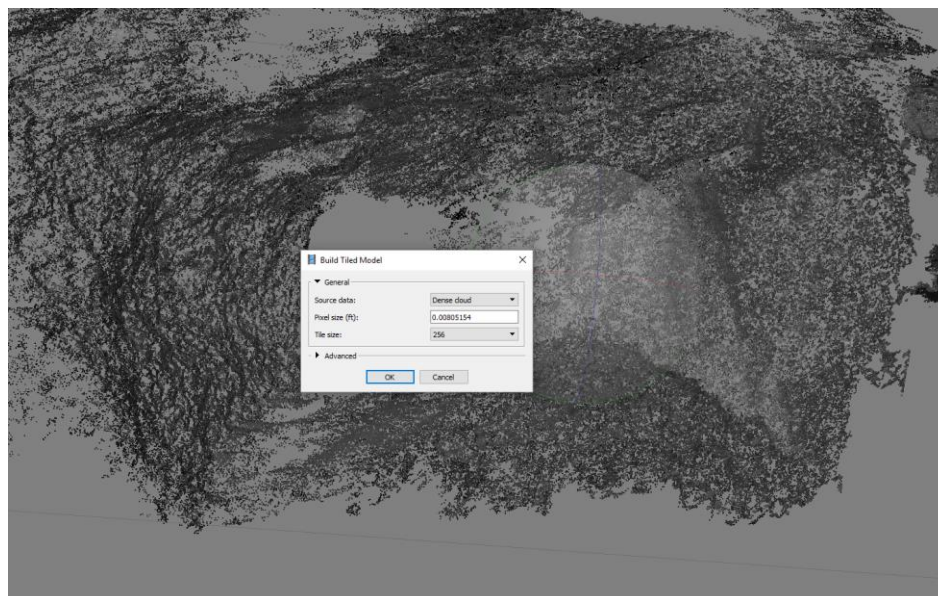
- e. If the coordinates of any control points (LED lights) are known, then they can be tagged in the individual photos and georeferenced under the “Reference” pane. Otherwise, the resultant point clouds can be co-registered to georeferenced point clouds using CloudCompare or Maptek I-Site Studio.

- f. After aligning the photos and generating tie points, select “Build Dense Cloud...” under the “Workflow” toolbar and use the “Ultra High” quality. It should be noted that “Ultra High” quality dense clouds (top image below) are better for generating tiled models, while “Medium” and “Low” quality dense clouds (respective middle and bottom images below) are better for generating point clouds that are more complete and have less holes in them.

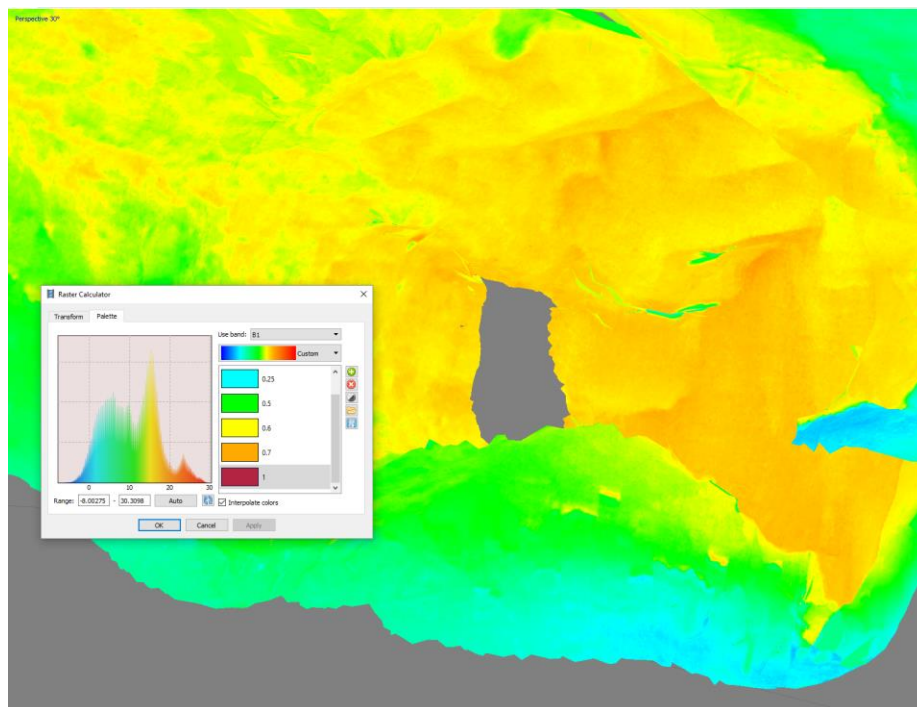
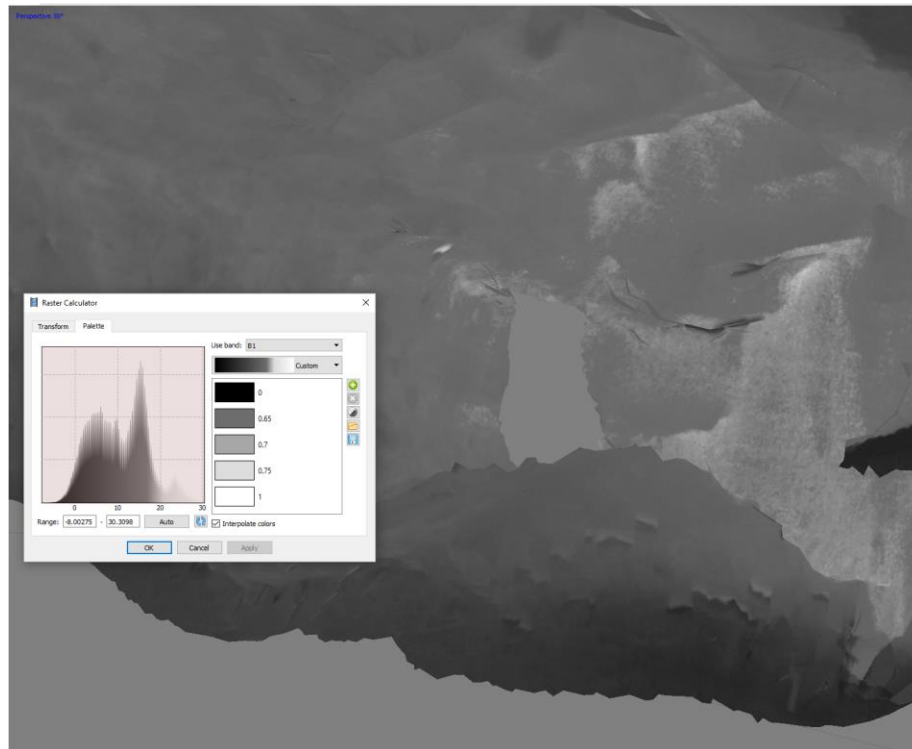




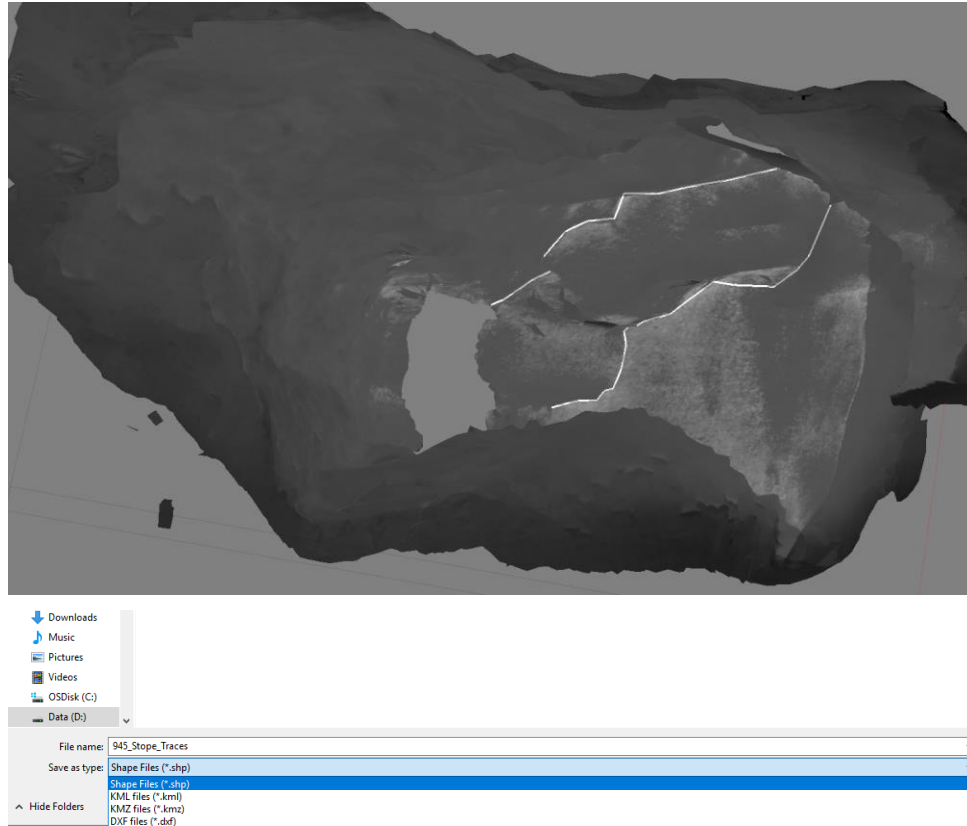
- g. After building the “Ultra High” quality dense cloud, select “Build Tiled Model...” under the “Workflow” toolbar and use the settings below.



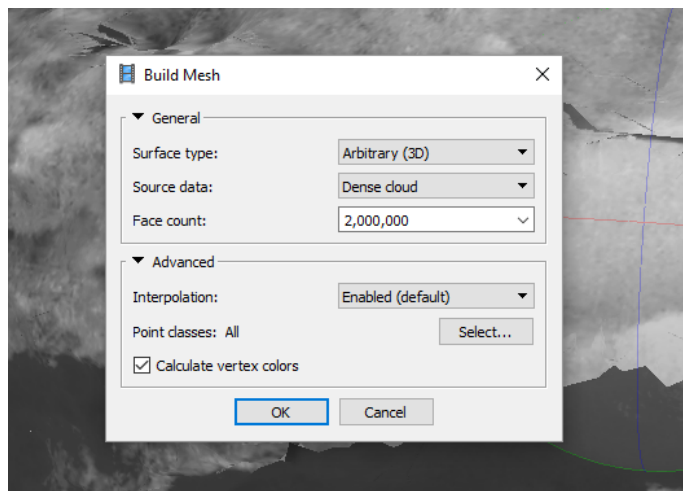
- h. After generating the tiled model, the “Raster Calculator” can be used to adjust the temperature scale (see top image below). Different palettes can be used to highlight structures (white traces in top image below or orange traces in bottom image), and it is useful to fine-tune the scale so that individual traces can appear.



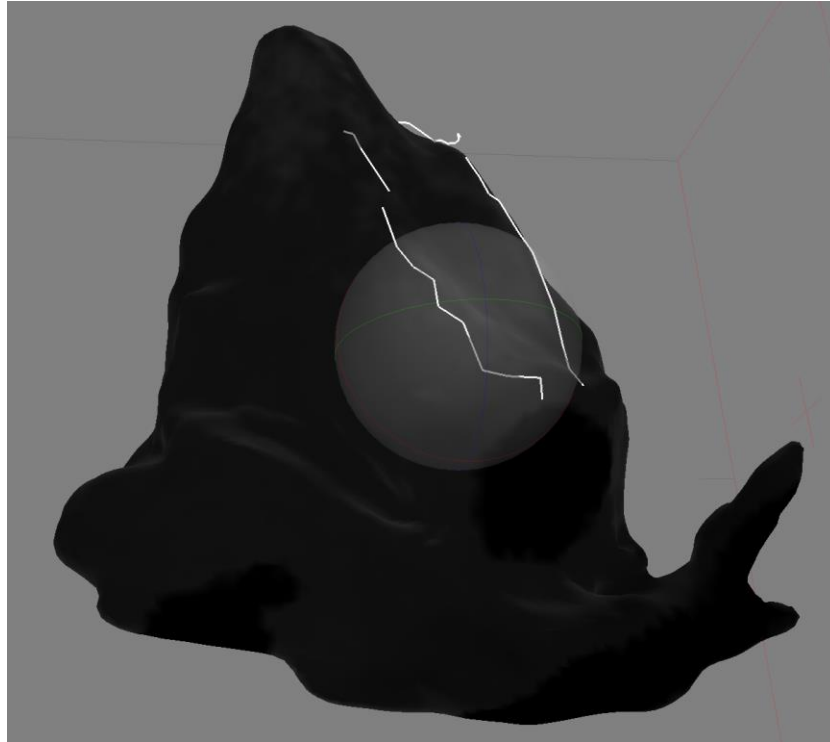
- i. Using the “Draw Polyline” tool, individual structures can be traced in 3D (top image below). If the model is georeferenced using ground control points or a co-registered point cloud, the polylines can be exported as georeferenced files for use in other software (bottom image below) by right-clicking on the “Shapes” under the Workspace file tree and selecting “Export Shapes...”.



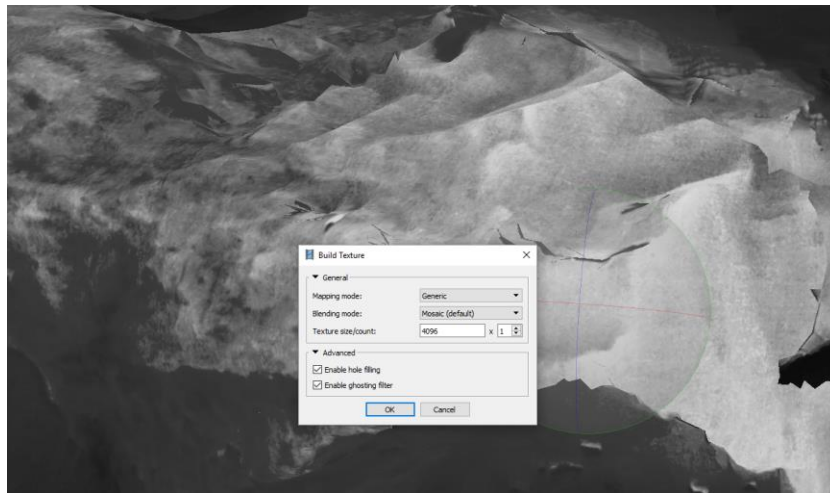
5. Exporting textured meshes from thermal models in Agisoft PhotoScan into CloudCompare for mapping.
 - a. Select the chunk that needs to be exported in the workspace and then select “Build Mesh...” from the “Workflow” menu. Use the settings below:



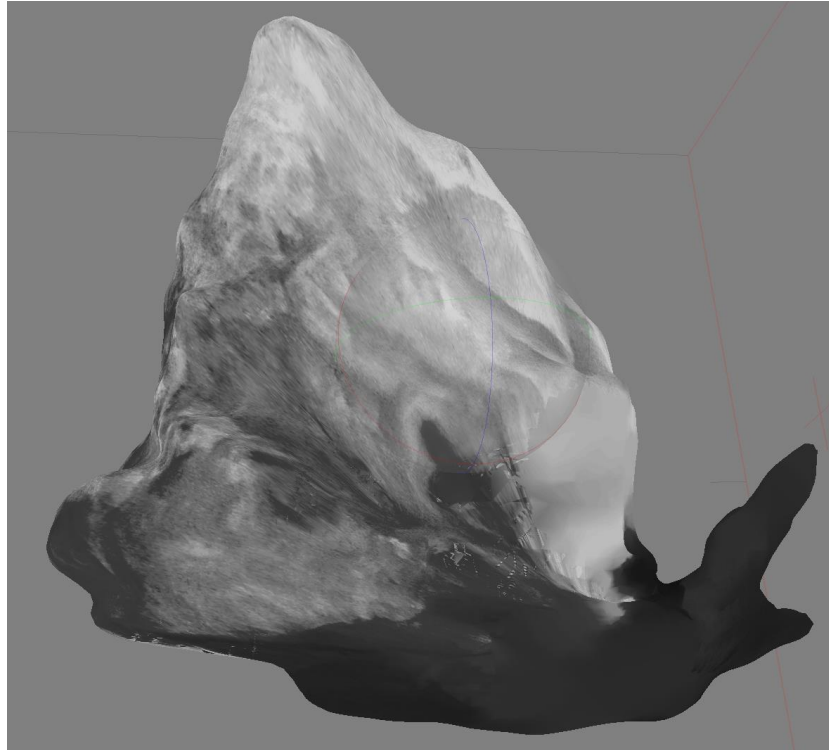
- b. The resultant mesh (3D model) will look like the one below for the 945-480 stope. Note that it will be a single color until a texture is built for it.



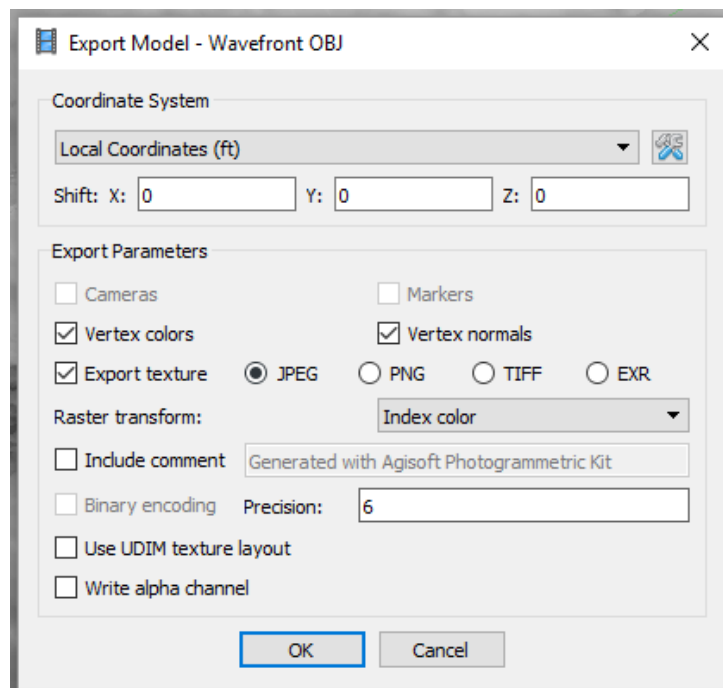
- c. Select the chunk that needs to be exported in the workspace and then select “Build Texture...” from the “Workflow” menu. Use the settings below:



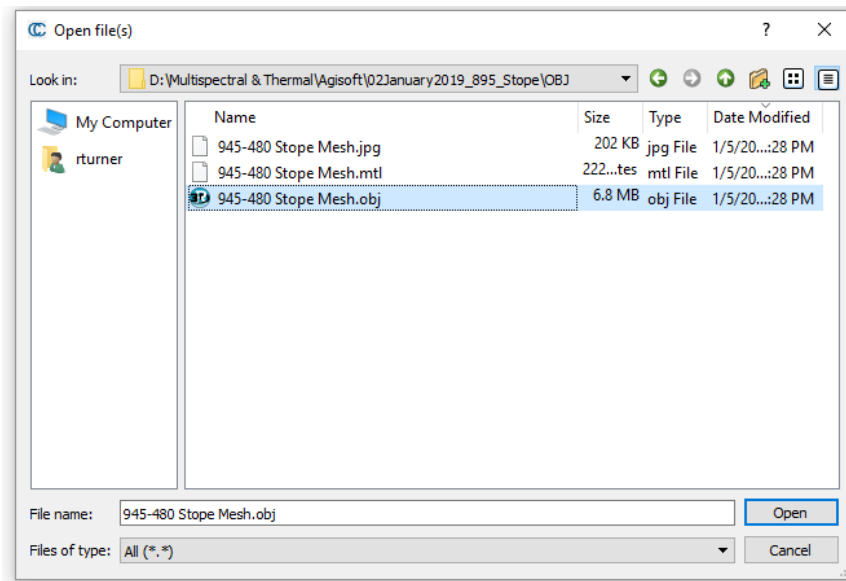
- d. After building the texture, select the 3D model again and a texture will be draped over it.



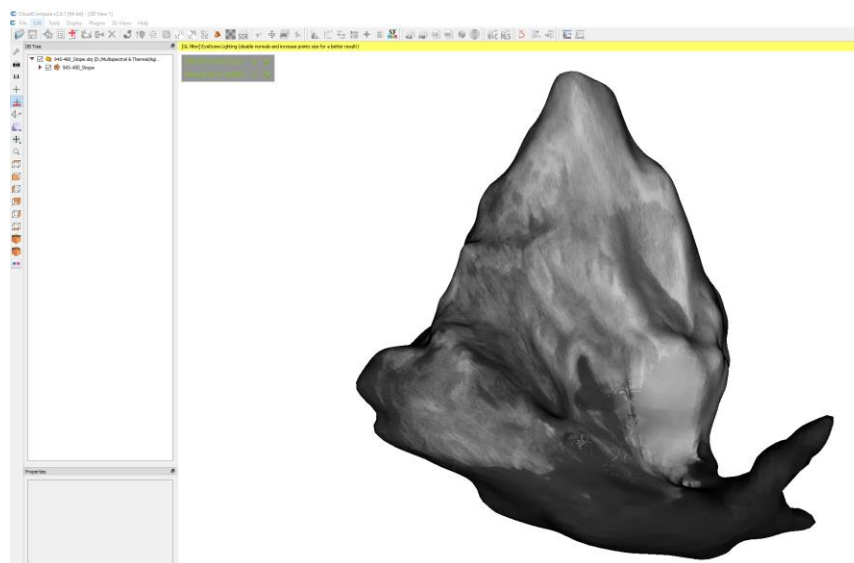
- e. Right-click on the “3D Model” in the Workspace and select “Export Model”. Export the model as an .obj file. Be sure that the file will be generated in its own folder or CloudCompare will not import the texture with the mesh. Use the settings below:



- f. Open CloudCompare and open the .obj file.



- g. The mesh should appear with the texture. Note that the raster values and brightness cannot be adjusted in CloudCompare. This will have to be done in Agisoft PhotoScan.



- h. Once in CloudCompare, the mesh can be co-registered with georeferenced data and structural features can be mapped using the “Compass” plugin.

APPENDIX G: WORKFLOW FOR CAPTURING & PROCESSING MULTISPECTRAL IMAGERY

1. With MicaSense RedEdge-M attached to drone, ensure there is an SD card in the camera and connect the camera to its power supply. This will automatically turn on the camera.
2. Using a WiFi enabled device (smartphone, tablet, PC, etc.), search for the RedEdge-M's WiFi access point and enter in the password:

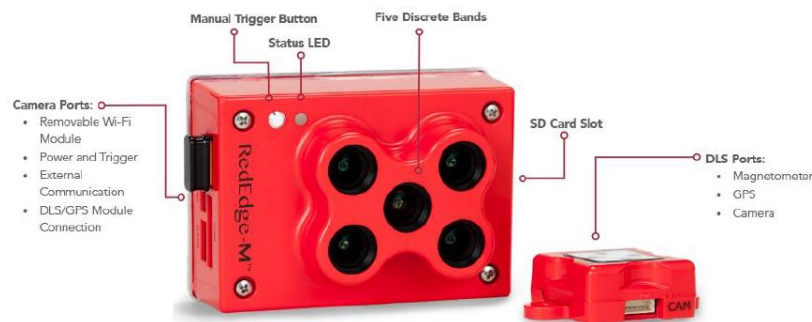
Access Point: *rededgeRMXX-XXXXXXX-XX* (X's are the serial numbers of the camera)

Password: *micasense*

3. Once connected to the camera, open a web browser and navigate to the following address:
192.168.10.254
4. Navigate to the "Live View" page, click the radio icon labeled "Streaming", and select "All Bands" in the drop-down menu to verify that all of the lenses are streaming imagery and working correctly.
5. If the drone is underground, turn on the onboard lighting (in this case the StratusLED ARM LED Module) and ensure that all other light sources in the area are turned off.



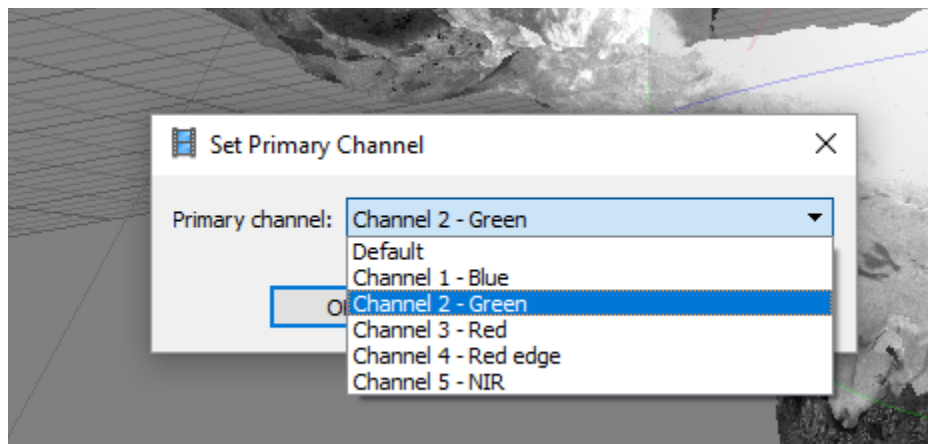
6. With the on-board lighting turned on, position the MicaSense reflectance panel perpendicular to the camera and use the live view to ensure that the panel takes up 50% of the image and that there are no shadows. Use the "Manual Trigger" button on the camera to capture at least 2 sets of images of the reflectance panel (see figure below from MicaSense, 2017).



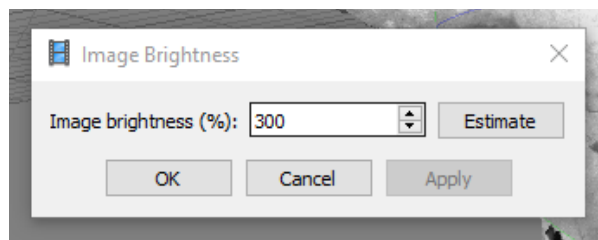
7. In the web browser, navigate to the “Settings” page and set the “Auto-Capture Mode” to “Timer”. Set the “Timer Period (sec)” to 1 second and then press the “Save” icon.
8. Under the “Settings” page, go to “Advanced Configuration” and verify that the “RAW Format” is set to “TIFF (16-bit)” and then press the “Save” icon.
9. When the drone is ready to start its mission, select the “Start” icon on the “Settings” page and use the same icon to press “Stop” when the mission is complete.
10. When the mission is complete, repeat the process of manually collecting 2 sets of images of the reflectance panel.
11. Download the TIFF files (they will appear as entirely black images in Windows Explorer) and import them into Agisoft PhotoScan. Note that each set of photos will have its own folder on the SD card and these sets reflect when the camera was turned on, images were manually captured, or images were captured in “Timer” mode. Combine the reflectance panel images with the “Timer” images for each mission.

12. Workflow for Agisoft PhotoScan:

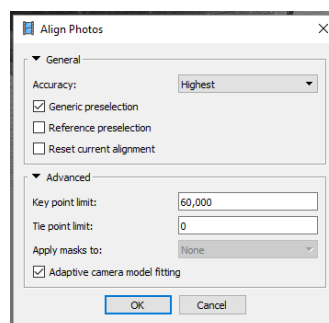
- a. Create a new chunk, import the multispectral photos (TIFF format) into the chunk, and right-click on the chunk to select “Set Primary Channel...”. PhotoScan will recognize that the photos are from a multispectral camera and will have 5 channels to choose from (not including “Default”). Select “Channel 1 – Blue”. Note that the chunk should be duplicated so that there are 5 chunks in total and so that the chunks are using the same set of photos. Each primary channel (blue, green, red, red edge, and near infrared (NIR)) will be assigned to an individual chunk and each chunk will be processed independently of the other chunks.



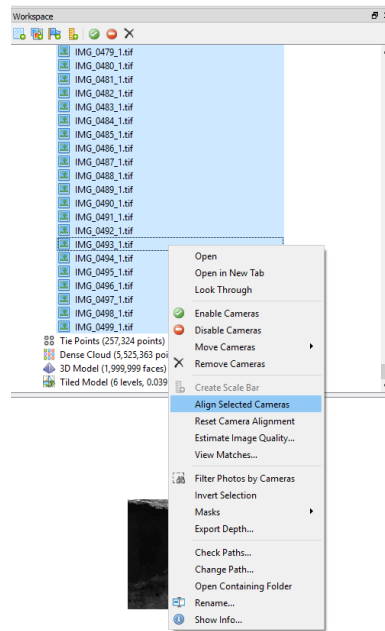
- b. After selecting the primary channel, right-click on the chunk again and select “Set Brightness”. Using the window that appears, set the brightness level manually or automatically using the “Estimate” button until the lighting in the TIFF files are satisfactory. Note that this can be adjusted after generating 3D point clouds and meshes.



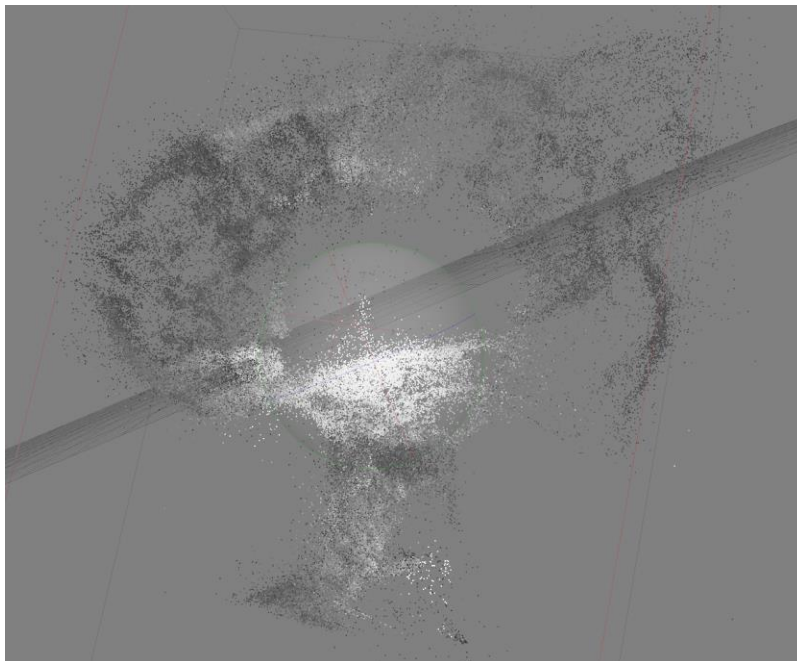
- c. With the individual chunk highlighted, navigate to the “Workflow” pane and select “Align Photos...”. Use the settings shown below:



- d. If not all of the photos aligned (excluding the reflective panel images), open the “Cameras” folder in the chunk and select all of the photos. Then right-click the selection and select “Align Selected Cameras” to align the remaining photos.

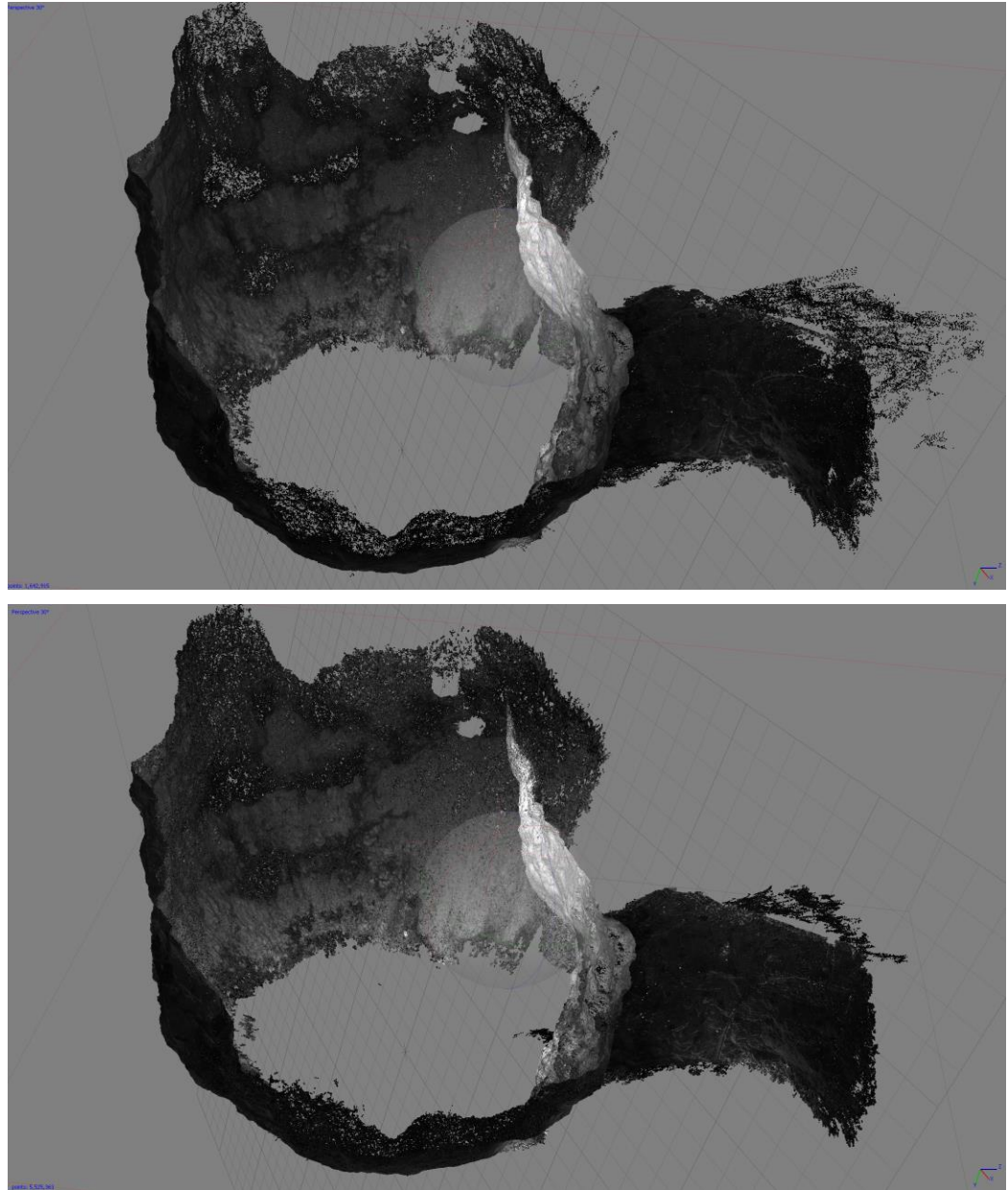


- e. After the photos are aligned select the “Tie Points” layer for the chunk and verify that the point cloud is satisfactory. The tie points for the 102 stope using the green band are shown below.

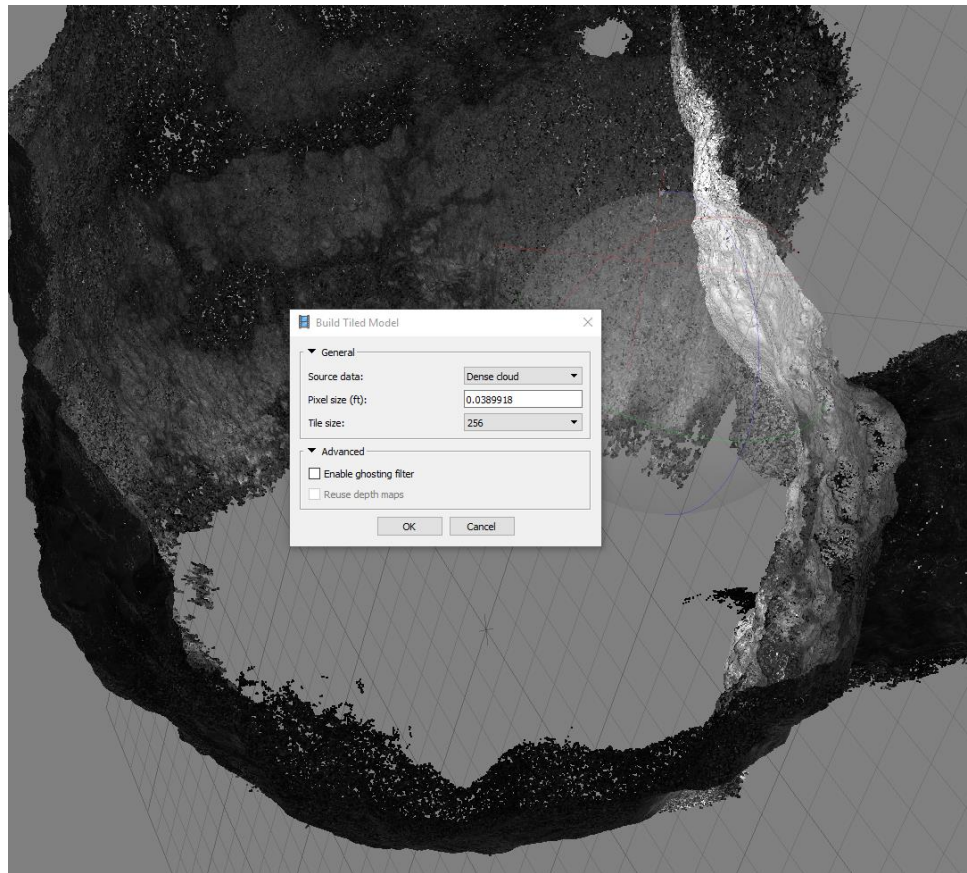


- f. If the coordinates of any control points (LED lights or reflective spheres) are known, then they can be tagged in the individual photos and georeferenced under the “Reference” pane. Otherwise, the resultant point clouds can be co-registered to georeferenced point clouds using CloudCompare or Maptek I-Site Studio.

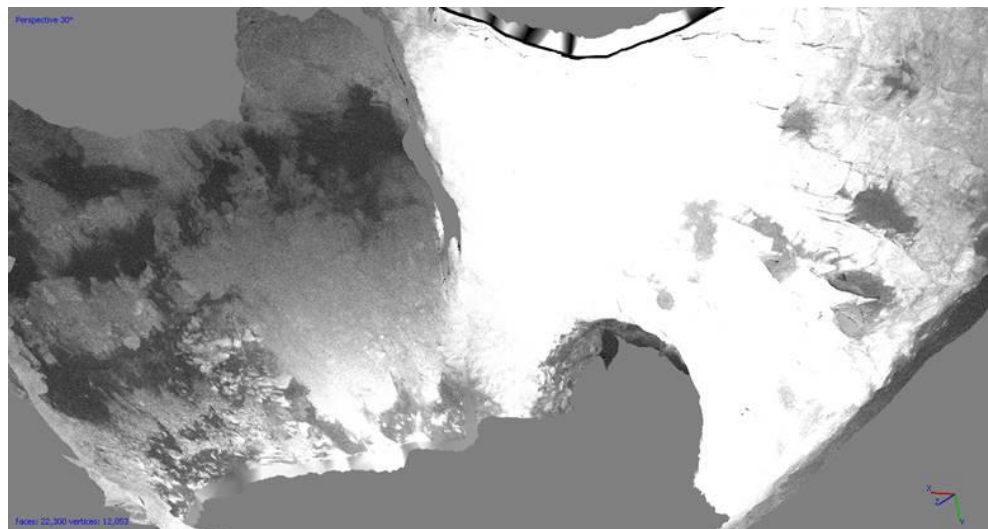
- g. After aligning the photos and generating tie points, select “Build Dense Cloud...” under the “Workflow” toolbar and use the “Medium” or “High” quality options. It should be noted that “Medium” (top image below of 102 stope using the green band) or “High” quality dense clouds (bottom image below of 102 stope using the green band) are better for generating tiled models.

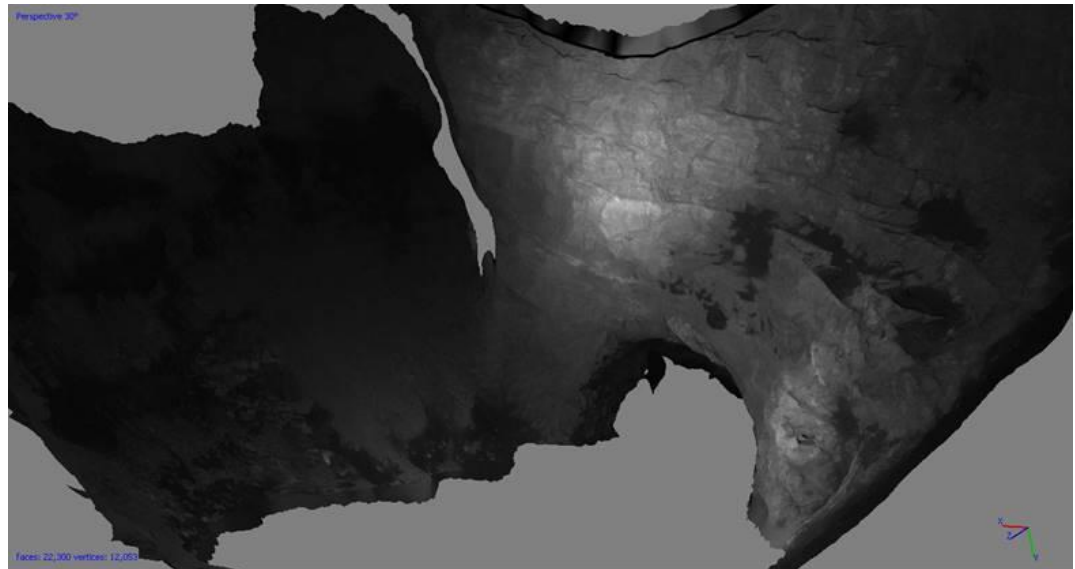


- h. After building the “Medium” or “High” quality dense cloud, select “Build Tiled Model...” under the “Workflow” toolbar and use the settings below.

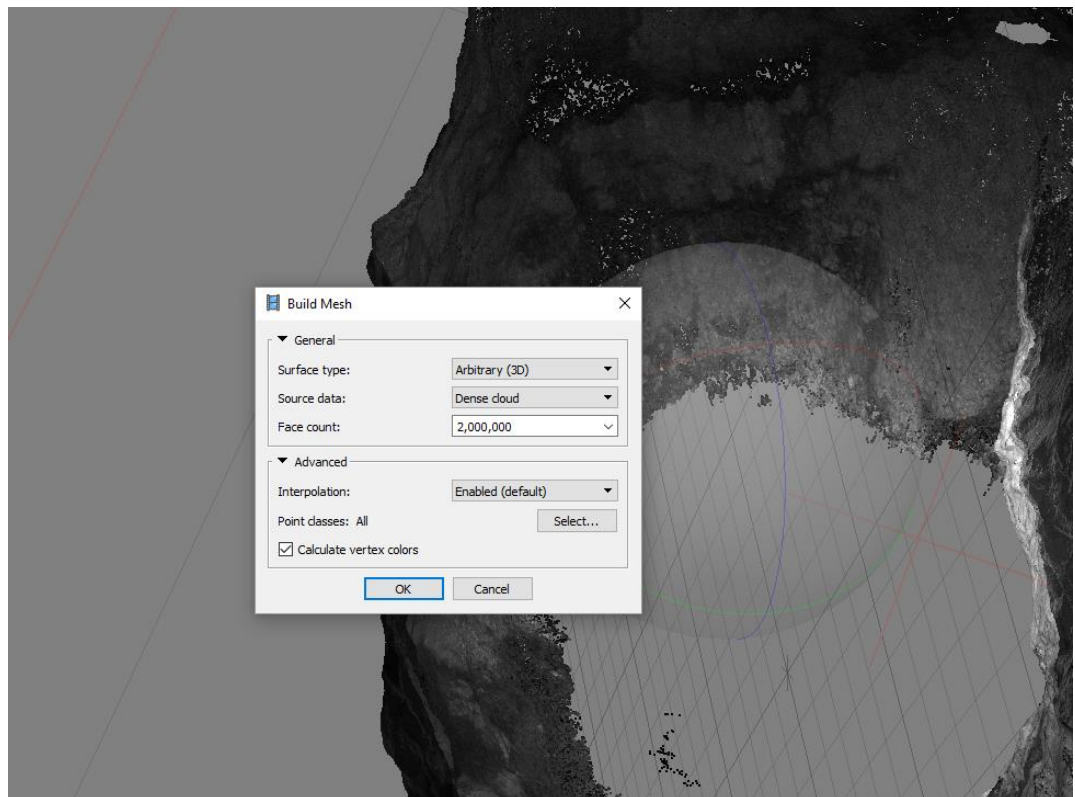


- i. After generating the tiled model, the “Set Brightness” tool (right-click the chunk) can be used to adjust the intensity of lighting in each image. Different brightness levels can be used to highlight structures. The images below show the 102 stope (green band) at 700 percent brightness (top image) and 100 percent brightness (bottom image).

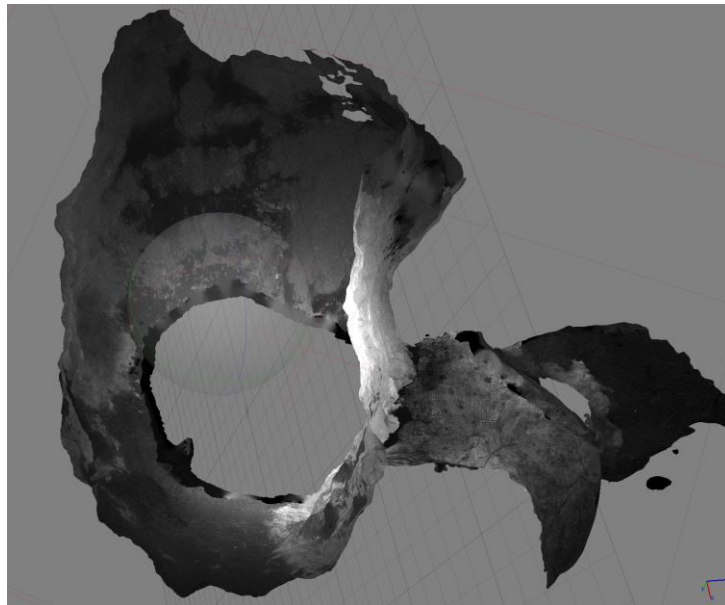




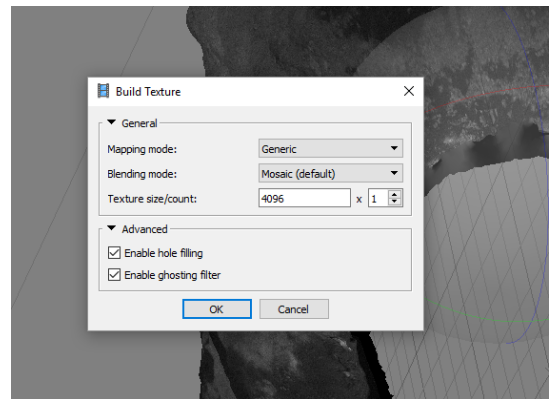
- j. Repeat these steps for each band (green, blue, red, red edge, and NIR) using dedicated chunks.
13. Exporting textured meshes and point clouds from multispectral models in Agisoft PhotoScan into CloudCompare for mapping.
 - a. Select the chunk that needs to be exported in the workspace and then select “Build Mesh...” from the “Workflow” menu. Use the settings below:



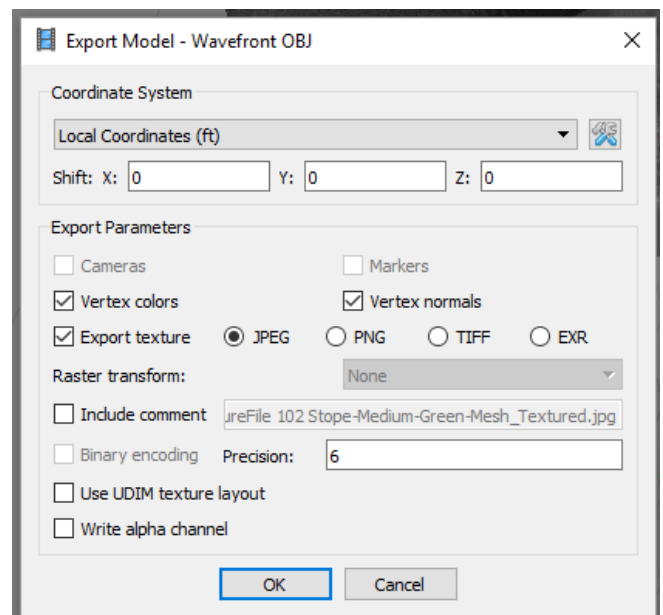
- b. The resultant mesh (3D model) will look similar to the dense cloud model.



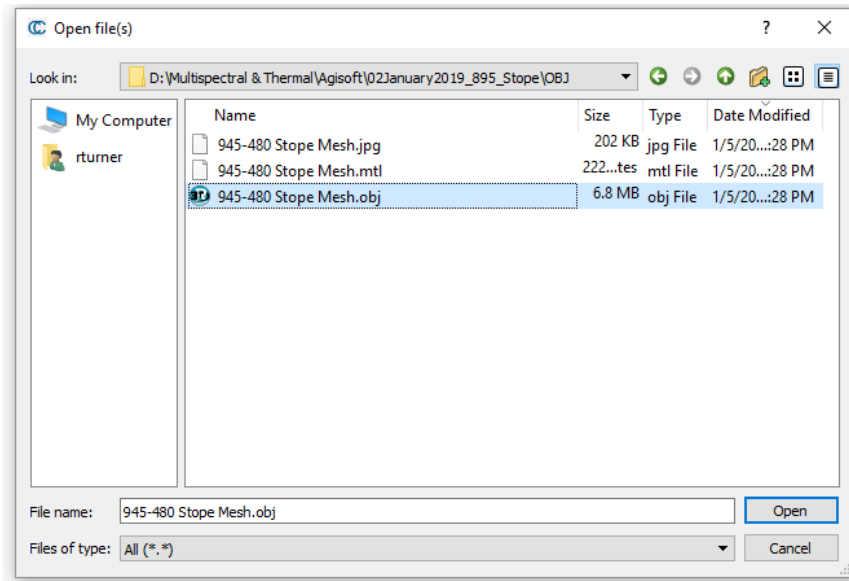
- c. Select the chunk that needs to be exported in the workspace and then select “Build Texture...” from the “Workflow” menu. Use the settings:



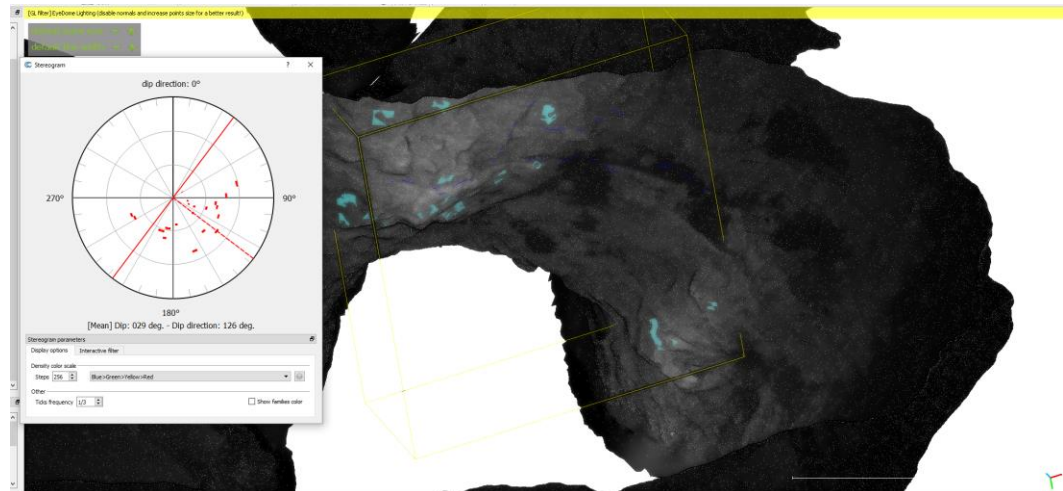
- d. Right-click on the “3D Model” in the Workspace and select “Export Model”. Export the model as an .obj file. Be sure that the file will be generated in its own folder or CloudCompare will not import the texture with the mesh. Use the settings:



- e. Open CloudCompare and open the .obj file.



- f. The mesh should appear with the texture. Note that the primary channel and brightness values cannot be adjusted in CloudCompare. This will have to be done in Agisoft PhotoScan.
- g. Once in CloudCompare, the mesh can be co-registered with georeferenced data and structural features can be mapped using the “Compass” plugin. Be sure that the vertices are turned on for the mesh so they can be selected when making structural measurements. Below is an example of the 102 stope (green band) being measured in CloudCompare.



APPENDIX I: TECHNOLOGY READINESS

Table I.1. NASA Technology Readiness Levels (NASA, 2013).

TRL	Definition	Hardware Description	Software Description	Exit Criteria
1	Basic principles observed and reported	Scientific knowledge generated underpinning hardware technology concepts/applications.	Scientific knowledge generated underpinning basic properties of software architecture and mathematical formulation.	Peer reviewed publication of research underlying the proposed concept/application
2	Technology concept or application formulated	Invention begins, practical application is identified but is speculative, no experimental proof or detailed analysis is available to support the conjecture.	Practical application is identified but is speculative, no experimental proof or detailed analysis is available to support the conjecture. Basic properties of algorithms, representations & concepts defined. Basic principles coded. Experiments performed with synthetic data.	Documented description of the application/concept that addresses feasibility and benefit
3	Analytical and/or experimental critical function or characteristic proof-of-concept	Analytical studies place the technology in an appropriate context and laboratory demonstrations, modeling and simulation validate analytical prediction.	Development of limited functionality to validate critical properties and predictions using non-integrated software components	Documented analytical/experimental results validating predictions of key parameters
4	COMPONENT or breadboard validation in laboratory	A low fidelity system/component breadboard is built and operated to demonstrate basic functionality and critical test environments and associated performance predictions are defined relative to the final operating environment.	Key, functionally critical, software components are integrated, and functionally validated, to establish interoperability and begin architecture development. Relevant Environments defined and performance in this environment predicted.	Documented test performance demonstrating agreement with analytical predictions. Documented definition of relevant environment.
5	COMPONENT or breadboard validation in a relevant environment	A mid-level fidelity system/component breadboard is built and operated to demonstrate overall performance in a simulated operational environment with realistic support elements that demonstrates overall performance in critical areas. Performance predictions are made for subsequent development phases.	End-to-end Software elements implemented and interfaced with existing systems/simulations conforming to target environment. End-to-end software system, tested in relevant environment, meeting predicted performance. Operational Environment Performance Predicted. Prototype implementations developed.	Documented test performance demonstrating agreement with analytical predictions. Documented definition of scaling requirements
6	SYSTEM/ SUBSYSTEM model or prototype demonstration in a relevant environment	A high-fidelity system/component prototype that adequately addresses all critical scaling issues is built and operated in a relevant environment to demonstrate operations under critical environmental conditions.	Prototype implementations of the software demonstrated on full-scale realistic problems. Partially integrate with existing hardware/software systems. Limited documentation available. Engineering feasibility fully demonstrated.	Documented test performance demonstrating agreement with analytical predictions
7	System prototype demonstration in space	A high fidelity engineering unit that adequately addresses all critical scaling issues is built and operated in a relevant environment to demonstrate performance in the actual operational environment and platform (ground, airborne or space).	Prototype software exists having all key functionality available for demonstration and test. Well integrated with operational hardware/software systems demonstrating operational feasibility. Most software bugs removed. Limited documentation available.	Documented test performance demonstrating agreement with analytical predictions
8	Actual system completed and flight qualified through test and demonstration	The final product in its final configuration is successfully demonstrated through test and analysis for its intended operational environment and platform (ground, airborne or space).	All software has been thoroughly debugged and fully integrated with all operational hardware and software systems. All user documentation, training documentation, and maintenance documentation completed. All functionality successfully demonstrated in simulated operational scenarios. V&V completed..	Documented test performance verifying analytical predictions
9	Actual system flight proven through successful mission operations	The final product is successfully operated in an actual mission.	All software has been thoroughly debugged and fully integrated with all operational hardware/software systems. All documentation has been completed. Sustaining software engineering support is in place. System has been successfully operated in the operational environment.	Documented mission operational results

Table I.2. Top: Definitions of levels of ingress protection against dust (DSM&T, 2018). Bottom: Definitions of levels of ingress protection against water (DSM&T, 2018).

Level	Object size protected against	Effective against
0	Not protected	No protection against contact and ingress of objects
1	>50mm	Any large surface of the body, such as the back of the hand, but no protection against deliberate contact with a body part.
2	>12.5mm	Fingers or similar objects.
3	>2.5mm	Tools, thick wires, etc.
4	>1mm	Most wires, screws, etc.
5	Dust Protected	Ingress of dust is not entirely prevented, but it must not enter in sufficient quantity to interfere with the satisfactory operation of the equipment; complete protection against contact.
6	Dust Tight	No ingress of dust; complete protection against contact.

Level	Object size protected against	Effective against
0	Not protected	–
1	Dripping water	Dripping water (vertically falling drops) shall have no harmful effect.
2	Dripping water when tilted up to 15°	Vertically dripping water shall have no harmful effect when the enclosure is tilted at an angle up to 15° from its normal position.
3	Spraying water	Water falling as a spray at any angle up to 60° from the vertical shall have no harmful effect.
4	Splashing water	Water splashing against the enclosure from any direction shall have no harmful effect.
5	Water jets	Water projected by a nozzle (6.3mm) against enclosure from any direction shall have no harmful effects.
6	Powerful water jets	Water projected in powerful jets (12.5mm nozzle) against the enclosure from any direction shall have no harmful effects.
7	Immersion up to 1m	Ingress of water in harmful quantity shall not be possible when the enclosure is immersed in water under defined conditions of pressure and time (up to 1 m of submersion).
8	Immersion beyond 1m	The equipment is suitable for continuous immersion in water under conditions which shall be specified by the manufacturer. Normally, this will mean that the equipment is hermetically sealed. However, with certain types of equipment, it can mean that water can enter but only in such a manner that it produces no harmful effects.

Table I.3. Safety and risk assessment table used by Barrick.

LIKELY HOD*	The outcome is certain to occur more than once during the period.	>95% Probability	Extremely Likely	Medium	Medium	High	High	High
	The outcome is expected to occur at least once during the period.	56%-95 Probability	Very Likely	Low	Medium	Medium	High	High
	The outcome is possible during the period.	31%-55% Probability	Likely	Low	Medium	Medium	High	High
	The outcome is not expected to occur during the period.	5%-30% Probability	Unlikely	Low	Low	Medium NEAR EARTH	Medium	High
	Unless there are exceptional circumstances, the outcome will not occur.	<5% Probability	Extremely Unlikely	Low FLYABILITY	Low	Low EMESENT INKONOVA	Medium	Medium
				Insignificant	Minor	Moderate	Major	Significant
			+/- <\$100k cash flow impact; Unplanned discrete operational delays (<1 week); Minor first aid treated onsite; minor reversible health effects of no concern; Environmental damage is easy to remediate	+/- \$100K-\$250K cash flow impact; Unplanned short term (up to 1 month) operational delays and/or suspension; Minor injury treated offsite; reversible health effects of no concern, no disability; Minor environmental damage	+/- \$250K-\$500K cash flow impact; Unplanned mid-term (up to 3 months) operational delays and/or suspension; Reportable injury (MTI, RD, LTI); reversible health effect resulting from acute short term exposure or progressive chronic condition; Moderate environmental damage	+/- \$500K-\$1M cash flow impact; Unplanned long-term (up to 6 months) suspension; Injury leading to permanent disability or exposures resulting in irreversible health effect of concern; Major environmental damage	+/- >\$1M cash flow impact; Unplanned shutdown (>6 months); Significant environmental damage; Single fatality; Health effects resulting in multiple disabling illness leading to early mortality	
IMPACT **								
* Based on probability that the predicted outcome/event will occur during the specified time frame, generally understood as the current 12 month period								
** Based on identified events, the impact of risk being realized on the achievement of related strategic objectives/priorities over the specified time frame as defined by metrics relevant to risk area/function (see support details); Operating Unit and Functional matrices to be scaled against the Enterprise matrix								